

Continuous-Flow Separation of Cells in a Lab-on-a-Chip using "Liquid Electrodes" and Multiple-Frequency Dielectrophoresis

THÈSE N° 4099 (2008)

PRÉSENTÉE LE 4 JUILLET 2008

À LA FACULTE SCIENCES ET TECHNIQUES DE L'INGÉNIEUR
LABORATOIRE DE MICROSYSTÈMES 4
PROGRAMME DOCTORAL EN MICROSYSTÈMES ET MICROÉLECTRONIQUE

ÉCOLE POLYTECHNIQUE FÉDÉRALE DE LAUSANNE

POUR L'OBTENTION DU GRADE DE DOCTEUR ÈS SCIENCES

PAR

Nicolas DEMIERRE

ingénieur en microtechnique diplômé EPF
de nationalité suisse et originaire de Saint-Martin (FR)

acceptée sur proposition du jury:

Prof. Y. Leblebici, président du jury
Prof. Ph. Renaud, directeur de thèse
Prof. N. de Rooij, rapporteur
Dr A. González Oliva, rapporteur
Prof. A. van den Berg, rapporteur



ÉCOLE POLYTECHNIQUE
FÉDÉRALE DE LAUSANNE

Suisse
2008

À mes parents

*Contradiction is not a sign of falsity,
nor the lack of contradiction a sign of truth.*

Blaise Pascal (1623 - 1662)



Abstract

This thesis reports on the integration of continuous-flow cell separation method for lab-on-a-chip applications. Cell separation methods are widely used in biology to prepare samples prior to analysis. There is a need for a highly sensitive separation method that is capable to quickly isolate a particular cell type in a single manipulation step.

We attempt to provide such a separation method that discriminates between cell types according to their dielectric properties such as the membrane permittivity and the cytoplasm conductivity. The dielectric properties are intrinsic to each cell type and thus prevent the need of a specific cell labeling as discriminating factor. To guaranty a high throughput, the cell separation method we propose is performed in a continuous flow.

The continuous-flow cell separation method presented in this thesis makes use of electrical forces to achieve the separation of different cell types. Dielectrophoresis is a phenomenon that describes the electrical force exerted on a dielectric particle such as a biological cell in presence of a non-uniform AC electric field. The combination of several dielectrophoretic forces at multiple frequencies produces a distinct dielectric response for each cell type.

The method is integrated into a microfluidic platform of 20 *mm* long by 15 *mm* wide. The microfabrication of the device consists of two successive steps of photolithography to define the metal electrodes in platinum and the microfluidic network in SU-8 photoresist. In the so-called separation chamber, an array of "liquid electrodes" is localized along the 20 μm deep central channel. The technological development of "liquid electrodes" allow us to produce horizontal dielectrophoretic force and the array of these electrodes opposes two fields of such forces. This opposition of two force fields defines

an equilibrium position towards which the cells that flow through the central channel are focused. There is a relationship between the equilibrium position and the dielectric properties of the cells which allows a flow-through dielectric characterization of the cells by the cell position readout.

Using this microfluidic platform that integrate a method of continuous-flow cell separation based on multiple-frequency dielectrophoresis, we succeeded in purifying fractions of viable and nonviable yeast cells that were initially mixed. Due to its sensitivity, the method also allowed to increase the infection rate of a cell culture up to 50% of parasitemia percentage, which facilitates the study of the parasite cycle. The method was finally applied to the biological issue of cell synchronization. By isolating cells that are at a particular phase within their cell cycle, our method prevents the use of metabolic agents in order to arrest a cell culture by disrupting the cell physiology. The synchronization method we proposed and based on multiple-frequency dielectrophoresis is to our best knowledge the most powerful one in terms of synchrony level reported so far.

keywords: *microfluidics, lab-on-a-chip, μ TAS, continuous flow, cell separation, cell isolation, cell synchronization, red blood cell, yeast cell, parasite, dielectrophoresis, multiple-frequency dielectrophoresis, dielectric properties, opacity, equilibrium, microfabrication, "liquid electrode".*

Version abrégée

Cette thèse porte sur l'intégration d'une méthode de séparation de cellules en flux continu pour une application de lab-on-a-chip (laboratoire sur puce). Les méthodes de séparation de cellules sont largement utilisées en biologie pour préparer un échantillon avant une analyse. Cependant, il manque une méthode de séparation à haute résolution capable d'isoler rapidement un type de cellules particulier en une seule étape de manipulation.

Nous désirons procurer une telle méthode de séparation qui différencie des cellules selon leurs propriétés diélectriques telles que la perméance de la membrane ou la conductivité du cytoplasme. Les propriétés diélectriques sont intrinsèques à chaque type de cellules et ainsi évitent le recours à un marquage des cellules comme facteur de discrimination. Pour garantir un bon rendement, la méthode de séparation que nous proposons est effectuée dans un flux continu.

La méthode de séparation de cellules en flux continu présentée dans cette thèse utilise des forces électriques afin de séparer différents types de cellules. La diélectrophorèse est un phénomène qui décrit la force électrique qui s'applique sur une particule diélectrique telle qu'une cellule biologique en présence d'un champ électrique AC non uniforme. La combinaison de plusieurs forces diélectrophorétiques à fréquences multiples induit une réponse diélectrique distincte pour chaque type de cellules.

Cette méthode est intégrée dans une plateforme microfluidique de 20 *mm* de long par 15 *mm* de large. La micro-fabrication du dispositif comprend deux étapes successives de photolithographie pour structurer les électrodes métalliques en platine et le réseau microfluidique en résine photosensible SU-8. Dans ce qui est appelé la chambre de séparation, un réseau d' "électrodes liquides" est disposé le long du canal central qui a une profondeur

de 20 μm . Le développement technologique des "électrodes liquides" nous a permis de produire des forces diélectrophorétiques horizontales ainsi que d'opposer deux champs de ces telles forces grâce à l'arrangement de ces électrodes en réseau. L'opposition des deux champs de forces définit une position d'équilibre vers laquelle sont dirigées les cellules qui s'écoulent dans le canal central. Il existe une relation entre la position d'équilibre et les propriétés diélectriques des cellules qui permet de caractériser diélectriquement les cellules par la lecture de leur position.

En utilisant la plateforme microfluidique qui intègre la méthode de séparation de cellules en flux continu basée sur la diélectrophorèse à fréquences multiples, nous sommes parvenus avec succès à purifier des populations de cellules vivantes et mortes qui étaient initialement mélangées. Grâce à sa sensibilité, la méthode a également permis d'augmenter le pourcentage de cellules infectées au sein d'une culture cellulaire jusqu'à des taux de 50% ce qui facilite l'étude du cycle du parasite. Cette méthode a finalement été appliquée à un problème biologique de synchronisation de cellules. En isolant les cellules qui sont à un stade particulier dans leur cycle cellulaire, notre méthode évite le recours à des agents métaboliques afin de bloquer des cellules à un stade particulier en perturbant leur physiologie. La méthode de synchronisation que nous proposons basée sur la diélectrophorèse à multiple fréquences est à notre connaissance la plus performante des méthodes rapportées jusqu'alors en terme de niveau de synchronisation.

mots-clés: *microfluidique, lab-on-a-chip, μTAS , flux continu, séparation de cellules, isolation de cellules, synchronisation de cellules, globule rouge, levure, parasite, diélectrophorèse, diélectrophorèse à fréquence multiples, propriétés diélectriques, opacité, équilibre, micro-fabrication, "électrode liquide".*

Acknowledgements

The outcome of this thesis is the result of many efforts, fruitful collaborations and lots of support of any kinds. This section aims expressing my gratitude to people who relied on me and somehow contributed to this work.

I would like to express my deepest gratitude to Professor Philippe Renaud for offering me a PhD position and introducing me to the world of miniaturization. I appreciated the trust and the liberty he conferred me. The European Community-funded CellPROM project under the 6th Framework Programme, contract No. NMP4-CT-2004-500039 is acknowledged for the financial support.

I express my gratitude to Professor Albert van den Berg, Professor Nico de Rooij, Dr. Abel Oliva for having accepted to be members of the jury of my thesis and Prof. Yusuf Leblebici for having playing the role of president of the jury. It was an honor for me to present you my research and to share with you this unique moment of the private thesis defense. Additional thanks go to Abel and his collaborators, Elisabete and Tiago, for their enthusiasm and competencies and for the nice moments of work (including overnight working...) and distraction we spent together either in Oeiras or in Lausanne.

I would like to acknowledge Professor Yves Barral from the Institute of Biochemistry of EPFZ and his Ph.D. student Alex Rauch. They welcomed us and helped us in addressing the issue of cell synchronization by providing us with GFP-tubulin yeast cells. Your support was essential.

I warmly acknowledge Dr. Alejandro Marabi, from the Nestlé Research Center, for his collaboration and support in the field of microcalorimetry,

which was also a focus of my research but not presented in this manuscript. His innovative insights extended the application field of our technological developments to the food industry.

Je voudrais remercier maintenant tous mes proches de l'EPFL, que ce soient des amis, des collègues ou ex-collègues, qui ont transformé ces années de thèse en une période inoubliable. Merci aux anciens qui sont parti trop tôt, Shady, Urban, Pontus et Mario, pour m'avoir accueilli et transmis une part de leur expérience.

Un grand merci à mes collègues actuels, Nicolas Du, Lynda, Harsha, Alessandro, Matteo, Sebastien, Raph F, Ludovica, Mina, Joel and Harald, qui partiront pour leur part après moi et qui donnent du piment à la vie de groupe par leur personnalités diverses.

Je remercie également ceux qui ont eu le courage et la patience nécessaire pour partager mon bureau, Marc T, Marc B, André M, Anja et tout particulièrement Raph. Ils ont su créer une ambiance motivante et amusante de par leur bonne humeur.

Je voudrais également remercier celui qui effraie les doctorants, celui qui manie le crayon rouge mieux que quiconque, Arnaud, pour son aide et ses conseils précieux durant les phases d'écriture.

Je remercie profondément Thomas qui a contribué de manière essentielle aux résultats de cette thèse de par son enthousiasme et ses connaissances hors normes. Un grand merci à Ana qui est davantage une amie qu'une collègue (mais oui) et qui m'a particulièrement beaucoup aidé et encouragé durant les derniers mois de thèse.

Un tout grand merci également aux secrétaires, Claudia, Sylvie, Marie et tout particulièrement notre encyclopédie sportive Rose-Mary, qui apportent quotidiennement joie et bonne humeur.

J'en profite également pour remercier mes étudiants de semestre ou master, Claudia, Cyntia, Laurent, Richard, Robin et Pascal, qui ont contribué à différentes parties de cette thèse en apportant une approche et des idées nouvelles.

Je remercie les membres du CMI pour leurs supports et patience dans les étapes de microfabrication ainsi qu'aux membres des ateliers de mécanique

ATPR et des circuits imprimés ACORT pour leurs travaux minutieux. Merci aussi aux différents collaborateurs des laboratoires de micro-systèmes 1, 2 et 3 que j'ai eu le plaisir de côtoyer régulièrement dans le corridor du 3^{ème} étage du BM. Et merci à tous les travailleurs de l'ombre que j'aurais oubliés de mentionner!

Je tiens à remercier sincèrement mes amis de l'EPFL, Marc, Ben, André N, Fabien, Pierrick et Steve, pour les nombreux bons moments partagés durant ces dernières années, que ce soient les pauses de midi ou les apéros du vendredi. J'espère en vivre encore de nombreux autres!

Merci à mes amis de toujours, Nicolas, Vincent, Doudou, Jérôme, Dodo et tant d'autres pour m'avoir permis de me changer les idées en votre compagnie lors de nombreux événements festifs entre autres!!!

Je remercie infiniment mes parents pour m'avoir toujours laissé choisir ma voie en me faisant confiance et pour m'avoir toujours soutenu aussi bien financièrement que moralement. Je vous en suis profondément reconnaissant car je n'y serais pas arrivé sans votre aide. Merci aussi à ma soeur Noémie et mon frère Alexandre pour leurs encouragements.

Un merci tout particulier à Roger Speidel qui très tôt déjà m'a sensibilisé aux multiples facettes de notre planète en me transmettant jour après jour une partie de ses vastes connaissances. Je t'en suis profondément reconnaissant, ces moments privilégiés et malheureusement trop courts resteront à jamais gravés dans ma mémoire.

Et je finirai par remercier de tout coeur Marion, qui m'a sans cesse soutenu, qui m'a supporté dans les moments difficiles (comme les quelques mois de rédaction) et qui donne au quotidien du goût et des couleurs à ma vie.

MERCI à vous tous, sans qui cette aventure ne serait restée qu'un rêve!



Contents

Abstract	ix
Version abrégée	xi
Acknowledgements	xiv
Nomenclature	xxiv
1 Introduction	1
1.1 The Origins of microfluidics	1
1.2 Towards a lab-on-a-chip	3
1.3 Scope of this thesis	5
1.4 Microfluidics concepts	6
1.4.1 Handling of liquid	6
1.4.2 Handling of particles in liquid	7
1.5 Physics of microfluidics	8
1.6 On-chip continuous-flow separation methods	10
1.6.1 Definition	10
1.6.2 Main characteristic features	12
1.6.3 State of the art	12
1.6.3.1 Acoustic separation	13
1.6.3.2 Magnetic separation	14
1.6.3.3 Fluidic-only separation	15

CONTENTS

1.6.3.4	Adhesion-based separation	15
1.6.3.5	Electrical separation	16
1.6.4	Discussion	20
1.7	Research Strategy	21
1.7.1	Motivations	21
1.7.2	Main objectives	22
1.8	Thesis structure	23
Bibliography		33
2	AC electrokinetics: fundamentals and modeling	35
2.1	Interfacial polarization	35
2.2	Induced dipole moment of dielectric particles	37
2.2.1	Model of homogeneous sphere	37
2.2.2	Multi-shell model	39
2.2.3	Model of common particles	40
2.2.3.1	Model of a polystyrene bead	40
2.2.3.2	Red blood cell	40
2.2.3.3	Viable yeast cell	41
2.2.3.4	Nonviable yeast cell	43
2.3	Dielectrophoresis	43
2.3.1	Dielectrophoresis with "liquid electrodes"	45
2.3.2	Numerical calculation of the electric field	48
2.3.2.1	In the access channel: from 2D to 3D	49
2.3.2.2	In the central channel: from 3D to 2D	50
2.3.3	Estimation of the electrical force	51
2.3.4	Scaling considerations	53
2.4	Multiple-frequency dielectrophoresis	54
2.4.1	Superposition of dielectrophoresis	55
2.4.2	The effective Clausius-Mossotti factor	56

2.4.3	Opposition of dielectrophoretic forces	57
2.4.3.1	Definition of equilibrium position	57
2.4.4	Particular case of multiple-frequency dielectrophoresis	59
2.4.4.1	Effect of close frequencies	59
2.4.5	Set of electrical signals for continuous-flow separation of cells . .	60
Bibliography		65
3 Microfluidic platform using "liquid electrodes"		67
3.1	The "liquid electrode"	67
3.1.1	General concept	67
3.1.2	Array of "liquid electrodes"	70
3.2	Chip design	70
3.2.1	Electrodes	70
3.2.2	Fluidic network	73
3.3	Microfabrication	73
3.4	Chip interfaces	75
3.4.1	Fluidic setup	75
3.4.2	Electrical setup	76
Bibliography		79
4 Electrical manipulation and characterization of particles		81
4.1	Materials and methods	81
4.1.1	Suspension medium	81
4.1.2	Preparation of suspended particles	81
4.1.3	Particle tracking	82
4.1.4	Image analysis	82
4.2	Deviation of particles	83
4.3	Focusing of particles	85
4.3.1	Effect of the particle size	88

CONTENTS

4.3.2	Focusing at two frequencies	88
4.4	Dielectric characterization of particles	91
4.4.1	Force balance	91
4.4.2	Definition of "opacity"	93
	Bibliography	95
5	Continuous-flow separation of cells using MFDEP	97
5.1	Materials and methods	97
5.1.1	Suspension medium	99
5.1.2	Preparation of yeast cells	99
5.1.3	Culture of infected RBCs	99
5.1.4	Image analysis	100
5.2	Separation of beads and yeast cells	100
5.2.1	Characterization of dielectric properties	102
5.3	Separation of viable and nonviable yeast cells	104
5.3.1	Estimation of the dielectric response	107
5.4	Isolation of parasitized RBCs	109
5.4.1	Separation of infected and non-infected RBCs	109
5.4.2	Estimation of the enrichment factor	112
5.5	Synchronization of a cell culture	113
5.5.1	Cell model	115
5.5.2	Numerical modeling of budding yeast cell	116
5.5.3	Materials and methods	118
5.5.3.1	Microfluidic device	118
5.5.3.2	Sample preparation	119
5.5.4	Estimation of the synchrony level	119
5.5.5	Isolation of cells in division	119
	Bibliography	126

6 Conclusion and outlook	127
6.1 Summary of achievements	127
6.1.1 The "liquid electrode"	128
6.1.2 The electrode array	129
6.1.3 Multiple-frequency dielectrophoresis	130
6.1.4 Biological applications	131
6.2 Contribution to knowledge	132
6.3 Future perspectives	134
Bibliography	137
A Curriculum vitae	139
B Publications	141

CONTENTS

Nomenclature

Variables and constants

η	Viscosity	$[kg \cdot m^{-1} \cdot s^{-1}]$
γ	Radius ratio	[-]
λ	Electric-potential ratio	[-]
\mathbf{E}	Electric field	$[V \cdot m^{-1}]$
\mathbf{p}	Dipole moment	$[C \cdot m]$
\mathbf{v}	Velocity	$[m \cdot s^{-1}]$
ν	Volume	$[m^3]$
ω	Angular frequency	$[rad \cdot s^{-1}]$
ϕ	Scalar field of potential distribution	$[V]$
σ	Electrical conductivity	$[S \cdot m^{-1}]$
τ_{MW}	Maxwell-Wagner relaxation time	$[s]$
$\tilde{\epsilon}$	Complex permittivity	$[F \cdot m^{-1}]$
\tilde{f}_{CM}	Clausius-Mossotti factor	[-]
ϵ	Permittivity	$[F \cdot m^{-1}]$
a	Radius of particle	$[m]$
d	Characteristic geometrical dimension	$[m]$

NOMENCLATURE

f	Frequency	[Hz]
f_{co}	Crossover frequency	[Hz]
f_{fric}	Friction factor	[kg · s ⁻¹]
f_{MW}	Maxwell-Wagner frequency	[Hz]
l	Characteristic dimension	[m]
Re	Reynold's number	[-]
V	Electric potential	[V]

Abbreviations

μ -TAS	Micro-total-analysis systems
AIDS	Acquired immunodeficiency syndrome
BEM	Boundary element method
BSA	Bovine serum albumine
CM	Clausius-Mossotti
DACS	Dielectric-activated cell sorting
DEP	Dielectrophoresis
DIC	Differential interference contrast
DNA	Deoxyribonucleic acid
eDEP	Electrodeless dielectrophoresis
EOF	Electro-osmotic flow
EP	Electrophoresis
EPFL	École Polytechnique Fédérale de Lausanne, Switzerland
ETHZ	École Polytechnique Fédérale de Zürich, Switzerland

FACS	Fluorescence-activated cell sorting
FEM	Finite element method
FFF	Field-flow fractionation
GFP	Green fluorescent protein
HIV	Human immunodeficiency virus
IBM	International Business Machines Corporation
iDEP	Insulator-based dielectrophoresis
IMT	Institute of microtechnology, Switzerland
ISAS	Institute for Analytical Sciences, Germany
IVD	In-vitro diagnostics
KTH	Royal Institute of Technology, Sweden
LOC	Lab-on-a-chip
MDT	Microfluidic diagnostic technology
MEMS	Micro-electro-mechanical Systems
MFDEP	Multiple-frequency dielectrophoresis
MIT	Massachusetts Institute of Technology, USA
MST	Microsystem technology
nDEP	Negative dielectrophoresis
PBS	Phosphate buffer solution
PCB	Printed circuit board
PCR	Polymerase chain reaction
PDE	Partial differential equations

NOMENCLATURE

pDEP	Positive dielectrophoresis
PDF	Pressure-driven flow
PDMS	Polydimethylsiloxane
PPE	Parasitemia percentage
RBC	Red blood cell
rms	Root mean square
TAS	Total-analysis systems
twDEP	Traveling wave dielectrophoresis
UV	Ultraviolet

Chapter 1

Introduction

Summary This first chapter gives the main aspects related to this thesis. A first section introduces the reader to the world of miniaturized systems, from the semiconductor industry to the integration of complex biological functions in lab-on-a-chips. The decrease in dimensions resulting from the miniaturization of systems has drastic consequences on the physics and induces particular phenomena characteristic of the microscale. The miniaturization is advantageously exploited to develop integrated methods of cell separation. The state of the art and best achievements of continuous-flow separation are summarized and discussed in the second part of the chapter. Then our research strategy and main objectives to further develop such techniques are described. Finally this first chapter ends with the outline of the whole manuscript.

1.1 The Origins of microfluidics

Today the microfluidics community is spread worldwide, including the most famous universities¹ and companies². However, it was a completely different story twenty years ago, but microfluidics has been a fast growing field and is even expected to be a key technology of the 21st century (Daw and Finkelstein, 2006) with novel applications without macroscopic equivalent (Dittrich and Manz, 2006). Due to its dimensions

¹Harvard, Stanford, MIT, KTH, ISAS, Twente Univ., IMT and EPFL

²Agilent Technologies, Evotec Technologies, Caliper Life Sciences, Hitachi, IBM and Fluidigm Technology

1. INTRODUCTION

comparable to the ones of living organisms, microfluidics offers innovative technological opportunities for obtaining new information about biological systems (El-Ali *et al.*, 2006).

Whitesides (2006) defines microfluidics as the science and technology of systems dealing with small amounts of fluids (typically picoliter to nanoliter), using micrometric fluidic networks. The origins of microfluidics date from the 80's and lie in microanalytical methods. A detailed overview of this period can be read in the book of Tabeling (2003). This period stands for a breakthrough in science with the emergence of a new fabrication technology, called microfabrication or micromechanics (Madou, 2002). The fast development of micromechanics was driven by the industry of silicon microprocessors between 1970 and 1980. Micromechanics is a set of basic techniques such as selective deposition and etching of materials on a silicon substrate and allows producing miniaturized systems, layer by layer, with typical dimensions of a few microns to hundreds of microns. The fundamental process used to structure layers of materials on a substrate is the photolithography. It allows to transfer a pattern from a design or from a mask to a photo-sensitive polymer - or photoresist - that is deposited on the substrate by selective ultraviolet-light (UV) radiation. The UV radiation induces chemical reactions that locally degrade or polymerize the resist according to its chemistry. Only part of the initial homogeneous layer of photoresist remains on the substrate after the photo-chemical reaction and consecutive chemical development that reveals the pattern on the resist. The remaining resist subsequently serves as mask for the next steps of microfabrication. Photolithography and other microfabrication techniques were widely used to produce systems of increasing complexity. The microsystems then included mechanical functions as well as electrical functions and were therefore called micro-electro-mechanical systems (MEMS). In comparison to integrated circuits (ICs) for semiconductor industry, microsystem technology (MST) contains three-dimensional features and moving parts. The new field of integrated actuators and sensors was promoted by MST and by its ability in solving problems that were so far not addressable by ICs alone. This field development is further motivated by the success of integrated sensors, in particular accelerometers, in the automotive market.

MEMS later extended to new fields such as chemistry and biology with the requirement

of handling liquids in order to fulfill more complex functions. The integration of fluids handling on MEMS gives birth to microfluidics. Although microfluidics is recognized as a scientific disciplinary only from the early 90's, the first microfluidic system has already been presented by Terry *et al.* in 1979. They developed a gas chromatograph and were able to separate a simple mixture of chemical compounds in a matter of seconds. Another example also considered as one of the first microfluidic systems is the ink jet printer head presented in 1977 by Bassous *et al.*. The main challenge was the integration of a fast enough actuator on the micromachined nozzles to deliver reproducible droplets. Major efforts were then focused on the fabrication of microfluidic components such as microvalves (Tiren *et al.*, 1989), micropumps (van Lintel *et al.*, 1988) and flow sensors (Johnson and Higashi, 1987). Smits (1990) combined microfluidics components, microvalves and micropumps, to increase the functionality of their system. Similarly, Van der Schoot *et al.* (1991) added a chemical analysis system to their micropump. As pointed out by Gravesen *et al.* (1993), the main advantages of micromechanical analysis systems are small volume of reactants, high sensitivity, high throughput due to parallelization and short response time. Moreover, their small sizes make the installation of these systems possible in portable equipments with low power consumption. Microfluidics, as a development of the MEMS industry, is emerging and conquering an extensive field of application, where its advantages push away the limits of our understanding of the physics (Feynman, 1992).

1.2 Towards a lab-on-a-chip

Further developments of microfluidic systems were mainly focused on materials carried or dragged by the fluid rather than the fluid itself as it was the case in the basic fluidic components mentioned previously. The material is for instance of chemical or biological nature. The fluid, generally a liquid, is used to move complex materials in suspension such as living microorganisms, single cells or proteins. The manipulation of chemical and biological materials brings new opportunities to microfluidics, in particular in the emerging field of molecular biology and in particular genomics, *e.g.* gene typing or sequencing. A decade of abundant integrations of chemical and biological manipulations on the chip format largely contributed to advances in biology at the single-cell level (Andersson and Van den Berg, 2004). The control of fluids and biological materials allowed

1. INTRODUCTION

miniaturizing functions such as cell culture in 3D matrix, sample preparation, material extraction and analysis. Many developments were performed to combine several lab processes in order to get fully functional and autonomous platforms to investigate cellomics, extensively described by Andersson and Van den Berg (2003). Lab-on-a-chip (LOC) is introduced in the 90's to describe microfluidic systems integrating single or multiple laboratory's processes down to the chip format. At the same period, Reyes *et al.* (2002) and Auroux *et al.* (2002) proposed micro-total-analysis-system (μ TAS) as an alternative of the term LOC. The difference between the two terms, LOC and μ TAS, is confused and both are often used indistinctly.

A few technological breakthroughs contributed largely to the fast growth of LOCs. The main breakthrough is a rapid prototyping method for microfluidic systems presented by Duffy *et al.* (1998). Its interest is reflected by the nearly thousand citations in the scientific literature. It consists of casting a polymer - poly(dimethylsiloxane) or (PDMS) - with a silicon-based master prior to its curing. The fabrication of microfluidic components becomes extremely simple and affordable, promoting an intense exploratory research at the early stages of development. Moreover, PDMS is a soft and transparent elastomer and is gas permeable which make it the perfect candidate for working with living organisms. Another relevant development coming from a collaboration between EPFL and IBM and proposed by Lorenz *et al.* (1997) consists of an epoxy-based photoresist, SU-8, that can be directly used as a structural material. In academic research, SU-8 is widely used to create microchannels with height ranging approximately from 1 micrometer to 1 millimeter.

Miniaturization increases the surface to volume ratio and speed up thermal processes like heating/cooling and enables therefore to perform efficient DNA amplification by polymerase chain reaction (PCR) procedure at the LOC format which represents a biological breakthrough (Woolley *et al.*, 1996). Microformat PCR is the basis of integrated analysis genetic microsystems (Lagally and Soh, 2005) for in-vitro diagnostics (IVD) and point-of-care (POC) applications. The use of LOCs in these two fields, referred to as microfluidic diagnostic technology (MDT), are likely to become very important with the personalization or the healthcare monitoring and home-testing for either treating or anticipating disease as thought by Whitesides (2006) and Yager *et al.* (2006). On

the research side and besides genomics (Ramsay, 1998), LOC is expecting to be a key player in the field of drug discovery (Dittrich and Manz, 2006).

1.3 Scope of this thesis

We intend to develop a miniaturized platform capable of separating different cell types. The applications are focused on the medical and the biological fields where the particles are likely to be living cells such as blood cells or other types of cells in suspension (in contrast to adherent cells which would be more complicated to manipulate). In these application fields where throughput and cell sampling are an issue, continuous-flow separation methods are generally preferred to batch methods. Although many continuous-flow separation methods have already been reported, a powerful and flexible integrated label-free technique that can be applied over a large panel of cell types is still lacking. This is our motivation to develop and provide a sorting method that separate various cell types with higher efficiency and resolution than current reported techniques.

Many biological applications of cell manipulation and analysis combine microfluidics with electric fields such as for instance cell counting (Koch *et al.*, 1999), flow cytometry (Gawad *et al.*, 2001) and cell separation (Fiedler *et al.*, 1998 and Gascoyne and Vykokouk, 2002). The electric fields generate forces on living cells that depend on their dielectric properties (intrinsic properties). We propose to separate cell types on a chip by exploiting differences in their response to an AC electric field. The manipulation of individual cells requires tools whose size is comparable to the one of cells. Therefore, this platform has to be produced with microfabrication techniques and must contain an embedded microfluidic network to manipulate cells suspended in a liquid. Basics of microfluidics as well as some particular physical phenomena exclusively occurring at the microscale are introduced in section 1.4 and section 1.5 respectively.

1. INTRODUCTION

1.4 Microfluidics concepts

1.4.1 Handling of liquid

Obviously in microfluidic applications, liquids need to be moved through microchannels. There are three main techniques to manipulate liquids on chips (Stone *et al.*, 2004):

Pressure driven flow The most obvious actuation technique is called pressure-driven flow (PDF). In analogy to electricity, a pressure difference between the inlet and the outlet forces the liquid to flow through the channel. The flow rate and velocity are defined by the fluidic resistance of the channel and the pressure difference. The no-slip condition at the channel's walls induces a parabolic velocity profile, following the Poiseuille's law. The simplest way of getting a PDF is by using a syringe pump that imposes a constant flow rate. A nice alternative, suitable for small-dimension microfluidics, is the control of a single or differential pressure directly applied onto liquid reservoirs. An ingenious pneumatic pressure control for driving fluids in microfluidic networks has been recently proposed by Braschler *et al.* (2007).

Electro-osmotic flow Another actuation method is of electrical nature and called electro-osmotic flow (EOF). It comes from charges located at the surfaces of a channel made of glass for instance. When filled with an electrolytic solution, an accumulation of mobile counter charges occurs in the vicinity of the surfaces for respecting global electrical neutrality. These bulk-solution charges can be moved by applying an electric field along the channel. When moving, charges drag the liquid due to the viscous force, with a flat velocity profile.

Capillarity A liquid can also be moved in a capillary or microchannel due to surface tension which is an energy associated with the surface contact between solid/liquid, solid/gas or liquid/gas. Depending on the materials and physical properties such as hydrophobicity, a liquid could naturally flow until it reaches the microchannel outlet in order to minimize the total system energy.

1.4.2 Handling of particles in liquid

In biological applications, the liquid is usually used for moving and manipulating particles in suspension, like living cells in physiological solution. In a moving liquid, the particles are pulled by a viscous drag force and strictly follow the streamlines, in the absence of other external forces. In the case of PDF, the movement of particles in a microchannel in terms of speed and trajectory is controlled by the pressure difference and the channel geometry. Thus particles can be driven to reaction chambers and integrated detectors for flow-through analysis (Huang *et al.*, 2003 and Breslauer *et al.*, 2006).

In other applications such as concentration, isolation, focusing or sorting, the particles would rather be moved within the liquid than kept in the same streamline all along the fluidic path. This movement requires an additional force as described by Yi *et al.* (2006). The additional force can simply be produced by a mechanical filter structure designed such that liquid can flow through while larger particles are retained (Crowley and Pizziconi, 2005). Umehara *et al.* (2003) used an optical force to trap and move particles in a microfluidic chamber. The optical manipulation is often valued in biological applications since it is a non-contact and contamination-free method. Wiklund *et al.* (2001) and Nilsson *et al.* (2004) opposed an acoustic force to the viscous drag force for concentrating the particles at the nodes of ultrasonic standing waves. Han and Frazier (2004) manipulated particles with magnetophoresis by taking advantages of the native magnetic properties of cells. The last method cited here and certainly the most widely used is of electrical nature; electrophoresis (EP) or dielectrophoresis (DEP). Basically, EP moves charged particles in a uniform electric field and DEP moves polarizable particles in a non-uniform electric field. Further details are found in Morgan and Green (2002) and Jones (1995). Marx *et al.* (1997) and Huang *et al.* (1997) used DEP as a levitating force acting against gravity in combination with a perpendicular PDF to achieve sorting of different particles. This method is referred to as field-flow fractionation (FFF). DEP is also used for focusing or aligning flowing particles prior to analysis in order to increase sensitivity and throughput as presented by Holmes *et al.* (2006).

1.5 Physics of microfluidics

In microfluidics, the standard constructs of classical meter-scaled physics do not always hold true. This divergence is even more emphasized when the dimensions are further downscaled to the nanometer range. In the frame of this thesis, dimensions are typically ranging from tens to hundreds of micrometers and the study of the corresponding physics and characteristic phenomena is therefore limited to this dimension range. It is of great importance to fully understand the physics governing the phenomena occurring at the microscale to address issues in life sciences with the best performances. Beebe *et al.* (2002) said that new designs must be made to take advantage of forces that work at the microscale. Decreasing dimensions l results in an increase of the surface area ($\propto l^2$) to volume ($\propto l^3$) ratio. Effects such as electrostatics and wetting (surface tension) thus dominate volume effects such as inertia or thermal mass. Laminar flow, fluidic resistance and diffusion are other dominant effects of the microfluidics physics.

The main characteristics of microfluidics physics is the quasi permanent laminar regime for the flow of liquids. The viscous forces dominate over the inertial forces and the resulting laminar flow is linear and predictable (Squires and Quake, 2005). The flow regime is characterized by a dimensionless number, the Reynolds number (Re) which depends on the properties of the liquid involved such as viscosity, density and velocity and on a characteristic geometrical dimension. Calculated values lower than 2300, which generally holds true in microfluidics, indicates a regime of laminar flow (in opposition to turbulent flow). In a laminar flow, the streamlines never cross each other. The mixing of confluent liquids is therefore strictly limited to the diffusive process which becomes important when the dimensions are small and induces small diffusive times. By understanding and leveraging microscale phenomena, microfluidics can be used for applications with new functionalities that can only be performed due to the physics specific to the microscale (Beebe *et al.*, 2002).

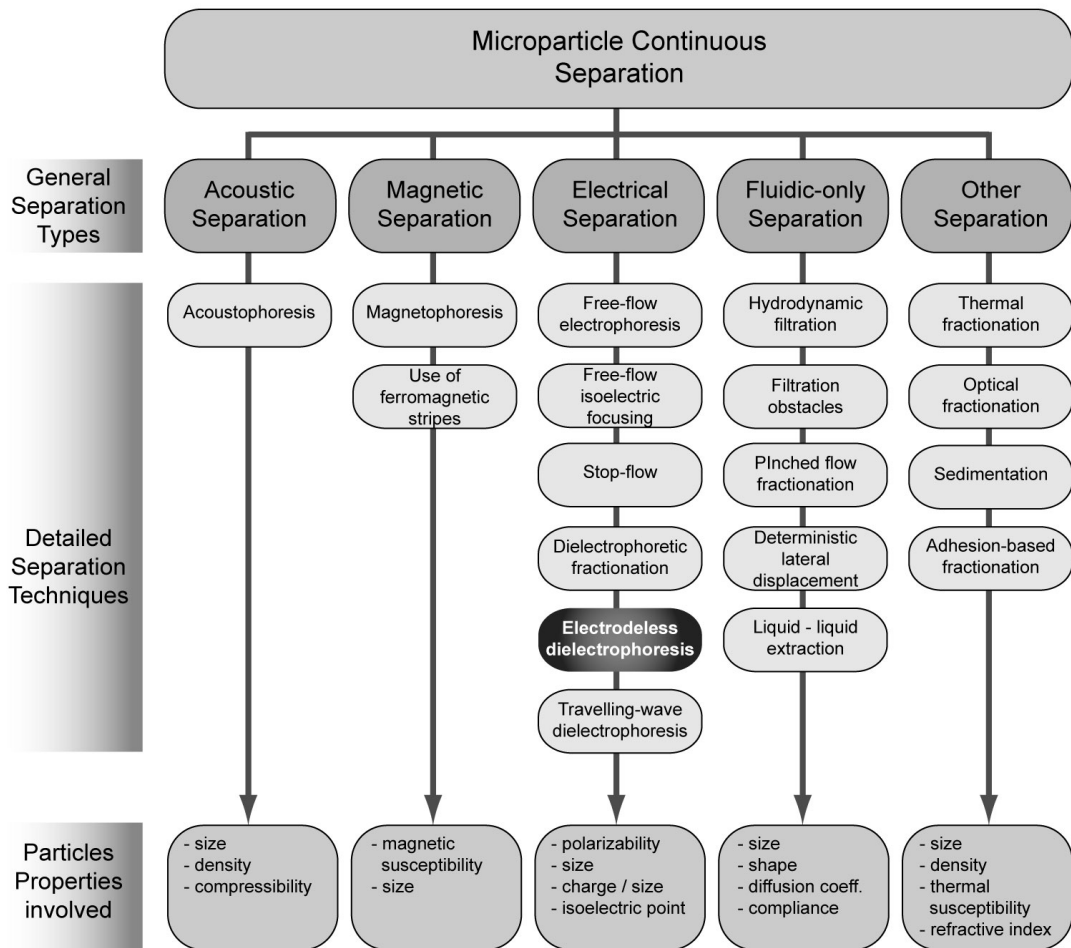


Figure 1.1: Chart summarizing the main methods of continuous-flow separation that are currently encountered in literature. The black box, electrodeless dielectrophoresis, is the principle on which the continuous-flow separation presented in this manuscript is based. *Adapted from Pamme (2007) and Kersaudy-Kerhoas et al. (2008).*

1. INTRODUCTION

1.6 On-chip continuous-flow separation methods

1.6.1 Definition

During the last two decades, numerous miniaturizations of standard chemical and biological lab-procedures on a chip format have proliferated, taking advantage of the physics at the microscale. A fundamental issue of any chemical or biological analysis is the sample preparation which includes the separation of components into homogeneous fractions. The isolation of a particular cell type from a complex biological tissue allows to better characterize its properties and to better understand its interactions with its environment. Biological research at the single cell level benefits from the recent progress in continuous-flow separation on chip. Diagnostics is particularly demanding in separation technology (Kersaudy-Kerhoas *et al.*, 2008). The management of HIV (human immunodeficiency virus) disease - AIDS (acquired immunodeficiency syndrome) - (Rodriguez *et al.*, 2005), cancer and prenatal diagnosis (Bianchi and Hanson, 2006) are relevant examples among numerous others where separation is a key issue in the follow-up of the disorder. In general, integrated sample separation and analysis are potentially less time consuming and less invasive than conventional tests. Pharmaceutical and food industry also require separation techniques to isolate and sample synthesized solid products or to carefully monitor potentially harmful bacterial activity for instance (Yang *et al.*, 2006).

On-chip methods of sorting - or separation - are able to isolate a targeted cell type. The numerous reported sorting methods in literature (some of them are detailed and referenced later in this section) can be classified in two groups according to their operation mode; either in continuous mode or semi-continuous mode, which is made of repetitive cycles of operations such as loading, sorting and sampling. The continuous mode means that the separation is performed in a continuous flow where two or more cell types initially mixed get spatially separated downstream from the separation chamber. In the framework of this thesis, we adopt the precise definition of continuous-flow separation given by Pamme (2007):

"The sample is fed into a separation chamber continuously and subjected to a force at an angle, often perpendicular, to the direction of the flow. The

1.6 On-chip continuous-flow separation methods

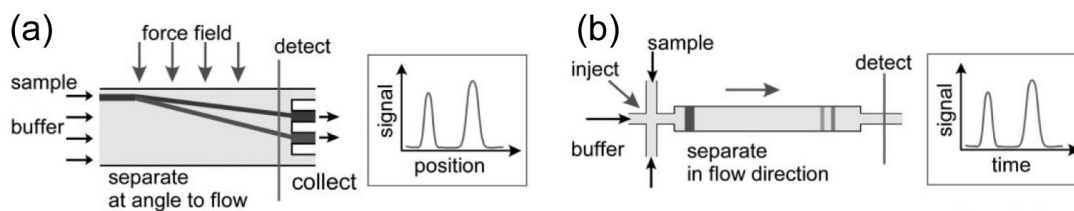


Figure 1.2: Illustration of the typical continuous-flow separation in (a) in opposition to a batch separation procedure in (b). In the continuous-flow separation, the sample is continuously fed into the separation chamber where a force generally acts perpendicular to the flow to laterally (spatially) separate the different species. The separated fractions can be continuously and simultaneously sampled at different channel outlets. In the batch separation or semi-continuous separation, the species are separated in time and are therefore sampled sequentially and not simultaneously in the same channel outlet. *Adapted from Pamme (2007).*

sample components respond differently to this force and are thus deflected from the direction of flow and can be collected at different outlets."

The important aspect in continuous-flow separation is that the components are laterally separated from each other and therefore they can be sampled simultaneously at different positions in the continuous flow or at different outlets when the channel is split into several outlets. This is different from separations where the components are separated in time, such as in chip chromatography, rather than separated in space and need to be sampled sequentially in the similar outlet channel. These aspects are illustrated in the figure 1.2 which was also published by Pamme (2007). The additional force acting on the different species involved in the separation can be of different nature such as acoustic, magnetic and electrical. The different forces are also based on different properties of the particles to separate. Thus for instance, an acoustic force depends on particle properties such as the size, the density and the compressibility while an electrical force depends on the size and the polarizability. The chart in figure 1.1 summarizes the main methods of continuous-flow separation according to the techniques and properties involved.

Characteristics of continuous-flow separations allow them to easily combine with other upstream and downstream functions to address complex issues in the medical and

1. INTRODUCTION

biological fields. They are described in the next section. The manuscript is thereafter essentially focused on the continuous-flow techniques of particle separation. Some techniques of continuous-flow separations are further described in detail in the state-of-the-art section.

1.6.2 Main characteristic features

This section summarizes the main advantages of the continuous-flow separation that make it particularly interesting for LOC applications where they are generally preferred to batch or semi-continuous separations (Pamme, 2007). The sample injection of a continuous-flow separation is simple and avoids the need of accurately control femtoliter volumes. In typical continuous-flow separation the flow velocity can reach a few millimeters per second which is rather easy to obtain and control with PDF. In some separation, flowrate fluctuations are tolerated and thus preserve the performances, which make the technique even more robust regarding the sample injection. Another advantage is the instantaneous estimation of the separation efficiency by observing the output positions of the separated components due to the separation occurs in space rather than in time. Indeed, there is no delay between the adjustment of experimental parameters and the resulting effects on the separation efficiency. This is essential in industrial applications of the separation where the automatic control is based on a feedback loop. The spatial separation allows a simultaneous and continuous sampling of each fractions at different portions of the output channels which provides, in combination with the parallelization, high-throughput performances. Lastly, continuous-flow separation is suitable for integration on chip format and, according to the nature of the separating force, requires light operation setup.

1.6.3 State of the art

There is a large panel of miniaturized cell sorting methods based on different physical properties of the components to be sorted like DNA, proteins, microorganisms and single cells, which are our focus. Many methods and corresponding cell properties are listed in reviews published by Pamme (2007), Gascoyne and Vykoukal (2002) and Hughes (2002) and are summarized in the chart of figure 1.1. There are two approaches of miniaturized cell sorting. One option is to first measure a property of the cells

1.6 On-chip continuous-flow separation methods

and then sort them based on the results obtained. Using this approach, fluorescence-activated cell sorting (FACS) (Wolff *et al.*, 2003) and dielectric-activated cell sorting (DACS) (Cheung *et al.*, 2005) have been integrated on chip. The other possibility is to use forces that act directly on the cells which means that the sorting is performed without prior measurement. We focus on this second approach because it is potentially simpler, making it more attractive for point-of-care devices.

1.6.3.1 Acoustic separation

Acoustic-based separation are performed using forces that are generated from ultrasonic waves. The movement imparted on cells and due to the acoustic force is called acoustophoresis. The generation of the acoustic force requires a specific channel design as resonator to establish and maintain a standing wave. The trapping sites correspond to the nodes and antinodes of the standing wave. According to cell properties such as size, density and compressibility, the cells that flow in the separation chamber are subjected to an acoustic force and migrate either towards the nodes or towards the antinodes. For example, Laurell *et al.* (2007) spatially controlled the size-dependent positioning of particles in a flow by utilizing forces that were generated by an acoustic standing-wave (figure 1.3b) to separate blood cells from lipids. Another integration of acoustic separation was presented by Wiklund *et al.* (2001). They reported on a size-selective separation of microspheres in small-diameter capillaries by creating traps from a longitudinal and hemispherical ultrasonic standing-wave that retained the larger particles. The fraction at the channel outlet is a homogeneous population of the smaller particles.

The integration of continuous-flow cell sorting based on acoustic forces requires the use of an external element such as piezoelectric transducers in combination with a resonating cavity to generate the standing wave. The positions and numbers of trapping sites (nodes and anti-nodes) are determined by the frequency of the standing wave by the geometry of the separation chamber. Trapping positions across the output channel can therefore only be tuned at a finite number of discrete positions.

1. INTRODUCTION

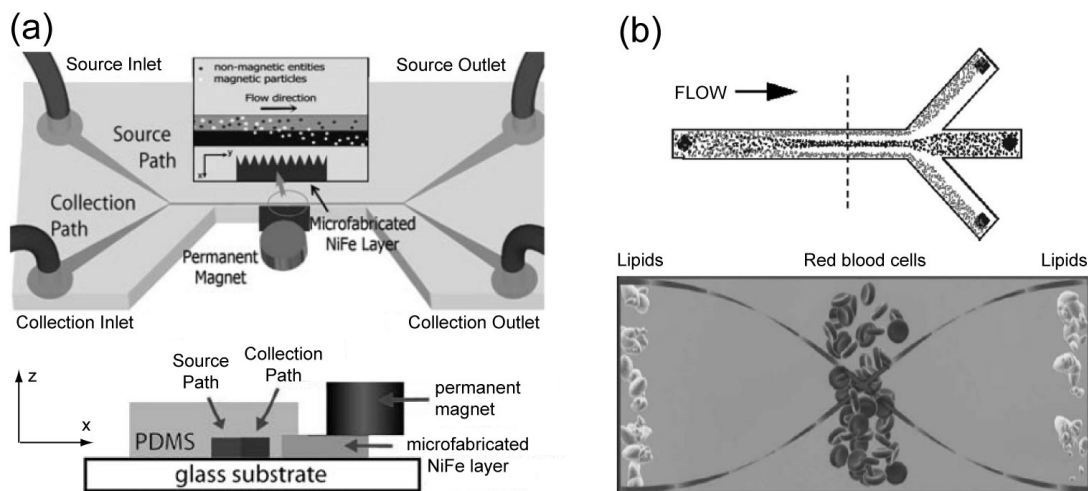


Figure 1.3: (a) Scheme of the mixed micromagnetic and microfluidic separation device that contains a microfabricated layer of soft magnetic material (NiFe) adjacent to a microfluidic channel. *Adapted from Xia et al. (2006)*. (b) Cross-section of channel with erythrocytes and lipid particles. When the ultrasound is turned on the two particle types are separated. *Adapted from Petersson et al. (2005)*.

1.6.3.2 Magnetic separation

Magnetic forces can also be used to move cells that flow in a separation chamber. The straightforward method to separate particles with magnetism is to position a permanent magnet aside a main channel that exerts a force on the flowing cells according to their native magnetic properties and size. It is usual in magnetic-based separation that the particles are labeled with magnetic tags if the native magnetic properties are too weak. This method is called magnetic-activated cell sorting (MACS) or magnetophoresis. Examples have been presented by Smistrup *et al.* (2005) and Xia *et al.* (2006) (figure 1.3a) to extract *E. coli* bacteria from red blood cells (RBCs).

Magnetic forces based on the native magnetic properties of living cells are generally weak. The use of labels is often required to increase the separation efficiency. The separation becomes subsequently more mediated by biochemistry or surface chemistry rather than intrinsic cell properties.

1.6.3.3 Fluidic-only separation

Cell properties such as size, shape and compliance have also been used for on-chip cell sorting based on geometries and flow profiles and hydrodynamic forces in the separation chamber. The fluidic-only separation are often called filtration methods (like the hydrodynamic filtration presented by Yamada and Seki (2005)). Generally based on the particles size, the fluidic-only separations are easy to operate and avoid the need of an external setup to generate an additional force such as acoustic, magnetic or electrical force. For instance, the diffusive filter presented by Sethu *et al.* (2006) (figure 1.4a) makes use of micro sieves that exploit the size and shape difference between the cell types to remove leukocytes from whole blood. Huang *et al.* (2004) reported on another system design that uses an asymmetric bifurcation of laminar flow around obstacles, which induces deterministic displacement that can be used for sorting particles based on their size. The device proposed by Yamada *et al.* (2004) and represented in figure 1.4b performs a size-based separation of particles in a pinched flow by constraining two confluent laminar flows. This ingenious technique allows the separation and isolation of several populations that have a specific size range and not only the isolation or extraction of the smallest or largest particles like in a basic filtration process.

1.6.3.4 Adhesion-based separation

The group of sorting methods mediated by the specific adhesion between the flowing cells and functionalized surfaces finds application in biological research. The cells that present a good affinity to the functionalized surface are slowed down, trapped or deviated while the cells without particular surface affinity continue flowing without disturbances. This provides the separation of the species based on physiological properties of the cells such as surface proteins. The adhesion-based separation allow for example to mimic physiological phenomena occurring in vessels. Such a separation has been used by Chang *et al.* (2005) to investigate the physiological process of leukocyte recruitment to blood vessel walls. A structure with functionalized pillars in a microchannel has been reported by Nagrath *et al.* (2007) to isolate rare circulating tumor cells. The separation in the microfluidic device was mediated by interactions of target cells with antibodies attached to microposts.

1. INTRODUCTION

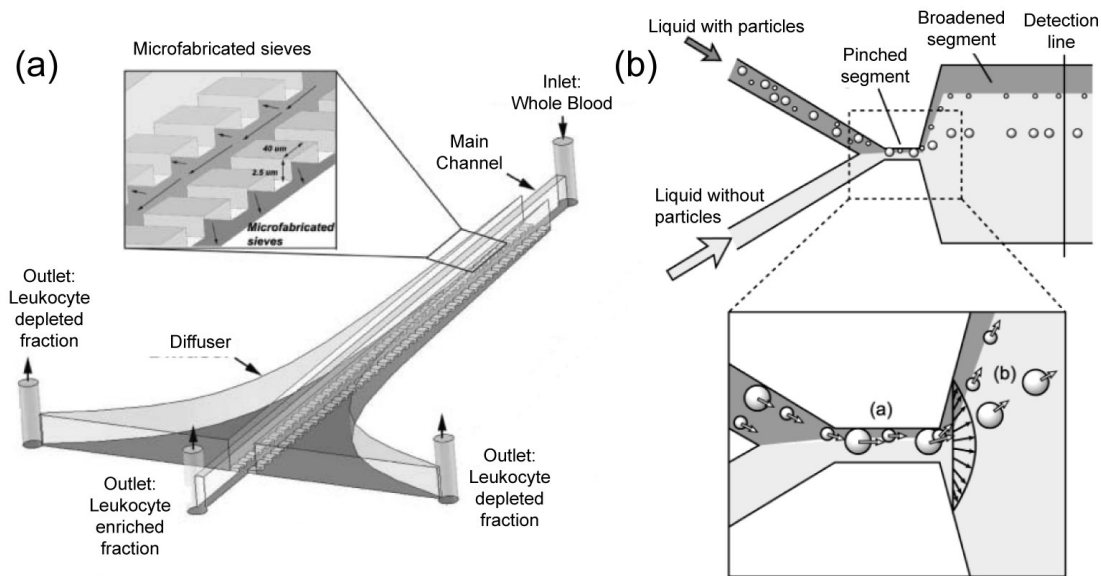


Figure 1.4: (a) Scheme of the diffusive filter for size based continuous-flow fractionation of erythrocytes from whole blood. *Adapted from Sethu et al. (2006).* (b) Principle of pinched flow fractionation. Particles are separated according to their sizes by the spreading flow profile at the boundary of the pinched and the broadened segments. *Adapted from Yamada et al. (2004).*

Although only a few adhesion-based separations in continuous-flow have been reported so far, they have the potential to address real biological problems and to characterize processes by reproducing nearly real physiological conditions.

1.6.3.5 Electrical separation

The last approach described here and probably the most popular one takes advantage of cell dielectric properties. From an electrical point of view, a cell can be described by an equivalent model containing a network of resistances and capacitances. It is an object with its own permittivity and conductivity which are indeed the dielectric properties of the cell. Sorting based on dielectric properties makes use of dielectrophoresis (DEP) (Hughes, 2002, Gascoyne and Vykoukal, 2002). Dielectrophoresis is a phenomenon in which a force is exerted on a dielectric particle when this latter is subjected to a non-uniform electric. First publications on DEP date back to 1951 and 1958 by Pohl.

1.6 On-chip continuous-flow separation methods

Readers can refer to a few books for a detailed description of the DEP phenomenology and theory (Pohl, 1978, Jones, 1995, Morgan and Green, 2002). The dielectrophoretic force (DEP-force) can move cells in a liquid due to the interaction between a polarizable particle and a non-uniform electric field. The phenomenon is called negative dielectrophoresis (nDEP) when the force repel the particles from regions of high electric-field strength. Inversely, it is called positive dielectrophoresis (pDEP) when the force attract the particles towards regions of high electric-field strength. DEP-based manipulations are non-invasive and prevent cell damage when limited to reasonable electric-field strengths (Pethig (1996) reported on cells that were cultured after DEP manipulations). The next sections describe some among the numerous DEP-based cell-sorting methods that are classified in four groups for the sake of clarity.

Stop-flow fractionation The first group of techniques consists of a separation chamber with an electrode array on the bottom which produces nDEP on a cell type that continues flowing while another cell type is trapped by attractive pDEP. Technically speaking, these sorting methods are generally performed in a semi-continuous mode. Nevertheless, there are often defined in literature as continuous-flow separation, in particular when the trapped population is out of interest. Thus, the injection and the sampling of the population of interest are considered continuous. A common design to produce well defined trapping sites are interdigitated electrodes of inverse polarities as well as castellation of electrodes (Markx and Pethig, 1995, Talary *et al.*, 1995). Flow separator devices have been demonstrated to be effective for sorting cancer cells (Gascoyne *et al.*, 1997), blood cells (Borgatti *et al.*, 2005) and yeast cells (Markx *et al.*, 1994). A similar principle has been presented by Fiedler *et al.* (1998), but with electrodes on the top and the bottom of a channel to produce 3D trapping cages. A similar method was presented by Yu *et al.* (2007) to separate viable and nonviable yeast cells using 3D silicon electrodes.

Dielectrophoretic fractionation Methods of dielectrophoretic fractionations could themselves be classified in different subgroups. One of these subgroup, called field-flow fractionation (FFF), includes sorting methods where a nDEP generated by a planar electrode array is used in combination with a PDF (Huang *et al.*, 1997, Markx *et al.*, 1997, Muller *et al.*, 2000). The nDEP acts horizontally as a levitation force against

1. INTRODUCTION

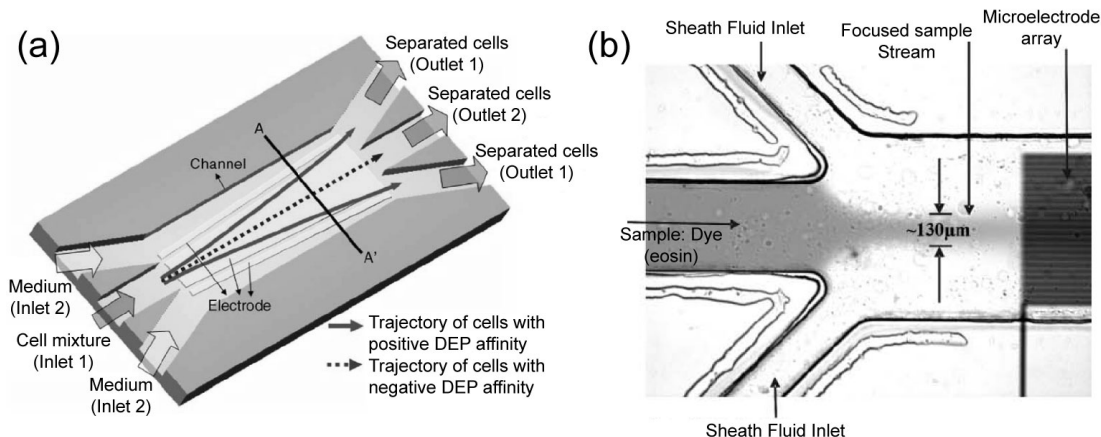


Figure 1.5: (a) Conceptual view of the hydrodynamic dielectrophoresis (DEP) process that continuously separate cell types with nDEP affinity to cell types with pDEP affinity. *Adapted from Doh and Cho (2005)*. (b) Image of the cell injector region, showing hydrodynamic focusing of the sample (eosin dye) by the support sheath flow. *Adapted from Li et al. (2007)*.

gravity and distributes cells in the parabolic velocity profile according to size and dielectric properties. The semi-continuous separation is achieved from the distribution of cell velocities and is therefore time-dependent. Fractionations of bioparticles including beads, bacteria and cancer cells have been reported.

Besides FFF, other methods of dielectrophoretic fractionation were reported to continuously separate cell types. For example, Kralj *et al.* (2006) proposed an interdigitated electrode array on the bottom of the chamber for continuously sorting cells. Their size-based separation is obtained from the differences in the nDEP amplitudes that are imparted on the different cell types. Although the separation method is continuous, focusing of the cells before separation is still required due to the influence of the initial positions of the cells (upstream from the separation chamber) to their output positions (downstream from the separation chamber). The flow separators presented by Doh and Cho (2005) (figure 1.5a) and Li *et al.* (2007) continuously sort viable and nonviable yeast cells by using an appropriate design of planar electrodes but still with the similar need of cell focusing prior to the separation.

In opposition to stop-flow fractionation presented above, these methods of dielectrophoretic fractionation allow to continuously separate species based on their dielectric properties. In that sense, they fit to the definition given in section 1.6.1. Their main drawback is the dependencies on the flow velocity and on the initial positions of the cells that require a focusing of the cells before the separation (an example of cell focusing using a sheath flow is shown in figure 1.5b).

Electrodeless dielectrophoresis The following group of techniques uses insulating obstacles along the path of an electric field to create regions of high and low field strengths, *i.e.* a non-uniform electric field. The obstacles squeeze the field lines and generate locally either pDEP to trap bioparticles or nDEP to repel them from these regions. The metal electrodes that generate the electric field can be located apart from the separation chamber. This principle is called "electrodeless dielectrophoresis" (eDEP) (Chou and Zenhausern, 2003, Masuda *et al.*, 1989) or "insulator-based dielectrophoresis" (iDEP). Barrett *et al.* (2005) and Kang *et al.* (2006) reported on continuous cell sorting with obstacles such as constriction and ridges respectively. Arrays of posts were used by Lapizco-Encinas *et al.* (2004) to separate live and dead bacteria. In his work, Zhang *et al.* (2006) replaced obstacles with a circular channel that favors the field lines to flow at the circle interior of the circle where the path is the shortest. A controllable separation of particles with different sizes was obtained by Barbulovic-Nad *et al.* (2006) by using a moveable droplet of oil as insulator.

Traveling-wave dielectrophoresis This group of techniques make use of a set of four electrical signals at the same frequency but at different phases to produce multiple dielectrophoresis. The set of electrical signals with phase shifts (generally 0° , 90° , 180° and 270°) is distributed to a planar electrode array and generates a traveling-wave dielectrophoresis (twDEP) in a channel. In a classical use of twDEP, the traveling wave moves trapping cages where are accumulated particles due to either nDEP or pDEP. By moving the trapping sites, twDEP also moves the captured particles along or across a separation chamber (Talary *et al.*, 1996, Morgan *et al.*, 1997). This technique is continuous even though the spatial separation remains time-dependant in the sense that the cells would move as long as they are in the separation chamber. Again, a better

1. INTRODUCTION

control of the spatial separation would require a prior step of particle focusing. Several electrical separation methods are sometimes combined to achieve a better separation efficiency. One example is presented by De Gasperis *et al.* (1999) where FFF and twDEP were associated in an application of 2-dimensional DEP-based cell separation.

1.6.4 Discussion

This section discusses the possibilities but also the major limitations of the DEP-based sorting methods. The separations based on electrical forces (DEP) are, in our opinion, one of the most appropriate techniques for the on-chip integration and control of a continuous-flow separation of cells. A few electrical methods presented in the previous sections are evaluated regarding quality factors such as throughput and selectivity. The choice of a method based on a continuous mode of operation definitely favors applications where the throughput and the recovering of multiple sub-populations are an issue.

Among the continuous-flow sorting methods based on DEP, many of them separate particles according to their size. This is limiting factor when working with living biological materials such as cells where size dispersion is an intrinsic characteristic of each cell population and changes over time. Hence, separations of cancerous cells, infected cells or nonviable cells, which present no significant changes in size, become challenging and is lacking selectivity. A good example of high-throughput continuous cell sorting is the one presented by Doh and Cho (2005) (refer to previous section and figure 1.5a). However, their method requires a fine tuning between the viscous drag force and the DEP-force to avoid sticking cells that undergo pDEP to the bottom electrodes. This would affect or damage the cells and eventually produce cell lysis. In addition, their separation is only based on the duality of nDEP and pDEP, *i.e.* one cell type present nDEP affinity while the another cell type present pDEP affinity for the same dielectrophoretic signal (same frequency of the electric field). This means that two different cell types, but presenting both nDEP or pDEP affinity, would not get separated. This characteristic of the separation method constrains the choice of experimental parameters and limits the cell types that could eventually be sorted. Another limitation comes from the time span that the particles to be sorted spent in the separation chamber. Indeed, this time span directly influences the spatial separation in many continuous-flow

separation methods. This is the reason why a focusing is often required to increase the separation efficiency, as well as a good control of the flow velocity.

In summary, DEP-based methods are suitable and potentially powerful for the integration on chip of a continuous-flow separation. However, the field is still lacking a universal method providing high throughput and high selectivity over a large frequency spectrum and over a large panel of cell types.

1.7 Research Strategy

1.7.1 Motivations

Our intention is to develop a continuous separation method that circumvents some of the major drawbacks highlighted above. In order to increase the performances of conventional reported methods in particular in term of flexibility, the method should be sensitive enough to separate cell types with tiny differences coming from various morphological or physiological changes. These differences could be for instance induced by the presence of a parasite inside the cells as well as differences in size, shape and internal arrangement of the cells, in particular during their cell cycle. To be optimal, the sorting method should avoid the need of a pre-focusing. This can be reached by limiting the dependency on the residence time of the cells in the separation chamber.

In this present research, dielectrophoresis has been selected as the separation principle. DEP-based separation techniques offer many advantages (refer to section 1.6.4) and are suitable for lab-on-a-chip applications in the biological and medical fields (Pethig and Markx, 1997). Moreover, DEP-based manipulation of cells on chip belongs to the core activities pursued in the Microsystem Laboratory of EPFL¹. For example, DEP has been previously used in microfluidic applications of flow cytometry by Gawad *et al.* (2001) and cell dipping by Seger *et al.* (2004). Furthermore, DEP-based separation methods require a standard technology of inexpensive and well established microfabrication processes. They are easily interfaced to conventional electronics and fluidic control (*e.g.* syringe pumps or a pressure box as proposed by Braschler *et al.*, 2007) to

¹lmis4.epfl.ch

1. INTRODUCTION

drive the electrical signals and the liquids respectively. DEP can discriminate between cells on the basis of physical or biochemical phenomena occurring inside the cells or at the cell surfaces in a non-invasive manner. Thus, a rich set of cell properties can be assessed to provide discriminating factors for the separation. Finally, DEP sorting does not usually require any cell modification or labeling and a high throughput is provided by the simultaneous manipulation of numerous cells.

1.7.2 Main objectives

The main objective of this thesis is the development of a novel integrated method of continuous-flow cell separation that addresses in priority the following issues:

- The selectivity of the separation method, or the discrimination between cell types, has to be improved and extended over a larger frequency spectrum. On the contrary of typical reported DEP-based method, our method should allow to separate two or several cells types that present the same DEP affinity (either nDEP or pDEP but at different strengths).
- We propose to replace the unique DEP-force at a single frequency often reported in literature by using electrical signals at multiple frequencies in order to improve the resolution and efficiency of the separation. This would generate a set of DEP-forces that could be potentially more sensitive to small changes in the frequency responses of different cell types. The method would be therefore applicable to a wider panel of biological separations of cell types.
- In some application where differences between cell types are small, the separation technique resorts to a cell labeling to increase the differences. However, a label-free separation technique preserves the cell physiology, prevents any modifications of sensitive biological materials and avoid a laborious sample preparation. The objective is to avoid the need of labels by improving the sensitivity of the separation method.
- The technology involved in the microfabrication of the device should be the simplest possible to assure reliability and repeatability of the chip production. In this direction, the technology previously described by Gawad *et al.* (2001) should

be replaced by a planar technology. A planar technology offers flexibility and prevent the alignment between the top and the bottom microelectrodes.

- Microelectrodes should be replaced by larger electrodes to improve the robustness of the separation and to extend the frequency range of operation due to the higher interfacial capacitance of the larger metal electrodes.

Our strategy is the miniaturization of a continuous-flow cell separation method in a microfluidic platform. The method uses electrical forces to separate cell types according to their intrinsic dielectric properties. The design of the microchip is a combination of few technological concepts and based on numerical modeling. First experiments run with well known material such as plastic beads serve as calibration of the chip and validation of the method before addressing real biological problems. By improving the resolution of the separation and the ease-of-use, our method could likely be applied to various research fields such as for example food engineering, fundamental biology, parasitology and diagnostics. We expect that advantages such as ease-of-use, efficiency and high-throughput would encourage physicians to use our sorting method in daily analysis.

1.8 Thesis structure

The dissertation is divided into six chapters. In chapter 1 is given a general introduction on microfluidics and lab-on-a-chips. The report is then focused on miniaturized continuous-flow separation methods and presents the state-of-the-art of the field. The main objectives of this thesis research are described at the end of this present chapter. Chapter 2 is dedicated to the theory of dielectrophoresis and to the modeling of the biological materials that are used in this research. Concepts of equilibrium, of opposition of two DEP-force fields and of multiple-frequency dielectrophoresis are introduced then. Chapter 3 deals with the presentation of the microfluidic platform in which the separation method is integrated. The "liquid electrode" is also described as well as the microfabrication procedure of its integration in the microfluidic platform. The first manipulations of particles in the microfluidic platform and based on dielectrophoresis are presented in chapter 4. They consist of first only deviating a stream of cells that flows through a central channel and then focusing it towards a controllable position

1. INTRODUCTION

across the central channel. Basics of dielectric characterization are finally described in this chapter. By considering the theory about multiple-frequency dielectrophoresis and the principle of equilibrium, the positions of the particles downstream from the separation chamber can be related their dielectric properties. Chapter 5 reports on the main achievements in the biological field obtained with our method. Besides applications of cell separation, biological issues such as the increase of an infection rate in a cell culture or the synchronization of a cell culture are addressed based on multiple-frequency dielectrophoresis. The main achievements in terms of technology, concepts and obviously applications are summarized in chapter 6 which is the conclusion of this thesis. Our work is compared to the state-of-the-art to show the contribution to knowledge. The last part of the manuscript is dedicated to perspectives with a particular emphasis on a few promising lab-on-a-chip applications in which our method could add value.

Bibliography

- Andersson H and Van den Berg A, 2003: *Microfluidic devices for cellomics: A review*. Sensors and Actuators, B: Chemical, *vol. 92*(3): 315–325.
- Andersson H and Van den Berg A, 2004: *Microtechnologies and nanotechnologies for single-cell analysis*. Current Opinion in Biotechnology, *vol. 15*(1): 44–49.
- Auroux PA, Iossifidis D, Reyes D and Manz A, 2002: *Micro total analysis systems. 2. Analytical standard operations and applications*. Analytical Chemistry, *vol. 74*(12): 2637–2652.
- Barbulovic-Nad I, Xuan X, Lee J and Li D, 2006: *DC-dielectrophoretic separation of microparticles using an oil droplet obstacle*. Lab on a Chip - Miniaturisation for Chemistry and Biology, *vol. 6*(2): 274–279.
- Barrett L, Skulan A, Singh A, Cummings E and Fiechtner G, 2005: *Dielectrophoretic manipulation of particles and cells using insulating ridges in faceted prism microchannels*. Analytical Chemistry, *vol. 77*(21): 6798–6804.
- Bassous E, Taub HH and Kuhn L, 1977: *Ink jet printing nozzle arrays etched in silicon*. Appl Phys Lett, *vol. 31*(2): 135–137.
- Beebe D, Mensing G and Walker G, 2002: *Physics and applications of microfluidics in biology*. Annual Review of Biomedical Engineering, *vol. 4*: 261–286.
- Bianchi D and Hanson J, 2006: *Sharpening the Tools: A summary of a National Institutes of Health workshop on new technologies for detection of fetal cells in maternal blood for early prenatal diagnosis*. Journal of Maternal-Fetal and Neonatal Medicine, *vol. 19*(4): 199–207.

BIBLIOGRAPHY

- Borgatti M, Altomare L, Baruffa M, Fabbri E, Breveglieri G, Feriotto G, Manaresi N, Medoro G, Romani A, Tartagni M, Gambari R and Guerrieri R, 2005: *Separation of white blood cells from erythrocytes on a dielectrophoresis (DEP) based 'Lab-on-a-chip' device*. International journal of molecular medicine, vol. 15(6): 913–920.
- Braschler T, Metref L, Zvitov-Marabi R, Van Lintel H, Demierre N, Theytaz J and Renaud P, 2007: *A simple pneumatic setup for driving microfluidics*. Lab on a Chip - Miniaturisation for Chemistry and Biology, vol. 7(4): 420–422.
- Breslauer D, Lee P and Lee L, 2006: *Microfluidics-based systems biology*. Molecular BioSystems, vol. 2(2): 97–112.
- Chang WC, Lee LP and Liepmann D, 2005: *Biomimetic technique for adhesion-based collection and separation of cells in a microfluidic channel*. Lab on a Chip - Miniaturisation for Chemistry and Biology, vol. 5(1): 64–73.
- Cheung K, Gawad S and Renaud P, 2005: *Impedance spectroscopy flow cytometry: On-chip label-free cell differentiation*. Cytometry Part A, vol. 65A(2): 124–132.
- Chou CF and Zenhausern F, 2003: *Electrodeless Dielectrophoresis for Micro Total Analysis Systems*. IEEE Engineering in Medicine and Biology Magazine, vol. 22(6): 62–67.
- Crowley T and Pizziconi V, 2005: *Isolation of plasma from whole blood using planar microfilters for lab-on-a-chip applications*. Lab on a Chip - Miniaturisation for Chemistry and Biology, vol. 5(9): 922–929.
- Daw R and Finkelstein J, 2006: *Lab on a chip*. Nature, vol. 442(7101): 367–367.
- De Gasperis G, Yang J, Becker FF, Gascoyne PRC and Wang XB, 1999: *Microfluidic Cell Separation by 2-dimensional Dielectrophoresis*. Biomedical Microdevices, vol. 2(1): 41–49.
- Dittrich P and Manz A, 2006: *Lab-on-a-chip: Microfluidics in drug discovery*. Nature Reviews Drug Discovery, vol. 5(3): 210–218.
- Doh I and Cho YH, 2005: *A continuous cell separation chip using hydrodynamic dielectrophoresis (DEP) process*. Sensors And Actuators A-Physical, vol. 121(1): 59–65.

- Duffy D, McDonald J, Schueller O and Whitesides G, 1998: *Rapid prototyping of microfluidic systems in poly(dimethylsiloxane)*. Analytical Chemistry, vol. 70(23): 4974–4984.
- El-Ali J, Sorger P and Jensen K, 2006: *Cells on chips*. Nature, vol. 442(7101): 403–411.
- Feynman RP, 1992: *There's plenty of room at the bottom*. Journal of Microelectromechanical Systems, vol. 1(1): 60–66.
- Fiedler S, Shirley S, Schnelle T and Fuhr G, 1998: *Dielectrophoretic Sorting of Particles and Cells in a Microsystem*. Analytical Chemistry, vol. 70(9): 1909–1915.
- Gascoyne P and Vykoukal J, 2002: *Particle separation by dielectrophoresis*. Electrophoresis, vol. 23(13): 1973–1983.
- Gascoyne PRC, Wang XB, Huang Y and Becker FF, 1997: *Dielectrophoretic separation of cancer cells from blood*. Ieee Transactions On Industry Applications, vol. 33(3): 670–678.
- Gawad S, Schild L and Renaud P, 2001: *Micromachined impedance spectroscopy flow cytometer for cell analysis and particle sizing*. Lab on a Chip - Minituarisation for Chemistry and Biology, vol. 1(1): 76–82.
- Gravesen P, Branebjerg J and Jensen O, 1993: *Microfluidics - A review*. Journal of Micromechanics and Microengineering, vol. 3(4): 168–182.
- Han KH and Frazier AB, 2004: *Continuous magnetophoretic separation of blood cells in microdevice format*. J Appl Phys, vol. 96(10): 5797–5802.
- Holmes D, Morgan H and Green N, 2006: *High throughput particle analysis: Combining dielectrophoretic particle focussing with confocal optical detection*. Biosensors and Bioelectronics, vol. 21(8): 1621–1630.
- Huang LR, Cox EC, Austin RH and Sturm JC, 2004: *Continuous Particle Separation Through Deterministic Lateral Displacement*. Science, vol. 304(5673): 987–990.
- Huang Y, Wang XB, Becker FF and Gascoyne PRC, 1997: *Introducing dielectrophoresis as a new force field for field-flow fractionation*. Biophysical Journal, vol. 73(2): 1118–1129.

BIBLIOGRAPHY

- Huang Y, Chen N, Borninski J and Rubinsky B, 2003: *A novel microfluidic cell-chip for single cell analysis and manipulation*. Proceedings of the IEEE Micro Electro Mechanical Systems (MEMS), pp. 403–406.
- Hughes M, 2002: *Strategies for dielectrophoretic separation in laboratory-on-a-chip systems*. Electrophoresis, vol. 23(16): 2569–2582.
- Johnson R and Higashi R, 1987: *Highly sensitive silicon chip microtransducer for air flow and differential pressure sensing*. Sensors and actuators, vol. 11(1): 63–72.
- Jones TB, 1995: *Electromagnetics of Particles* (Cambridge University Press, Cambridge).
- Kang K, Kang Y, Xuan X and Li D, 2006: *Continuous separation of microparticles by size with direct current-dielectrophoresis*. Electrophoresis, vol. 27(3): 694–702.
- Kersaudy-Kerhoas M, Kersaudy-Kerhoas M, Dhariwal R and Desmulliez M, 2008: *Recent advances in microparticle continuous separation*. Nanobiotechnology, IET, vol. 2(1): 1–13.
- Koch M, Evans A and Brunnschweiler A, 1999: *Design and fabrication of a micromachined Coulter counter*. Journal of Micromechanics and Microengineering, vol. 9(2): 159–161.
- Kralj J, Lis M, Schmidt M and Jensen K, 2006: *Continuous dielectrophoretic size-based particle sorting*. Analytical Chemistry, vol. 78(14): 5019–5025.
- Lagally E and Soh H, 2005: *Integrated genetic analysis microsystems*. Critical Reviews in Solid State and Materials Sciences, vol. 30(4): 207–233.
- Lapizco-Encinas B, Simmons B, Cummings E and Fintschenko Y, 2004: *Dielectrophoretic Concentration and Separation of Live and Dead Bacteria in an Array of Insulators*. Analytical Chemistry, vol. 76(6): 1571–1579.
- Laurell T, Petersson F and Nilsson A, 2007: *Chip integrated strategies for acoustic separation and manipulation of cells and particles*. Chemical Society Reviews, vol. 36(3): 492–506.

- Li YL, Dalton C, Crabtree HJ, Nilsson G and Kaler K, 2007: *Continuous dielectrophoretic cell separation microfluidic device*. Lab on a Chip - Miniaturisation for Chemistry and Biology, vol. 7(2): 239–248.
- Lorenz H, Despont M, Fahrni N, LaBianca N, Renaud P and Vettiger P, 1997: *SU-8: A low-cost negative resist for MEMS*. Journal of Micromechanics and Microengineering, vol. 7(3): 121–124.
- Madou MJ, 2002: *Fundamentals of microfabrication* (CRC Press).
- Markx G, Pethig R and Rousselet J, 1997: *The dielectrophoretic levitation of latex beads, with reference to field-flow fractionation*. Journal of Physics D: Applied Physics, vol. 30(17): 2470–2477.
- Markx GH and Pethig R, 1995: *Dielectrophoretic separation of cells: Continuous separation*. Biotechnology and Bioengineering, vol. 45(4): 337–343.
- Markx GH, Talary MS and Pethig R, 1994: *Separation of viable and non-viable yeast using dielectrophoresis*. Journal of Biotechnology, vol. 32(1): 29–37.
- Masuda S, Washizu M and Nanba T, 1989: *Novel method of cell fusion in field constriction area in fluid integrated circuit*. IEEE Transactions on Industry Applications, vol. 25(4): 732–737.
- Morgan H and Green NG, 2002: *AC Electrokinetics: Colloids and Nanoparticles* (Research Studies Press, Baldock, Hertfordshire, UK).
- Morgan H, Green NG, Hughes MP, Monaghan W and Tan TC, 1997: *Large-area travelling-wave dielectrophoresis particle separator*. Journal Of Micromechanics And Microengineering, vol. 7(2): 65–70.
- Muller T, Schnelle T, Gradl G, Shirley SG and Fuhr G, 2000: *Microdevice for cell and particle separation using dielectrophoretic field-flow fractionation*. Journal Of Liquid Chromatography & Related Technologies, vol. 23(1): 47–59.
- Nagrath S, Sequist LV, Maheswaran S, Bell DW, Irimia D, Ulkus L, Smith MR, Kwak EL, Digumarthy S, Muzikansky A, Ryan P, Balis UJ, Tompkins RG, Haber DA and Toner M, 2007: *Isolation of rare circulating tumour cells in cancer patients by microchip technology*. Nature, vol. 450(7173): 1235–1239.

BIBLIOGRAPHY

- Nilsson A, Petersson F, Jonsson H and Laurell T, 2004: *Acoustic control of suspended particles in micro fluidic chips*. Lab on a Chip - Miniaturisation for Chemistry and Biology, vol. 4(2): 131–135.
- Pamme N, 2007: *Continuous flow separations in microfluidic devices*. Lab on a Chip - Miniaturisation for Chemistry and Biology, vol. 7(12): 1644–1659.
- Petersson F, Nilsson A, Holm C, Jonsson H and Laurell T, 2005: *Continuous separation of lipid particles from erythrocytes by means of laminar flow and acoustic standing wave forces*. Lab on a Chip - Miniaturisation for Chemistry and Biology, vol. 5(1): 20–22.
- Pethig R, 1996: *Dielectrophoresis: Using inhomogeneous AC electrical fields to separate and manipulate cells*. Critical Reviews in Biotechnology, vol. 16(4): 331–348.
- Pethig R and Markx G, 1997: *Applications of dielectrophoresis in biotechnology*. Trends in Biotechnology, vol. 15(10): 426–432.
- Pohl H, 1951: *The motion and precipitation of suspensoids in divergent electric fields*. Journal of Applied Physics, vol. 22(7): 869–871.
- Pohl H, 1958: *Some effects of nonuniform fields on dielectrics*. Journal of Applied Physics, vol. 29(8): 1182–1188.
- Pohl HA, 1978: *Dielectrophoresis* (Cambridge University Press, London).
- Ramsay G, 1998: *DNA chips: State-of-the art*. Nature Biotechnology, vol. 16(1): 40–44.
- Reyes D, Iossifidis D, Auroux PA and Manz A, 2002: *Micro total analysis systems. 1. Introduction, theory, and technology*. Analytical Chemistry, vol. 74(12): 2623–2636.
- Rodriguez W, Christodoulides N, Floriano P, Graham S, Mohanty S, Dixon M, Hsiang M, Peter T, Zavahir S, Thior I, Romanovicz D, Bernard B, Goodey A, Walker B and McDevitt J, 2005: *A microchip CD4 counting method for HIV monitoring in resource-poor settings*. PLoS Medicine, vol. 2(7): 0663–0672.

- Seger U, Gawad S, Johann R, Bertsch A and Renaud P, 2004: *Cell immersion and cell dipping in microfluidic devices*. Lab on a Chip - Miniaturisation for Chemistry and Biology, vol. 4(2): 148–151.
- Sethu P, Sin A and Toner M, 2006: *Microfluidic diffusive filter for apheresis (leukapheresis)*. Lab on a Chip - Miniaturisation for Chemistry and Biology, vol. 6(1): 83–89.
- Smistrup K, Hansen O, Bruus H and Hansen M, 2005: *Magnetic separation in microfluidic systems using microfabricated electromagnets - Experiments and simulations*. Journal of Magnetism and Magnetic Materials, vol. 293(1): 597–604.
- Smits JG, 1990: *Piezoelectric micropump with three valves working peristaltically*. Sensors and Actuators, A: Physical, vol. 21(1-3): 203–206.
- Squires T and Quake S, 2005: *Microfluidics: Fluid physics at the nanoliter scale*. Reviews of Modern Physics, vol. 77(3): 977–1026.
- Stone H, Stroock A and Ajdari A, 2004: *Engineering flows in small devices: Microfluidics toward a lab-on-a-chip*. Annual Review of Fluid Mechanics, vol. 36: 381–411.
- Tabeling P, 2003: *Introduction a la microfluidique* (Editions Belin).
- Talary M, Mills K, Hoy T, Burnett A and Pethig R, 1995: *Dielectrophoretic separation and enrichment of CD34+ cell subpopulation from bone marrow and peripheral blood stem cells*. Medical and Biological Engineering and Computing, vol. 33(2): 235–237.
- Talary MS, Burt JPH, Tame JA and Pethig R, 1996: *Electromanipulation and separation of cells using travelling electric fields*. Journal of Physics D: Applied Physics, vol. 29(8): 2198–2203.
- Terry S, Jerman J and Angell J, 1979: *A gas chromatographic air analyzer fabricated on a silicon wafer*. IEEE Transactions on Electron Devices, vol. 26(12): 1880–1886.
- Tiren J, Tenerz L and Hok B, 1989: *Batch-fabricated non-reverse valve with cantilever beam manufactured by micromachining of silicon*. Sensors and actuators, vol. 18(3-4): 389–396.

BIBLIOGRAPHY

- Umehara S, Wakamoto Y, Inoue I and Yasuda K, 2003: *On-chip single-cell microcultivation assay for monitoring environmental effects on isolated cells*. Biochemical and Biophysical Research Communications, vol. 305(3): 534–540.
- Van der Schoot BH, Van den Berg A, Jeanneret S, de Rooij NF and Grisel A, 1991: *A miniaturized chemical analysis using two silicon micro pumps*. In Sensors, Actuators and Microsystems Conference, TRANSDUCERS 1991, pp. 789–791.
- van Lintel H, Van De Pol F and Bouwstra S, 1988: *Piezoelectric micropump based on micromachining of silicon*. Sensors and actuators, vol. 15(2): 153–167.
- Whitesides G, 2006: *The origins and the future of microfluidics*. Nature, vol. 442(7101): 368–373.
- Wiklund M, Nilsson S and Hertz H, 2001: *Ultrasonic trapping in capillaries for trace-amount biomedical analysis*. Journal of Applied Physics, vol. 90(1): 421–426.
- Wolff A, Perch-Nielsen I, Larsen U, Friis P, Goranovic G, Poulsen C, Kutter J and Telleman P, 2003: *Integrating advanced functionality in a microfabricated high-throughput fluorescent-activated cell sorter*. Lab on a Chip - Miniaturisation for Chemistry and Biology, vol. 3(1): 22–27.
- Woolley A, Hadley D, Landre P, DeMello A, Mathies R and Northrup M, 1996: *Functional integration of PCR amplification and capillary electrophoresis in a microfabricated DNA analysis device*. Analytical Chemistry, vol. 68(23): 4081–4086.
- Xia N, Hunt TP, Mayers BT, Alsberg E, Whitesides GM, Westervelt RM and Ingber DE, 2006: *Combined microfluidic-micromagnetic separation of living cells in continuous flow*. Biomedical Microdevices, vol. 8(4): 299–308.
- Yager P, Edwards T, Fu E, Helton K, Nelson K, Tam M and Weigl B, 2006: *Microfluidic diagnostic technologies for global public health*. Nature, vol. 442(7101): 412–418.
- Yamada M and Seki M, 2005: *Hydrodynamic filtration for on-chip particle concentration and classification utilizing microfluidics*. Lab on a Chip - Miniaturisation for Chemistry and Biology, vol. 5(11): 1233–1239.

- Yamada M, Nakashima M and Seki M, 2004: *Pinched flow fractionation: Continuous size separation of particles utilizing a laminar flow profile in a pinched microchannel*. Analytical Chemistry, vol. 76(18): 5465–5471.
- Yang L, Banada P, Chatni M, Seop Lim K, Bhunia A, Ladisch M and Bashir R, 2006: *A multifunctional micro-fluidic system for dielectrophoretic concentration coupled with immuno-capture of low numbers of Listeria monocytogenes*. Lab on a Chip - Miniaturisation for Chemistry and Biology, vol. 6(7): 896–905.
- Yi C, Li CW, Ji S and Yang M, 2006: *Microfluidics technology for manipulation and analysis of biological cells*. Analytica Chimica Acta, vol. 560(1-2): 1–23.
- Yu L, Iliescu C, Xu G and Tay F, 2007: *Sequential field-flow cell separation method in a dielectrophoretic chip with 3-D electrodes*. Journal of Microelectromechanical Systems, vol. 16(5): 1120–1129.
- Zhang L, Tatar F, Turmezei P, Bastemeijer J, Mollinger J, Piciu O and Bossche A, 2006: *Continuous electrodeless dielectrophoretic separation in a circular channel*. Journal of Physics: Conference Series, vol. 34(1): 527–532.

BIBLIOGRAPHY

Chapter 2

AC electrokinetics: fundamentals and modeling

Summary This chapter presents the fundamental aspects of AC electrokinetics involved in the manipulation of cells by multiple-frequency dielectrophoresis in an application of continuous-flow separation. It also describes the equivalent models of the biological materials that are separated. Finally, the dielectrophoretic force is characterized by the numerical calculation of the electric-field distribution within the microstructure.

2.1 Interfacial polarization

A dielectric spherical particle such as a biological cell gets polarized in reaction to an electric field. Each dielectric can be defined by its permittivity¹ ϵ and its conductivity² σ . Five different polarization mechanisms according to the frequency of the electric field can take place: electronic, atomic, orientational, interfacial and counterion polarizations. A relaxation frequency is associated to each polarization mechanism. The polarization occurs at frequencies below the relaxation frequency but disappears at frequencies above the relaxation frequency since the polarization mechanism does not have enough time to establish. Figure 2.1 shows the five relaxations - or dispersions - in ascending order of frequency. By examining better the frequency scale, it appears

¹The permittivity is the ability of a material to polarize in response to an electric field and store energy

²The conductivity is ability of a material to moves mobile charges in response to an electric field

2. AC ELECTROKINETICS: FUNDAMENTALS AND MODELING

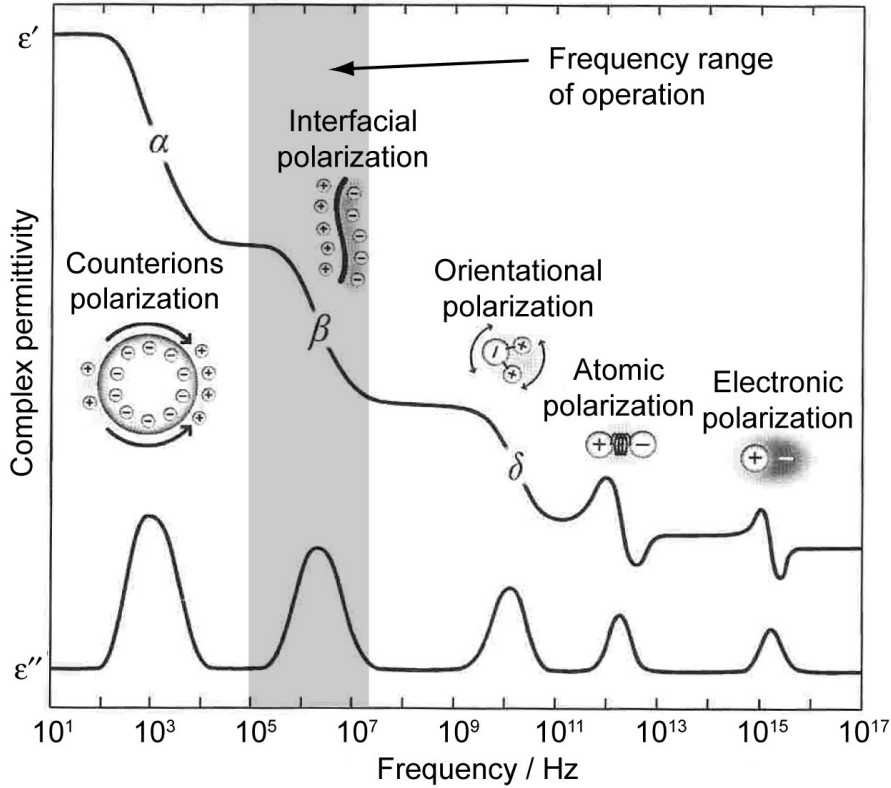


Figure 2.1: Contribution of the different polarization mechanisms of a dielectric particle to the frequency dependence energy storage expressed as the real part of the complex permittivity ϵ' and imaginary part ϵ'' which is associated to the energy dissipation.

that the β -dispersion is the only one in our frequency range of operation (typically from 10^5 to 10^7 Hz). This is referred to as the Maxwell-Wagner theory of interfacial polarization. Readers can refer to Morgan and Green (2002) for further details about the relaxations occurring at higher frequency orders.

An interfacial polarization occurs when an heterogeneous dielectric system is subjected to an electric field, *e.g.* a biological cell in a physiological solution. The mobile and surface charges accumulate at the interfaces of the dielectrics, giving rise to a polarization as a function of the angular frequency $\omega = 2\pi f$. The frequency-dependent expression of the complex permittivity $\tilde{\epsilon}$ from the Debye formulations (refer to Morgan and Green

2.2 Induced dipole moment of dielectric particles

(2002) for more detailed explanations) is expressed as:

$$\tilde{\epsilon} = \epsilon' - i\epsilon'' \quad (2.1)$$

It reflects the total energy that can be stored in the dielectric system and exhibits dispersions as shown in figure 2.1. If the system consists of a single dielectric particle in a suspending liquid, the interfacial polarization in reaction to an electric field gives rise to an induced dipole moment of the particle.

2.2 Induced dipole moment of dielectric particles

A system containing two dielectrics and immersed in an electric field is subjected to a charge build-up between the dielectrics. This effect results from the interfacial polarization and is irrespective to the system geometry. If the said system is a particle in a suspending liquid, charges move and accumulate at both sides of the particle to produce a dipole across this particle. The induced dipole moment is function of the dielectric properties of the particle and the medium as well as the angular frequency of the AC electric field. The two next sections derive the general expression for induced dipoles moment of spherical homogeneous particles and complicated shelled particles (Morgan and Green, 2002).

2.2.1 Model of homogeneous sphere

Let us consider first the model of the simplest case, *i.e.* the dipole moment \mathbf{p} of an homogeneous solid spherical particle of radius a . Such a particle could be a polystyrene or latex bead, two examples of microbeads widely used in dielectric spectroscopy and flow cytometry for calibration. The electric field, assumed to be uniform in this development, and the arising interfacial polarization induces a dipole moment as follows:

$$\mathbf{p} = 4\pi\epsilon_m \left(\frac{\tilde{\epsilon}_p - \tilde{\epsilon}_m}{\tilde{\epsilon}_p + 2\tilde{\epsilon}_m} \right) a^3 \mathbf{E} \quad (2.2)$$

where the subscripts p and m refer to the particle and the medium respectively, \mathbf{E} is the amplitude of the electric field and $\tilde{\epsilon}$ is the complex permittivity (see equation 2.1). The frequency dependance of the dipole is described in the brackets of equation 2.2

2. AC ELECTROKINETICS: FUNDAMENTALS AND MODELING

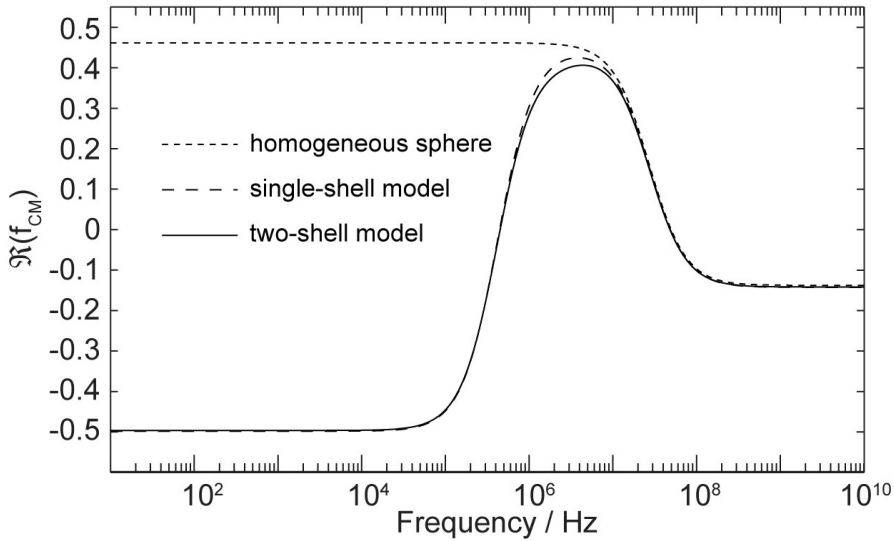


Figure 2.2: Typical curves of the real parts of the Clausius-Mossotti factors for the homogeneous sphere model, for the single-shell model and for the two-shell model. The shell models exhibit two distinguishable dispersions due to interfacial polarizations while the homogeneous sphere only one.

by the complex permittivities $\tilde{\varepsilon}_p$ and $\tilde{\varepsilon}_m$. The term in brackets is referred to as the Clausius-Mossotti (CM) factor \tilde{f}_{CM} :

$$\tilde{f}_{CM}(\tilde{\varepsilon}_p, \tilde{\varepsilon}_m) = \frac{\tilde{\varepsilon}_p - \tilde{\varepsilon}_m}{\tilde{\varepsilon}_p + 2\tilde{\varepsilon}_m} \quad (2.3)$$

The Clausius-Mossotti factor is bounded to $+1$ and $-\frac{1}{2}$ for the real part $\Re(\tilde{f}_{CM})$ and $+\frac{3}{4}$ and $-\frac{3}{4}$ for the imaginary part $\Im(\tilde{f}_{CM})$. If not stated otherwise, the CM factor stands for the real part only, since it is the only contribution to dielectrophoresis (the imaginary part contributing electrorotation, another AC electrokinetic effect). The plot of the CM factor as a function of the frequency exhibits a single dispersion shown in figure 2.2 (homogeneous sphere) with the following relaxation time τ_{MW} :

$$\tau_{MW} = \frac{\varepsilon_p + 2\varepsilon_m}{\sigma_p + 2\sigma_m} \quad (2.4)$$

where the corresponding frequency f_{MW} is called the Maxwell-Wagner relaxation frequency since the dispersion in the dipole moment is caused by the interfacial polarization. Remember that this dipole model is valid for an homogeneous particle in a

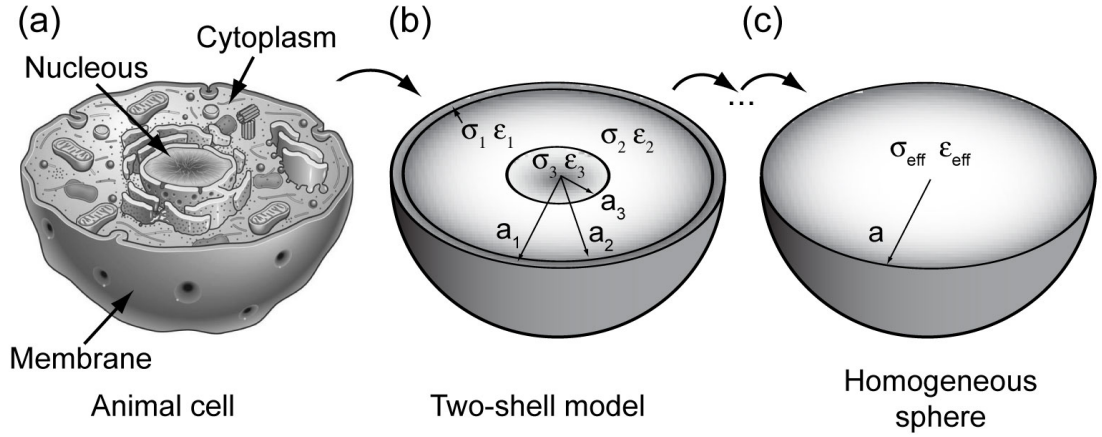


Figure 2.3: Equivalent dielectric modeling of an animal cell (a) (from www.oup.co.uk/oxed/children/oise/pictures/nature/animalcell) with a two-shell model (b) that represent the nucleus, the cytoplasm and the membrane. The two-shell model is transformed into an effective 0-shell model - or homogeneous sphere model - by analytical calculation (c).

uniform electric field. However, the model that only contains one interface and thus only one associated dispersion is inappropriate when working with most biological materials such as cells.

2.2.2 Multi-shell model

Biological materials like cells have complicated internal structures with components such as wall, membrane and nucleus. Thus the number of interfaces and dispersions are increased. One common approach to model cells is using concentric spheres called single- or multi-shell model (Huang *et al.*, 1992). Figure 2.3 shows a cell and the equivalent two-shell model. Analytical calculation brings iteratively the N-shell model to (N-1)-shell until an effective homogeneous 0-shell model (figure 2.3c). Here, the mathematical development is limited to a two-shell model which is sufficient for describing all the biological materials used in this work. In case of a single-shell model, the Clausius-Mossotti factor in equation 2.3 becomes:

$$\tilde{f}_{CM}(\tilde{\epsilon}_{12}, \tilde{\epsilon}_m) = \frac{\tilde{\epsilon}_{12} - \tilde{\epsilon}_m}{\tilde{\epsilon}_{12} + 2\tilde{\epsilon}_m} \quad (2.5)$$

2. AC ELECTROKINETICS: FUNDAMENTALS AND MODELING

where the subscript $_{12}$ indicates an effective complex permittivity that takes into account σ_1, ε_1 and σ_2, ε_2 . The effective complex permittivity $\tilde{\varepsilon}_{12}$ is:

$$\tilde{\varepsilon}_{12} = \tilde{\varepsilon}_1 \frac{\gamma_{12}^3 + 2 \frac{\tilde{\varepsilon}_2 - \tilde{\varepsilon}_1}{\tilde{\varepsilon}_2 + 2\tilde{\varepsilon}_1}}{\gamma_{12}^3 - \frac{\tilde{\varepsilon}_2 - \tilde{\varepsilon}_1}{\tilde{\varepsilon}_2 + 2\tilde{\varepsilon}_1}} \quad (2.6)$$

where $\gamma_{12} = a_1/a_2$ with a_1 and a_2 the radii of the concentric spheres (figure 2.3). In case of a two-shell model, the coefficient $\tilde{\varepsilon}_2$ of equation 2.6 becomes an effective value $\tilde{\varepsilon}_{23}$. It is function of σ_2, ε_2 and σ_3, ε_3 in a similar manner than described in equation 2.6:

$$\tilde{\varepsilon}_{23} = \tilde{\varepsilon}_2 \frac{\gamma_{23}^3 + 2 \frac{\tilde{\varepsilon}_3 - \tilde{\varepsilon}_2}{\tilde{\varepsilon}_3 + 2\tilde{\varepsilon}_2}}{\gamma_{23}^3 - \frac{\tilde{\varepsilon}_3 - \tilde{\varepsilon}_2}{\tilde{\varepsilon}_3 + 2\tilde{\varepsilon}_2}} \quad (2.7)$$

The typical curves of $\Re(\tilde{f}_{CM})$ for the single-shell and the double-shell models are shown in figure 2.2. The mathematical development of the multi-shell model can be extended to N shells and produce N+1 dispersions in the graph of $\Re(\tilde{f}_{CM})$. The complexity of the model obviously increases with the number of shells. The challenge is to define the simplest model that reasonably models a specific cell type according to the cell physiology (Pethig and Kell, 1987).

2.2.3 Model of common particles

2.2.3.1 Model of a polystyrene bead

An homogeneous sphere model is appropriate for simulating a bead made of an insulating material. Polystyrene beads with a radius of $5.14 \mu m$ are used in our experiments. The real part of their CM factor is plotted in figure 2.4a from the parameters listed in table 2.1 and taken from Arnold *et al.* (1987). The CM value is always negative and increases from -0.5 to -0.4 around $10^7 Hz$ due to the Maxwell-Wagner relaxation where the polarization is dominated by the permittivity over the conductivity.

2.2.3.2 Red blood cell

A single-shell model with parameters listed in table 2.1 and taken from Gascoyne *et al.* (2004) is used to describe the dielectric response of a red blood cell (RBC). The RBCs do not contain a nucleus and therefore require a unique shell equivalent for the membrane. The concentric sphere model is rather rough because of the complicated geometry of

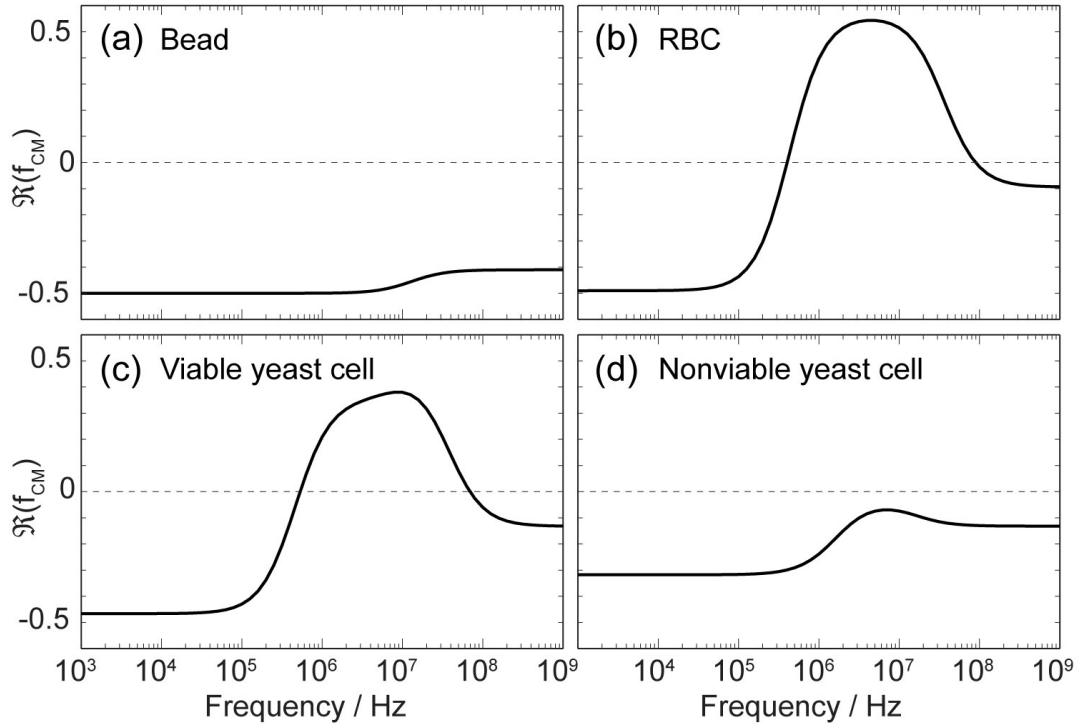


Figure 2.4: Real part of the Clausius-Mossotti factor: (a) 0-shell model of a polystyrene bead, (b) 1-shell model of a RBC, (c) 2-shell model of a viable yeast cell and (d) 2-shell model of a nonviable yeast cell. All the parameters are listed in table 2.1.

RBCs which looks more like an elongated donut. However, it is widely used although an oblate spheroid shell model has been proposed by Asami and Yonezawa (1995). The real part of the CM factor shown in figure 2.4 exhibits two dispersions. The point at which the sign changes in the first dispersion is called the crossover frequency f_{co} . This first dispersion is due to the membrane that starts driving current with increasing frequency and therefore the CM factor becomes positive due to the high conductivity inside the cell.

2.2.3.3 Viable yeast cell

The physiology of a yeast cell and in particular the presence of a "cell wall" around the cytoplasmic membrane necessitates a two-shell model (Huang *et al.*, 1992, Talary *et al.*,

2. AC ELECTROKINETICS: FUNDAMENTALS AND MODELING

Parameters	Bead	Red blood cell	viable yeast cell	nonviable yeast cell
$\sigma_m / S \cdot m^{-1}$	$60 \cdot 10^{-3}$	$60 \cdot 10^{-3}$	$60 \cdot 10^{-3}$	$60 \cdot 10^{-3}$
σ_1	$0.8 \cdot 10^{-3}$	$1 \cdot 10^{-6}$	$24 \cdot 10^{-3}$	$2.5 \cdot 10^{-3}$
σ_2	-	0.31	$0.25 \cdot 10^{-6}$	$160 \cdot 10^{-6}$
σ_3	-	-	0.3	$60 \cdot 10^{-3}$
$\varepsilon_m / F \cdot m^{-1}$	$78\varepsilon_0$	$78\varepsilon_0$	$78\varepsilon_0$	$78\varepsilon_0$
ε_1	$3.5\varepsilon_0$	$4.44\varepsilon_0$	$60\varepsilon_0$	$60\varepsilon_0$
ε_2	-	$59\varepsilon_0$	$6\varepsilon_0$	$6\varepsilon_0$
ε_3	-	-	$50\varepsilon_0$	$50\varepsilon_0$
a_1 / m	$2.57 \cdot 10^{-6}$	$3.6 \cdot 10^{-6}$	$4 \cdot 10^{-6}$	$3.5 \cdot 10^{-6}$
a_2	-	$a_1 - 4.5 \cdot 10^{-9}$	$a_1 - 0.22 \cdot 10^{-6}$	$a_1 - 0.22 \cdot 10^{-6}$
a_3	-	-	$a_2 - 8 \cdot 10^{-9}$	$a_2 - 8 \cdot 10^{-9}$

Table 2.1: List of parameters for the shell models

1996, Holzel and Lamprecht, 1992). The first shell stands for the cell wall (σ_1, ε_1), the second shell for the cytoplasmic membrane (σ_2, ε_2) while the inner sphere substitutes the cytoplasm (σ_3, ε_3). Works focused on the dielectric characterization of yeast cell from a double-shell model pretend that the cytoplasm can be reasonably replaced by an equivalent homogeneous medium even though the cytoplasm contains numerous biological constituents. Huang *et al.* (1992) have reported a cell-wall and cytoplasmic-membrane thicknesses of 220 nm and 8 nm as well as values of conductivities and permittivities as listed in table 2.1. The real part of the Clausius-Mossotti factor is plotted versus frequency in figure 2.4c and shows three dispersions coming from the three interfaces.

Asami *et al.* (1976) proposed to simplify the double-shell model to a single shell when the dielectric properties of the wall are within one order of magnitude close to the ones of the medium. Indeed, the role of permeation barrier in ions flux is mainly fulfilled by the cytoplasmic membrane whose pores are much smaller than the pores of the cell wall. However, what seems first to be a simplification actually imposes to be in particular experimental conditions. Alternatively, Raicu *et al.* (1996) proposed to neglect the cell-wall influence but to consider the inner vacuoles in order to explain a dispersion occurring at high frequency (which is above the frequency range considered in our work).

This dispersion can only be seen with high-frequency equipment of spectroscopy. These two specific cases diverge from standard conditions. This work only uses the general double-shell model for modeling a yeast cell.

2.2.3.4 Nonviable yeast cell

The last graph in figure 2.4 shows the CM factor for a nonviable yeast cell, as well modeled by a double-shell. The value is constantly negative for the parameters in table 2.1 but would get positive at low frequency at a lower medium conductivity, *e.g.* $\sigma_m/10$. A comparison of the dielectric properties of a nonviable yeast cell with a viable cell shows a drastic increase in the cytoplasmic-membrane conductivity and a decrease in the cytoplasm conductivity. Although the intrinsic physico-chemical properties of the cell are not completely understood, the first variation likely comes from a significant reduction of the specific membrane resistance. The membrane degradation results in an ion leakage and therefore in a drop of the cytoplasm conductivity. It is questionable if the drop of cytoplasmic conductivity is either really due the absence of physiological and metabolic mechanisms in the nonviable cells or only a morphologic consequence to heat treatment used to prepare a solution of nonviable yeast cell. This question, although very interesting, gets out of this work context.

2.3 Dielectrophoresis

As said in section 2.2, a dielectric particle such as a biological cell gets polarized when subjected to an electric field due to an induced dipole moment. The interaction of this induced dipole with the electric field gives raise to electrical forces. AC electrokinetics is the field that describes the movement of dielectric particles produced by AC electric fields, *e.g.* via electrical force. In the framework of this thesis, the wide field of AC electrokinetics is restricted to the study and to the use of dielectrophoresis (DEP). Dielectrophoresis is a phenomenon that describes the generation of an electrical force on a dielectric particle when this latter is subjected to a non-uniform electric field. The induced dipole moment of the dielectric particle (section 2.2) interacts with the non-uniform electric field to produce a net movement of the particle. According to the polarizability of the particle which can be larger or smaller than the one of its surrounding

2. AC ELECTROKINETICS: FUNDAMENTALS AND MODELING

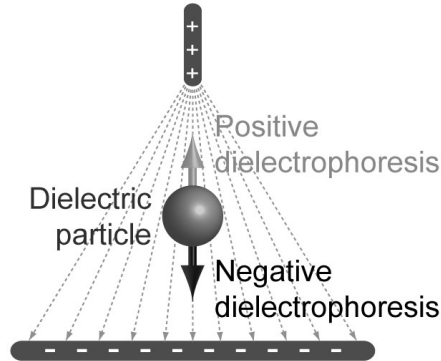


Figure 2.5: Representation of dielectrophoresis which describes an electrical force that is exerted on a dielectric particle when this latter is subjected to a non-uniform electric field. The particle moves towards the region of high electric-field strength if it is more polarizable than the medium (positive dielectrophoresis). Inversely, the particle moves back from the same region if it is less polarizable than the medium (negative dielectrophoresis).

medium, the particle moves towards of back from a region of high electric-field strength respectively. Figure 2.5 shows the two cases: negative dielectrophoresis (nDEP), when the particle is repelled from the region of high electric-field strength and positive dielectrophoresis (pDEP), when the particle is attracted towards this same region. The net force exerted on a particle due to dielectrophoresis is called the dielectrophoretic force (DEP-force). It is expressed as follows:

$$\mathbf{F}_{DEP} = (\mathbf{p} \cdot \nabla)\mathbf{E} \quad (2.8)$$

where \mathbf{p} is the dipole moment as described in equation 2.2 and the nabla operator ∇ stands for the gradient of the electric field. This expression of DEP is correct for the dipole approximation, *i.e.* the length of the dipole is smaller than the characteristic length of the field non-uniformity or the field does not vary significantly across the dimension of the dipole. For more general cases where this approximation is invalid, Jones (1995) presented a calculation based on higher order moments or multipoles using Maxwell stress tensor. The dipole approximation is valid throughout this research and the time-averaged DEP-force on the particle in an AC field becomes:

$$\langle \mathbf{F}_{DEP} \rangle = \pi \epsilon_m a^3 \Re(\tilde{f}_{CM}) \nabla |\mathbf{E}|^2 \quad (2.9)$$

where $\langle \rangle$ defines a time-averaged value of the variable in between. This equation shows the force dependencies on the particle volume, on the CM factor and on the gradient of the square of the field amplitude. This last factor ($\nabla|\mathbf{E}|^2$) is determined by the geometry of the device and by the electrical signals applied to the metal electrodes. The sign and the frequency dependence of the DEP-force of equation 2.9 are defined by the CM factor of equation 2.3. Negative values of the CM factor, meaning that the particle is less polarizable than its surrounding medium, induce nDEP whereas positive values, meaning that the particle is more polarizable than the medium, induce pDEP. The CM factor and therefore the DEP-force can either be negative or positive as a function of the frequency of the AC electric field. For example, the model presented in section 2.2.3 shows that a particle can be less polarizable at low frequency but more polarizable at frequencies above f_{co} .

Equation 2.9 shows that only the real part of the polarization $\Re(\mathbf{p})$ has to be considered in the definition of the DEP-force. This can be explained by the projection of \mathbf{p} on the electric-field vector which is the only contribution to a net movement of a dipole in a non-uniform electric field. The projection corresponds to the real part of \mathbf{p} since the electric field itself is defined as real. Oppositely, only the imaginary part of the polarization $\Im(\mathbf{p})$ contributes to the electrorotation, *i.e.* a phenomenon of AC electrokinetics that induces rotation of a dielectric particle subjected to a rotating electric field. The characterization of the electric-field distribution within our particular microstructure is needed in order to fully determine the DEP-force and to be able to calculate its value. This is addressed later on in section 2.3.2.

2.3.1 Dielectrophoresis with "liquid electrodes"

The general concept of dielectrophoresis presented in section 2.3 is adapted to our particular microstructure where the electric field and the non-uniformities of its distribution are produced by planar metal electrodes and by a patterned insulator respectively. This novel combination of planar electrodes with a patterned insulator to generate DEP is discussed in details later on in section 3.1. Basically, we propose a simple geometry where planar metal electrodes deposited on the bottom of dead-end chambers generate an electric field within the microstructure. These chambers are located perpendicular

2. AC ELECTROKINETICS: FUNDAMENTALS AND MODELING

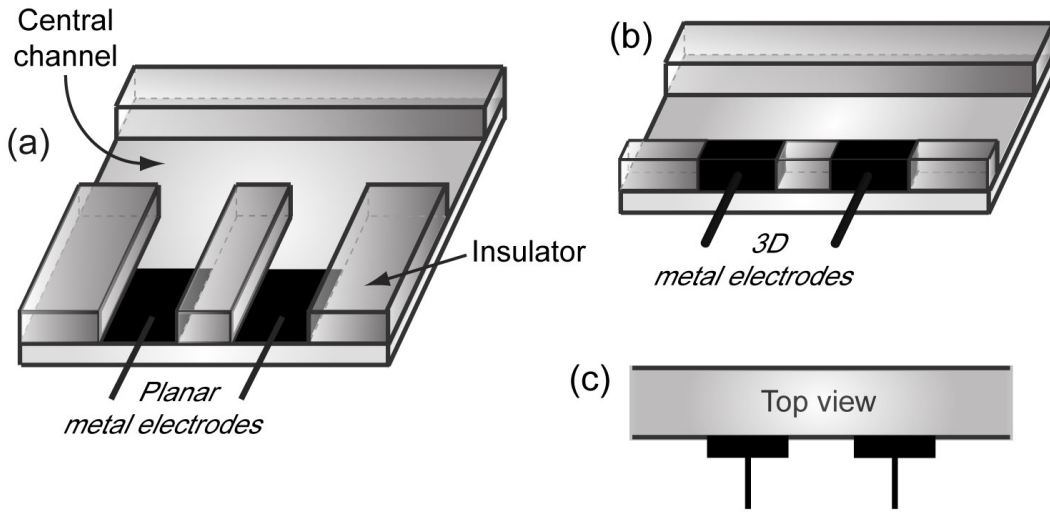


Figure 2.6: Schemes of the microstructure to manipulate particles flowing through a central channel with dielectrophoresis. The planar electrodes and the patterned insulator are represented in (a). The electrodes generate an electric field which is guided by the insulator through the central channel where non-uniformities are created by the geometry to produce a DEP-force. (b) shows an equivalent representation of the planar electrodes and the insulator that behave like 3D electrodes located in the sidewall of the central channel. (c) is the top view of (b), *i.e.* a simplified representation of (a) and (b).

to a central channel and are, like the central channel, defined by a patterned insulator. The planar electrodes, the insulator and the central channel are shown in figure 2.6a. The electric field is guided by the insulator through the central channel where the geometry defines its distribution and creates non-uniformities. Actually, the planar electrodes and the perpendicular dead-end chambers behave like 3D metal electrodes that would be located in the sidewall of the central channel as represented in figure 2.6b. The liquid boundaries between the central channel and the perpendicular dead-end chambers are referred to as "liquid electrodes". A simplified illustration of the "liquid electrodes" is represented in figure 2.6c. This arrangement generates a DEP-force in the central channel to manipulate the particles that are flowing through the central channel.

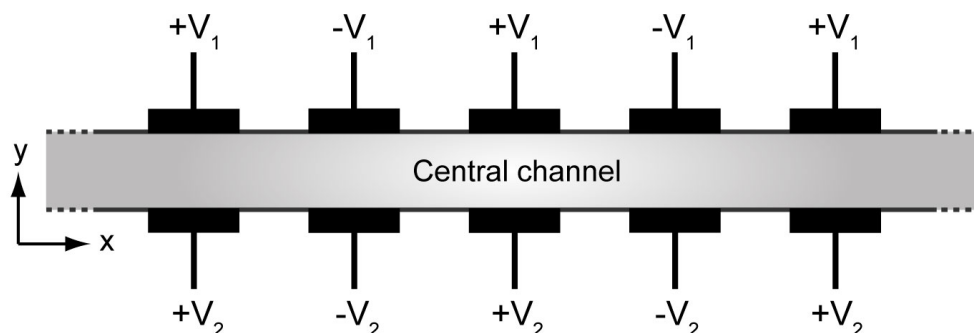


Figure 2.7: Scheme of an array of "liquid electrodes" located on both sides of a central channel. Considering a few precautions, electrical potentials applied to each side of the array ($+V_1$, $-V_1$, $+V_2$ and $-V_2$) produce two electric fields that do not interfere. Thus, each side of the array generates a DEP-force field that can either attract or repel the particles that flow through the central channel according to the nature of the DEP, either positive or negative respectively. The opposition of the forces allows application of cell focusing towards different positions across the central channel.

The characterization of the generated DEP-force in the central channel shows that this latter is horizontal, *i.e.* parallel to the channel bottom. This is due to the uniformity of the electric field across the channel height (this uniformity is discussed in section 2.3.2 based on numerical calculation). Thus the field gradient $\nabla|\mathbf{E}|$ only varies in an horizontal plane. The regions of highest field strength are located at the corners of the patterned insulator, *i.e.* between two "liquid electrodes". As seen by the dielectric particles that flow through the central channel, these regions act as attracting or repelling poles according to the nature of the dielectrophoresis, positive or negative respectively. As a result, the trajectories of the particles that flow through the central channel are modified by the effect of the DEP-force. Such a deflecting structure would find applications in cell dipping, where cells are moved from a first medium to a second one and brought back to the first medium in a well time-controlled manner as presented by Seger *et al.* (2004) and more recently by Tornay *et al.* (2008) also based on "liquid electrodes".

2. AC ELECTROKINETICS: FUNDAMENTALS AND MODELING

The number of "liquid electrodes" (two in figure 2.6) can be increased to improve the total efficiency of the deflecting structure. In our typical geometry, this number is defined by the electrical connectors used in the electrical interface (see section 3.7) and is equal to fifteen. It is also possible to locate "liquid electrodes" on the opposite side of the central channel by taking a few precautions to produce two counteracting DEP-force fields. Section 2.4 discusses considerations on the electrical signals that have to be applied to the metal electrodes to generate DEP-forces that do not interfere with each other. And thus, the resultant force is the superposition of each force contribution. Two opposite force fields can move the flowing particles laterally across the central channel in a control manner. Their effect can be combined to create an effective and tunable electrical focusing of a particle stream. These applications are presented in section 4.3.

2.3.2 Numerical calculation of the electric field

In order to evaluate the DEP-force, the electric field distribution within the microstructure needs to be known. However, the electric field distribution can not be simply calculated with analytical methods due to the complicated 3D geometry and in particular due to the fact that the electric field is generated by planar electrodes (2D). An analytical expression to describe the development of the electric-field lines within the microstructure is complicated and requires successive steps of conformal mapping. Propositions of analytical expressions can be found in Demierre *et al.* (2007) and Sun *et al.* (2007). In this thesis, numerical calculations are therefore preferred to analytical calculations. The objective of this section is to characterize the electric field in the 3D microstructure and to calculate its distribution in order to predict the DEP-forces in the central channel. The numerical characterization of the electric field is also used to discuss the assumption that the "liquid electrode" is an equipotential surface.

The electric fields that are considered in this work are restricted to a typical frequency range from 10^5 to 10^7 Hz. AC electric fields prevent electrochemical processes occurring at the metal-liquid interfaces. Furthermore, they allow to excite various dielectric-particle types at multiple frequencies to observe differences in their dielectric responses. An AC signals applied to the metal electrodes produce an electric field \mathbf{E} in

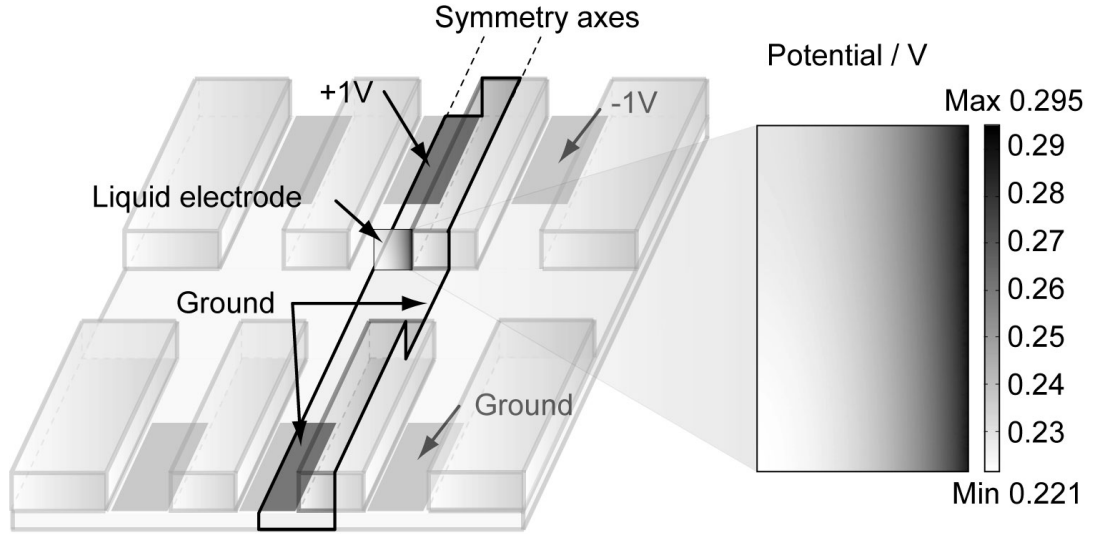


Figure 2.8: Drawing of the 3D geometry used for the numerical calculation with the boundary conditions. The geometry is only a small part of the whole structure thanks to the symmetrical and repetitive arrangement. On the right is shown the numerical result of the potential distribution at the "liquid electrode".

the microstructure as follows:

$$\mathbf{E} = -\nabla(\phi) \quad (2.10)$$

where $\phi(x, y, z)$ is the spatial distribution of potentials. The electric field distribution needs to be known in order to estimate the DEP-force in the channel. Here, we propose to address this problem using calculation based on numerical methods. The numerical calculations presented in this section are made using the commercial software *ComsolMultiphysics*[©] based on a finite element method (FEM).

2.3.2.1 In the access channel: from 2D to 3D

The first numerical calculation - or simulation - is to characterize the field lines and the equipotential surfaces in the access channel. Thanks to the symmetrical and repetitive geometry, only a part of the whole structure has to be simulated, from the half of the access channel to the half of the SU-8 finger between two electrodes as shown in figure 2.8. The geometrical dimensions of the 3D structure correspond to the case $d = 20 \mu m$

2. AC ELECTROKINETICS: FUNDAMENTALS AND MODELING

in figure 3.4b. A boundary condition of $+1 V$ is applied to the lower electrode while *ground* is applied to the upper electrode as well as to the symmetry axis in the central channel, all the others being electric insulation (figure 2.8). The result of the simulation shows how the field lines in the vicinity of the planar electrode go up and occupy the 3D volume. Moreover, the narrow access channel forces the field lines to run parallel, which creates vertical equipotential surfaces. The right part of figure 2.8 shows the potential distribution at the "liquid electrode", *i.e.* the surface boundary between the access channel and the central channel. The maximum and minimum potentials with $+1 V$ and *ground* at the boundaries are equal to $0.295 V$ and $0.221 V$ which gives a variability of $\approx 25\%$. Numerical calculation of the potential on the "liquid electrode" indicates an average homogeneity $> 98\%$ in the height and an average homogeneity $> 80\%$ in the width. Another result from the simulation, more as a design rule, is the minimum distance between the metal electrode and the central channel that should be equal or larger than the channel height. This rule allows the field lines to fully develop in the access channel and create vertical equipotential surfaces (homogeneity $> 98\%$).

This numerical calculation indeed confirms that our concept of "liquid electrode" can be reasonably seen as a vertical electrode on the sidewall of the central channel. The next step is the calculation of the field distribution in the central channel to predict the generated DEP-force.

2.3.2.2 In the central channel: from 3D to 2D

As just stated, the field distribution in the height is from now considered homogeneous. Consequently, the field distribution in the central channel is brought back to a 2D problem. A much higher spatial resolution of the calculation is obtained with a 2D simulation compared to a 3D simulation. This is easily understood by considering the maximum number of calculations that a computer can do. However, since the horizontal homogeneity is in the order of 80% , the "liquid electrode" is not simply replaced by a flat boundary at fixed equivalent potential but rather stays spatially apart from the central channel to which it is connected through the access channel. The length of the access channel is such that the potential drop in the 2D geometry fits the drop in the 3D structure. This latter roughly corresponds to $1.5 \times d$, the characteristic geometrical

dimension (refer to figure 3.4).

Again due to symmetry and repetition, the simulation is performed on a simpler geometry. We further assume that the last element of the electrode array do not produce any disturbance. It is important at this point to carefully mesh the geometry in order to get the best resolution possible at regions of strong field gradient, *i.e.* essentially at the corners. A grid of post-processed data (the norm of the electric field) is exported with a spatial grid pitch of half a micrometer. A similar procedure from 3D fluidic simulation is done to get the fluid-velocity fields in x and y directions at the mid-height plane. The two grids, electrical and fluidic, consist of input matrices for another commercial software *Matlab*[©] in which home-made scripts calculate a particle trajectory as a function of the DEP-force field, the flow velocity and the properties of the particle and the medium. Examples of calculated trajectories based on this method are shown in figure 4.1 in section 4.2. The main utility of the numerical calculation of the electric field is presented later on in section 4.4.2 where the readout of the positions of cells downstream from the electrode array is related to their intrinsic dielectric properties. It lies in the dielectric characterization of biological materials.

2.3.3 Estimation of the electrical force

The electric field calculated in the previous section is now used to evaluate the DEP-force in the central channel that acts on flowing particles. Besides numerical predictions, measurements of DEP-force from real particle-trajectories is performed in this section to corroborate the numerical model and the simulations. Estimating the DEP-force from a particle trajectory is generally complicated, as DEP-force and fluid flow are not at right angles. This complicates the separation of the two contributions on the trajectory of a particle. On exception is the symmetry axis of a single pair of "liquid electrodes" located on a single side of a central channel (show top-right image in figure 2.9). Along this particular axis, the DEP-force has a contribution in the y -direction whereas the viscous drag force from the flow is only acting in the x -direction. Thus, the y -velocity of a particle is due to the DEP-force, which is opposed to friction. By assuming an instantaneous acceleration, the DEP-force as a function as the particle

2. AC ELECTROKINETICS: FUNDAMENTALS AND MODELING

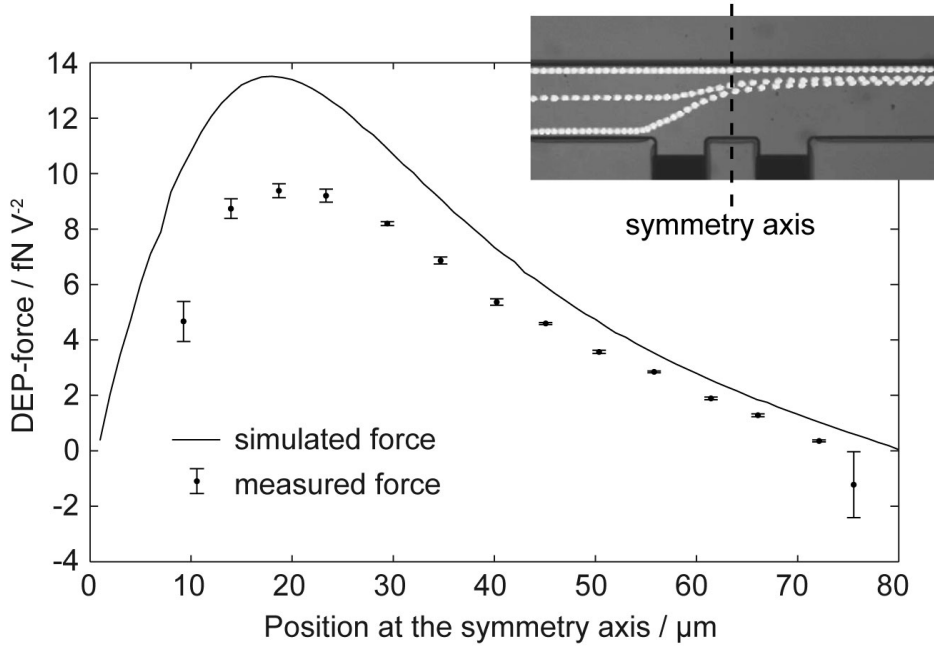


Figure 2.9: Numerical simulation and measurements of the dielectrophoretic force acting on flowing particles ($5.14 \mu m$ polystyrene beads with $\Re(\tilde{f}_{CM}) = -0.5$) at the symmetry axis of the simple structure containing one pair of "liquid electrodes". The channel width is $80 \mu m$, the electrode and insulator width is $56 \mu m$.

velocity \mathbf{v} has the following general expression (Morgan and Green, 2002):

$$\mathbf{F}_{DEP} = 6\pi\eta a(\mathbf{v} - \mathbf{v}_{flow}) \quad (2.11)$$

where η is the medium viscosity. It is therefore possible to evaluate the DEP-force at the symmetry axis by estimating the y-velocity of a particle from image analysis. The evaluated DEP-force normalized by the voltage in $fN \cdot V^{-2}$ is plotted as a function of the position in figure 2.9. Measurements on several particles are performed at 14 different positions across the channel. The mean value and the standard deviation are reported in the graph for each measurement point. The small deviations indicate that the evaluation method is robust even though the first and last deviations are larger than the others. This comes respectively from the need to use very small voltages to evaluate the DEP-force close to the lower sidewall and from the extremely weak DEP-force at the upper sidewall that makes the velocity estimation critical.

Figure 2.9 also compares the DEP-force estimated from particle trajectories to the numerical calculation. The behaviors are similar and the agreement is better and better with increasing distance from the electrodes. Close to the electrodes, the measured force is smaller than calculated. This can be mainly attributed to small differences between the simulated geometry and the real geometry obtained by microfabrication. Indeed, the corners of the patterned SU-8 appear rounded under microscopic image due to the step of photolithography.

A typical voltage of 25 V gives rise to a DEP-force on the order of 5 pN on the particles. However and as shown in the figure 2.9, the DEP-force quickly decreases with the distance from the "liquid electrodes" and even becomes negative for the measured values. The negative sign of the force indicates that the y-velocity was actually negative, *i.e.* the particle was moving from the upper sidewall towards the central channel. This effect is probably caused by locally enhanced field non-uniformities due to squeezing between the insulating particles and the insulating channel wall.

2.3.4 Scaling considerations

This section describes the effects of a scaling of the microstructure on the DEP-force. It also highlights major limitations in the miniaturization in order to maintain a significant effect of the DEP-force on the particles that flow in the central channel. These issues are discussed based on scaling laws (Castellanos *et al.*, 2003) that describe how physical phenomena such as DEP or particle movement vary with the characteristic dimension l . Equation 2.9 shows the proportionality of the DEP-force to the particle volume ν and to the gradient of the square of the electric-field amplitude $\nabla|\mathbf{E}|^2$. For a constant potential, they scale with l as follows:

$$\begin{aligned} \nu &\propto l^3 \\ \nabla|\mathbf{E}|^2 &\propto l^{-3} \\ \Rightarrow \langle F_{DEP} \rangle &\propto l^0 \end{aligned} \tag{2.12}$$

The most important physical value for an application of cell separation is the lateral movement imparted on the particles by the DEP-force. The movement of particles

2. AC ELECTROKINETICS: FUNDAMENTALS AND MODELING

induced by the DEP-force is opposed to a friction force. This friction force limits the velocity (DEP velocity, or \mathbf{v}_{DEP}) at which the particles can move. Assuming that inertia is negligible and that the maximum velocity is instantaneously reached, the velocity of the particle movement due to the DEP-force is expressed as follows:

$$\mathbf{v}_{DEP} = \frac{\mathbf{F}_{DEP}}{f_{fric}} = \frac{\pi\varepsilon_m a^3 \Re(\tilde{f}_{CM}) \nabla |\mathbf{E}|^2}{6\pi\eta a} \propto l^{-1} \quad (2.13)$$

where f_{fric} is friction factor for a spherical particle. Thus the movement scales with l^{-1} . This indicates that the efficiency of DEP in moving particles increases when the dimensions are reduced. In contrast, at small dimension, the movement due to thermal effect, *i.e.* the brownian motion, becomes significant. Finally, the ratio between the movement per second due to DEP and to thermal effect scales as:

$$\frac{\Delta x_{DEP}}{\Delta x_{brownian}} \propto l^{-\frac{1}{2}} \quad (2.14)$$

The concluding remark on the DEP scaling is that our device is suitable for further miniaturization where applications require the manipulation of small biological sample such as bacteria. However, the downscaling of the whole device might face some technological limitations such as the resolution of classical photolithography. Furthermore, the influence of brownian motion would get more and more important with the miniaturization and would for instance remix particles downstream from the separation chamber.

2.4 Multiple-frequency dielectrophoresis

So far, all the concepts presented deal with electrical signals at a single frequency for driving an electrode array (such as the one in figure 2.7). This section extends the use of single-frequency signals to the combination of several electrical signals at multiple frequencies to produce multiple-frequency dielectrophoresis (MFDEP). The electrical interface described later on in section 3.7 gives the possibility to apply independent electrical signals on the two sides of the electrode array (as shown in figure 3.2). Each signal can be itself a combination of several signals with different voltages and frequencies that are mixed together before being conditioned and driven to the metal electrodes. Thus, it is possible to configure a set of signals with multiple voltages and

frequencies according to the application.

An example of realization consists of mixing signals from two function generators through a power combiner module (as shown in figure 3.2). The combination of dielectrophoresis at multiple frequencies provides an efficient method for separating particles according to their dielectric response (Urdaneta and Smela, 2007). Only few works on MFDEP have been reported so far (Pethig *et al.*, 2003, Kaler *et al.*, 1992). Section 5 reports on the main results of our cell separation method using "liquid electrodes" and multiple-frequency dielectrophoresis.

2.4.1 Superposition of dielectrophoresis

In the general case where a dielectric particle is subjected to an electric field at multiple frequencies, its total polarization \mathbf{p}_{total} of equation 2.2 is a non-linear function of the total electric field in the time domain. The reason comes from the relaxation mechanisms that delay and spread the polarization response to multiple frequencies over time. The polarization is therefore a complicated function of the electric fields in the time domain. It is however a linear function of the electric field at multiple frequencies (n frequencies in the following equations) in the Fourier's domain:

$$\mathbf{p}_{total} = \sum_{i=1}^n \alpha_i \cdot \mathbf{E}_i = \sum_{i=1}^n \mathbf{p}_i \quad (2.15)$$

where α_i is a scalar factor that quantifies the dielectric response of the particle at the angular frequency ω_i of the electric field and \mathbf{E}_i is a real AC electric field that can be written $\mathbf{E}_i \cos(\omega_i t)$. The expression of the single-frequency dielectrophoresis (equation 2.8) becomes for multiple frequencies as follows:

$$\mathbf{F}_{DEP,total} = \left(\sum_{i=1}^n \mathbf{p}_i \cdot \nabla \right) \sum_{i=1}^n \mathbf{E}_i \quad (2.16)$$

The superposition principle of the electric fields says that the total electric field is the vectorial sum of the single contribution of each electric field in absence of the others. This simplifies equation 2.16 as follows:

$$\begin{aligned} \mathbf{E}_{total} &= \sum_{i=1}^n \mathbf{E}_i \\ \mathbf{F}_{DEP,total} &= (\mathbf{p}_{total} \cdot \nabla) \mathbf{E}_{total} \end{aligned} \quad (2.17)$$

2. AC ELECTROKINETICS: FUNDAMENTALS AND MODELING

Considering a particular case for $n = 2$ where $\mathbf{E}_1 = \mathbf{E}_1 \cos \omega_1 t$ and $\mathbf{E}_2 = \mathbf{E}_2 \cos \omega_2 t$:

$$\mathbf{F}_{DEP,total} = (\mathbf{p}_1 \cdot \nabla)\mathbf{E}_1 + (\mathbf{p}_2 \cdot \nabla)\mathbf{E}_2 + (\mathbf{p}_1 \cdot \nabla)\mathbf{E}_2 + (\mathbf{p}_2 \cdot \nabla)\mathbf{E}_1 \quad (2.18)$$

This expression still needs to be time averaged to define the total DEP-force acting on particles. It contains two kinds of terms; pure-product term of angular frequency and two cross-product term. The time-averaged value of the cross-product term is zero if we consider the two following assumptions:

- The two frequencies are much larger than the transit frequency of the particles, *i.e.* the particles see many periods of the two signals such that a time-averaging makes sense.
- The two frequencies have to be different enough such that the absolute value of the frequency difference is still much larger than transit frequency of the particles.

If these assumptions are respected, the time-averaged value of a cross-product for an AC electric field is:

$$\langle (\mathbf{p}_1 \cdot \nabla)\mathbf{E}_2 \rangle = \frac{1}{T} \int_0^T (\mathbf{p}_1 \cos(\omega_1 t) \cdot \nabla)\mathbf{E}_2 \cos(\omega_2 t) dt = 0 \quad (2.19)$$

Thus the time-averaged value of the total force in equation 2.18 becomes:

$$\langle \mathbf{F}_{total} \rangle = \langle (\mathbf{p}_1 \cdot \nabla)\mathbf{E}_1 \rangle + \langle (\mathbf{p}_2 \cdot \nabla)\mathbf{E}_2 \rangle = \sum_{i=1}^n \langle \mathbf{F}_i \rangle \quad (2.20)$$

This last equation means that the total DEP-force is the vectorial sum of all the force contributions at each frequency, as long as the above assumptions are fulfilled. This is comparable to the superposition principle of electric fields and was also previously reported by Kaler *et al.* (1992).

2.4.2 The effective Clausius-Mossotti factor

In order to describe the phenomenology of MFDEP, Urdaneta and Smela (2007) introduced an effective value of the Clausius-Mossotti factor $\Re(\tilde{f}_{CM,eff})$ based on the superposition principle of the DEP-forces (equation 2.20). This preserves better the

traditional formalism of the DEP-force which is the multiplication of an electric field with a frequency-dependant factor (bounded to -0.5 and +1) as follows:

$$\langle \mathbf{F}_{total} \rangle \propto \langle \Re(\tilde{f}_{CM,eff}) \rangle \cdot \nabla |\mathbf{E}_{total}|^2 \quad (2.21)$$

In this last equation, $\Re(\tilde{f}_{CM,eff})$ is a function of the $\Re(\tilde{f}_{CM})$ for each frequency and therefore describes the polarization resulting from all the frequencies. The nabla operator ∇ can be dropped when the divergence of each electric field is the same, as it is in our symmetrical electrode array. The time-averaged value of $\Re(\tilde{f}_{CM,eff})$ can be expressed as follows:

$$\langle \Re(\tilde{f}_{CM,eff}) \rangle = \frac{\sum_{i=1}^n \Re(\tilde{f}_{CM,i}) \cdot |\mathbf{E}_i|^2}{\sum_{i=1}^n |\mathbf{E}_i|^2} \quad (2.22)$$

Note that this expression for an effective and time-averaged CM factor is only valid under the two assumptions of the previous section (2.4).

2.4.3 Opposition of dielectrophoretic forces

This section extends the development of multiple-frequency dielectrophoresis to the case where two DEP-forces are not generated from a single side of the electrode array but are rather generated from both sides of the electrode array of figure 2.7. The principle of opposite dielectrophoresis is illustrated in figure 2.10. The scheme shows two electric-field distributions that are symmetrical, with an horizontal symmetry axis. The same principle is applied to the electrode array of figure 2.7 where each side generates a DEP-force field. Likewise the scheme in figure 2.10a, the two DEP-force fields are symmetric. Their distributions have *i.e.* the same x component but the inverse y component (see axis definition in figure 2.7). Again, the superposition principle of the DEP-forces can be used to calculate the total DEP-force only if the two assumptions of section 2.4 are fulfilled. If this is the case, the two DEP-forces can be controlled externally by adjusting the voltages and the frequencies of the electrical signals.

2.4.3.1 Definition of equilibrium position

In some cases, the opposition of two DEP-forces defines spatially a position of equilibrium - or equilibrium line - where the y component of the resultant DEP-force is

2. AC ELECTROKINETICS: FUNDAMENTALS AND MODELING

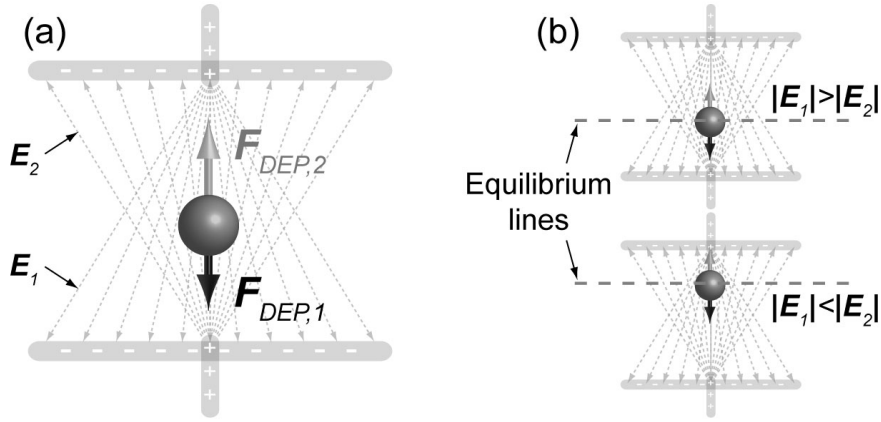


Figure 2.10: (a) Opposition of two symmetrical electric fields whose non-uniformities generate two counteracting nDEP-forces ($\mathbf{F}_{DEP,1}$ and $\mathbf{F}_{DEP,2}$). In (b) the two counteracting forces spatially define an equilibrium line where y component of the resultant force ($\mathbf{F}_{DEP,1} + \mathbf{F}_{DEP,2}$) is equal to zero. The equilibrium line can be shifted at different location by adjusting the amplitudes of the electric fields $|\mathbf{E}_1|$ and $|\mathbf{E}_2|$.

equal to zero. The equilibrium is approximately a line parallel to the x -axis (see axis definition in figure 2.7), along the central channel, as represented in figure 2.10b. The requirement to create positions of equilibrium is on the nature of the dielectrophoresis. This latter has to be negative such that each side of the electrode array repels the particles towards the opposite side with a DEP-force that has the general shape of figure 2.9. The equilibrium line can be moved across the central channel by adjusting the electrical signals. Indeed, the position of the equilibrium line is determined by the respective values of the two counteracting DEP-forces, which are externally controlled by the electrical signals applied to the metal electrodes. Two particular cases when $|\mathbf{E}_1| > |\mathbf{E}_2|$ and when $|\mathbf{E}_1| < |\mathbf{E}_2|$ are represented in figure 2.10b.

The principle of equilibrium is essential in our method of continuous-flow cell separation. The definition of an equilibrium line is possible due to the opposition of two horizontal DEP-forces, which are themselves possible due to the use of "liquid electrodes". This principle of equilibrium is used in focusing applications (section 4.3) as well as in applications of continuous-flow cell separations (5).

2.4.4 Particular case of multiple-frequency dielectrophoresis

Certain applications based on MFDEP require several signals at different frequencies. For example, our method of continuous-flow cell separation necessitates one signal on one side of the electrode array and two superimposed signals at different frequencies on the other side (an example is illustrated in figure 3.2). The single signal and one of the two superimposed signals have to be at sufficiently low frequency such that both of them produce nDEP to focus the cells that flow through the central channel towards an equilibrium line. The two low frequencies have to be close enough in order to produce the same dielectric response of the cells. Here can arise some troubles with MFDEP. If the frequencies are too close, then the second assumption of section 2.4 is no longer respected and the time-averaged value of $|\mathbf{E}_{total}|^2$ does not follow the superposition principle anymore:

$$\langle |\mathbf{E}_{total}|^2 \rangle \neq \sum_{i=1}^2 \langle |\mathbf{E}_i|^2 \rangle \quad (2.23)$$

In this particular case, when two frequencies are really close, the development of the left-hand term in equation 2.23 contains cross-product terms that are not canceled by the time-averaging:

$$\begin{aligned} \langle |\mathbf{E}_{total}|^2 \rangle &= \langle |\mathbf{E}_1|^2 \cos^2 \omega_1 t \rangle + \langle |\mathbf{E}_2|^2 \cos^2 \omega_2 t \rangle + \\ &\quad \langle |\mathbf{E}_1|^2 |\mathbf{E}_2|^2 \cos \omega_1 t \cos \omega_2 t \cos \varphi \rangle \\ &= \dots + \langle |\mathbf{E}_1|^2 |\mathbf{E}_2|^2 \frac{1}{2} [\cos(\omega_1 + \omega_2)t + \cos(\omega_1 - \omega_2)t] \cos \varphi \rangle \end{aligned} \quad (2.24)$$

where φ is the angle between the two electric-field vectors \mathbf{E}_1 and \mathbf{E}_2 which gives a spatial dependency of the total force. Moreover, the total force is time dependent since the time-averaged value of $\cos(\omega_1 - \omega_2)t$ is different from zero. In summary, $\langle \mathbf{F}_{DEP, total} \rangle = f(\mathbf{x}, t)$ when ω_1 and ω_2 are too close. This gives raise to beat effects that are generally not desired in focusing and separation applications. They could eventually be used in other application to move particles step by step in an electrode array or to sweep the output positions from one side to the other with the focused particle stream.

2.4.4.1 Effect of close frequencies

When two close frequencies are required by the application but when the spatial and the time dependencies have to be avoided, the solution is to use quadrature signals to drive

2. AC ELECTROKINETICS: FUNDAMENTALS AND MODELING

the electrode array, *i.e.* two signals at the same frequency but with a 90 degrees phase shift. Thus, the cross-product of equation 2.24 becomes $(\cos \omega t \sin \omega t)$ whose time-averaged value is zero. This cancels the time and the spatial dependencies and it gives the possibility to add the effects of two different electric fields at the same frequency. For this particular case, the time-averaging of the total DEP-force in equation 2.16 becomes identical to equation 2.20 and is expressed as follows:

$$\langle \mathbf{F}_{DEP,total} \rangle = \langle \mathbf{F}_{DEP,1} \rangle + \langle \mathbf{F}_{DEP,2} \rangle \quad (2.25)$$

This particular configuration of quadrature signals is used later on in this work for applications of continuous-flow separation of cells.

2.4.5 Set of electrical signals for continuous-flow separation of cells

The method of continuous-flow cell separation that is proposed in this thesis makes use of three electrical signals to drive the electrode array where the separation occurs. The configuration of the electrical signals is kept homogeneous throughout the manuscript for the sake of clarity. The whole electrode array contains two rows of fifteen "liquid electrodes" each. The two rows are driven by independent signals. The left and right side are defined as they would be seen by a flowing particle. In figure 2.7, the left side corresponds to the upper side of the top view.

The left side is driven by the superposition of two electrical signals (V_1 in figure 2.7 is equal to $V_{11} + V_{12}$). One of them has a low and constant frequency ($< 100 \text{ kHz}$) whereas the second one has a frequency that varies during the experiments to achieve the best performances in terms of separation efficiency. Their respective amplitudes are also adjusted to achieve high separation efficiency. On the other side of the array, a single signal at low and constant frequency ($< 100 \text{ kHz}$) is applied (V_2 in figure 2.7). The definition of the two low frequencies considers the theory about multiple-frequency dielectrophoresis of previous sections. Thus these signals are generally at same frequency with a 90 degrees phase shift, *i.e.* quadrature signals. The three amplitudes and frequencies differ from one application to another according to the biological materials that have to be separated.

2.4 Multiple-frequency dielectrophoresis

Conceptually, the two signals at low frequencies, one on each side of the array, are used to focus the cells towards an equilibrium line. Therefore, these electrical signals have to generate nDEP-forces to allow the focusing. Moreover, their frequencies need to be close enough such that they produce the same dielectric response of the different cell types. Otherwise, the cell types would not be focused towards the same equilibrium line (this is illustrated in section 4.3.2) and the subsequent dielectric characterization would be disturbed. The separation of the different cell types is obtained by the addition of the third electrical signal. This third signal is set at a particular frequency for which the dielectric responses of the cell types differ. Thus the positions of equilibrium, that were equal for all cell types so far, are modified differently for each cell type since each cell type perceives a distinct set of DEP-forces. Given the configuration of the three electrical signals, the resultant DEP-force, or the total DEP-force, exerted on cells is the superposition of the three DEP-forces according to the theory of multiple-frequency dielectrophoresis.

2. AC ELECTROKINETICS: FUNDAMENTALS AND MODELING

Bibliography

- Arnold WM, Schwan HP and Zimmermann U, 1987: *Surface Conductance and Other Properties of Latex-Particles Measured by Electrorotation*. Journal of Physical Chemistry, vol. 91(19): 5093–5098.
- Asami K and Yonezawa T, 1995: *Dielectric behavior of non-spherical cells in culture*. Biochimica et Biophysica Acta - General Subjects, vol. 1245(3): 317–324.
- Asami K, Hanai T and Koizumi N, 1976: *Dielectric properties of yeast cells*. Journal of Membrane Biology, vol. 28(2-3): 169–180.
- Castellanos A, Ramos A, Gonzalez A, Green N and Morgan H, 2003: *Electrohydrodynamics and dielectrophoresis in microsystems: Scaling laws*. Journal of Physics D: Applied Physics, vol. 36(20): 2584–2597.
- Demierre N, Braschler T, Linderholm P, Seger U, Van Lintel H and Renaud P, 2007: *Characterization and optimization of liquid electrodes for lateral dielectrophoresis*. Lab on a Chip - Miniaturisation for Chemistry and Biology, vol. 7(3): 355–365.
- Gascoyne P, Satayavivad J and Ruchirawat M, 2004: *Microfluidic approaches to malaria detection*. Acta Tropica, vol. 89(3): 357–369.
- Holzel R and Lamprecht I, 1992: *Dielectric properties of yeast cells as determined by electrorotation*. Biochimica et Biophysica Acta - Biomembranes, vol. 1104(1): 195–200.
- Huang Y, Holzel R, Pethig R and Wang XB, 1992: *Differences In The Ac Electrodynamic Of Viable And Nonviable Yeast-Cells Determined Through Combined Dielectrophoresis And Electrorotation Studies*. Physics In Medicine And Biology, vol. 37(7): 1499–1517.

BIBLIOGRAPHY

- Jones TB, 1995: *Electromagnetics of Particles* (Cambridge University Press, Cambridge).
- Kaler K, Xie JP, Jones T and Paul R, 1992: *Dual-frequency dielectrophoretic levitation of Canola protoplasts*. *Biophysical Journal*, vol. 63(1): 58–69.
- Morgan H and Green NG, 2002: *AC Electrokinetics: Colloids and Nanoparticles* (Research Studies Press, Baldock, Hertfordshire, UK).
- Pethig R and Kell D, 1987: *The passive electrical properties of biological systems: Their significance in physiology, biophysics and biotechnology*. *Physics in Medicine and Biology*, vol. 32(8): 933–970.
- Pethig R, Talary M and Lee R, 2003: *Enhancing Traveling-Wave Dielectrophoresis with Signal Superposition*. *IEEE Engineering in Medicine and Biology Magazine*, vol. 22(6): 43–50.
- Raicu V, Raicu G and Turcu G, 1996: *Dielectric properties of yeast cells as simulated by the two-shell model*. *Biochimica et Biophysica Acta - Bioenergetics*, vol. 1274(3): 143–148.
- Seger U, Gawad S, Johann R, Bertsch A and Renaud P, 2004: *Cell immersion and cell dipping in microfluidic devices*. *Lab on a Chip - Miniaturisation for Chemistry and Biology*, vol. 4(2): 148–151.
- Sun T, Green N, Gawad S and Morgan H, 2007: *Analytical electric field and sensitivity analysis for two microfluidic impedance cytometer designs*. *IET Nanobiotechnology*, vol. 1(5): 69–79.
- Talary MS, Burt JPH, Tame JA and Pethig R, 1996: *Electromanipulation and separation of cells using travelling electric fields*. *Journal of Physics D: Applied Physics*, vol. 29(8): 2198–2203.
- Tornay R, Braschler T, Demierre N, Steitz B, Finka A, Hofmann H, Hubbell J and Renaud P, 2008: *Dielectrophoresis-based particle exchanger for the manipulation and surface functionalization of particles*. *Lab on a Chip - Miniaturisation for Chemistry and Biology*, vol. 8(2): 267–273.

BIBLIOGRAPHY

Urdaneta M and Smela E, 2007: *Multiple frequency dielectrophoresis*. *Electrophoresis*, vol. 28(18): 3145–3155.

BIBLIOGRAPHY

Chapter 3

Microfluidic platform using "liquid electrodes"

Summary In this chapter is introduced the concept of "liquid electrode" which is an essential aspect of this thesis. The chip design is then presented, showing how the concept of "liquid electrode" is integrated into a microfluidic platform. Finally, the steps of microfabrication are described, as well as the fluidic and electrical interfaces that connect the microfluidic device to pneumatic pressure and function generators respectively.

3.1 The "liquid electrode"

3.1.1 General concept

An essential aspect of our continuous-flow cell separation method is the generation of the dielectrophoretic forces and its consequences. To do so, we propose an arrangement of planar metal electrodes and a patterned insulator based on the principle of iDEP. This arrangement aims to replace the use of microelectrodes on the top and the bottom of a microchannel as often encounter in diverse microfluidic applications. The insulator defines the fluidic network whose main parts are the central channel and several perpendicular dead-end chambers. For the sake of clarity, we defined a particular terminology which is represented in figure 3.1a. Here, in contrast to classical designs

3. MICROFLUIDIC PLATFORM USING "LIQUID ELECTRODES"

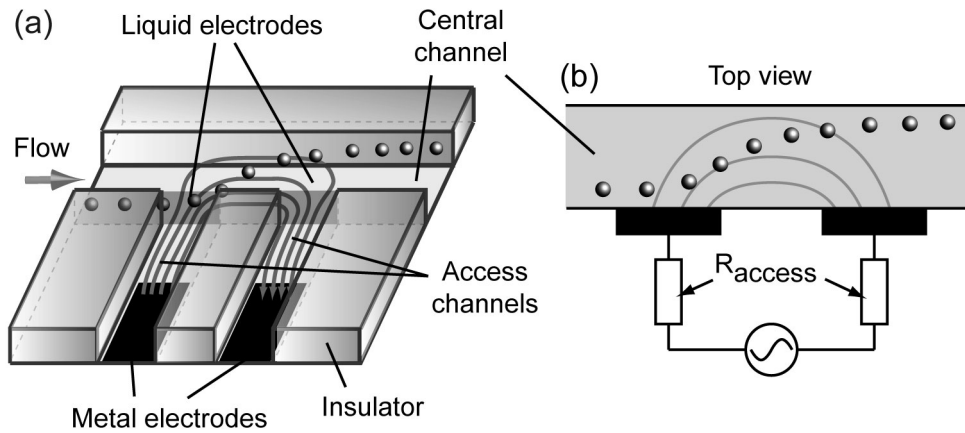


Figure 3.1: (a) 3D scheme of the basic geometrical arrangement of metal electrode and patterned insulator used for deviating flowing cells. The two equipotential surfaces located at the junctions of the access channels and the central channel are referred to as "liquid electrodes". (b) The electrical model of the "liquid electrode" is represented by a vertical metal electrode on the sidewall of the central channel with an access resistance.

of microelectrodes, the metal electrodes are deposited on the bottom of the perpendicular dead-end chambers, *i.e.* apart from the central channel. The metal electrodes are planar and large, which provide high interfacial capacitance and robustness regarding eventual metal degradations. They are connected to the central channel through narrow channels that are called access channels. When a potential difference is applied to a pair of metal electrodes, an electric field is created and a current flows from the first metal electrode through the access channels and the central channel to the second metal electrode. The current path is defined by the geometry of the insulator that actually guides the electric-field lines and determines the electric-field distribution within the central channel as shown in figure 3.1a). The vertical surface boundaries between the access channels and the central channel are referred to as "liquid electrodes". We call them electrodes because they are approximately equipotential surfaces (refer to the numerical calculations of section 2.3.2) through which current is injected. The homogeneous distribution of potentials of the "liquid electrodes" is a consequence of the access channels that force the electric-field lines to run in parallel. The "liquid electrodes" can be conceptually seen as vertical electrodes located on the sidewalls of the

central channel (refer to the drawings (a) and (b) of figure 2.6). An example of such vertical electrodes on the sidewall has been recently reported by Wang *et al.* (2007). For potentially similar performances in DEP-based cell manipulations, their structure is more complicated to integrate into a microfluidic device and requires costly processes of microfabrication.

The potentials of the "liquid electrodes" are different from the potentials applied at the metal electrodes that lie behind because of the potential drop in the access channels. A numerical calculation (similar to the one of section 2.3.2) can be used to estimate the resistance of the central channel and the access channel. The appropriate model for the "liquid electrode" is a vertical electrode with an known access resistance, as shown in figure 3.1b.

The distribution of the electric field within the central channel is determined by the insulator geometry rather than by the metal electrodes themselves. Even though the metal electrodes are horizontal and located on the bottom of the chambers, the current is injected into the main channel through vertical equipotential surfaces that are referred to as "liquid electrodes". Hence, the field distribution is homogeneous across the height of the central channel. The non-uniformities of the electric field appear mainly at the corners of the insulator geometry, *i.e.* at the surface of the "liquid electrode". Thus, the DEP-force generated by these electric-field non-uniformities acts horizontally, as previously described in section 2.3. This DEP-force acts on flowing particles and moves them towards the opposite side of the central channel as schematized in figure 3.1a.

The "liquid electrode" provides some major advantages over classical microelectrodes. The larger surfaces of the planar metal electrodes increase the interfacial capacitance and can therefore inject comparatively more current, in particular at low frequencies. The large surfaces also provide robustness and stability of the DEP-force. Indeed, a small defect of the metal electrode would not disturb the field distribution. The integration of "liquid electrodes" in a microfluidic device for manipulating particles has been patented by Renaud *et al.* in 2006. The granting procedure is still in progress.

3. MICROFLUIDIC PLATFORM USING "LIQUID ELECTRODES"

3.1.2 Array of "liquid electrodes"

As outlined in theoretical section 2.3.1, a pair of "liquid electrodes" as shown in figure 3.1a can generate a nDEP-force which is able to push the particles towards the opposite side of the central channel. The single pair of "liquid electrodes" can be duplicated in order to improve the efficiency of the deviation by adding the effect of each pair. Moreover, the theoretical section 2.4.3 proposed to oppose two DEP-forces in order to create positions of equilibrium towards which particles are focused. These equilibrium positions define actually a line in the direction of the central channel. Its position across the central channel is determined by the amplitudes of the two counteracting DEP-forces. The opposition of this second DEP-force is simply achieved by repeating the arrangement of "liquid electrodes" of the first side of the central channel on its other side. The resulting structure is a central channel that have a row of "liquid electrodes" on its both sides. The final arrangement is represented in figure 3.2. The number of "liquid electrodes" of each row is theoretically unlimited but practically restricted to fifteen because of the electrical interface (described later on in section 3.4.1).

The whole electrode array represented the figure 3.2 allows to generate two opposite electric fields. Using the principle of multiple-frequency dielectrophoresis described in section 2.4, the superposition of electrical signals at multiple frequencies, that are independently applied to the both sides of the electrode array, allows to configure as many different set of DEP-forces as required by the applications. Thus, this structure can be used in applications of deviation and focusing of particles or continuous-flow separation of cells.

3.2 Chip design

This section reports on the integration and the design of "liquid electrodes" in a microfluidic platform that consists of two main parts: the electrodes and the fluidic network.

3.2.1 Electrodes

The role of the integrated electrodes is to bring the the electrical signals from outside the microfluidic platform towards a precise location inside the chip, *i.e.* the central

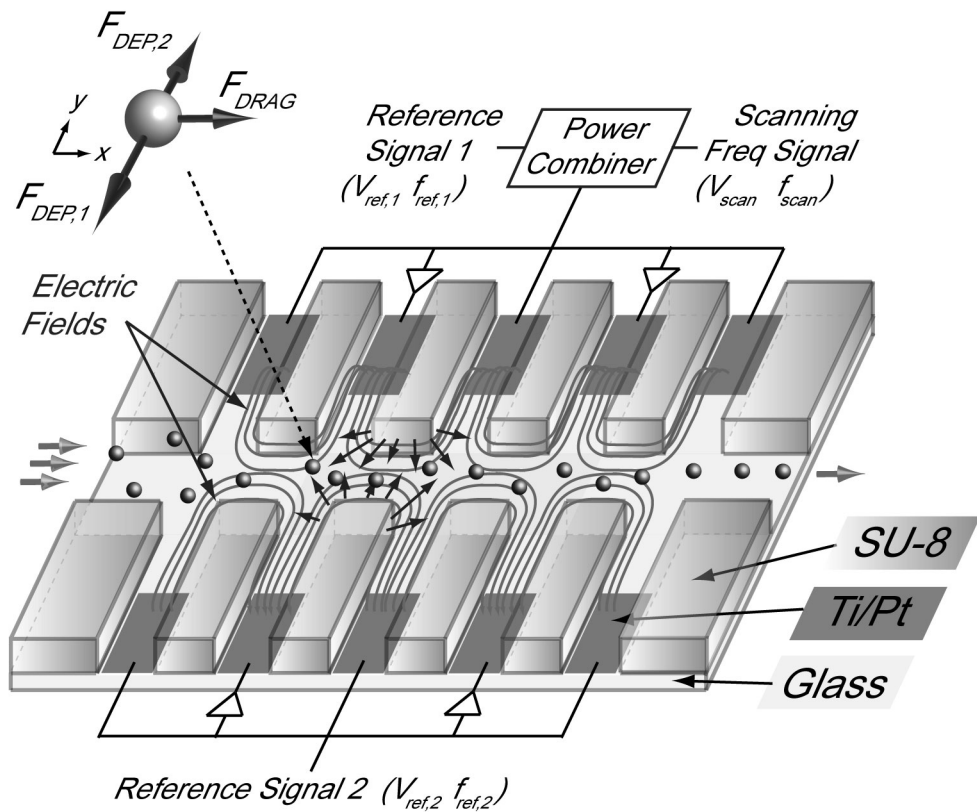


Figure 3.2: 3D scheme of the geometrical arrangement of "liquid electrodes". A combination of metal electrodes (black rectangles) with a patterned insulator (transparent volumes) is used to generate an electric field (represented by the black curved arrows) within the central channel where particles flow. Single- or multiple-frequencies signals are applied to the metal electrodes in order to create two opposite DEP-forces. The increased view of a bead (on the top left corner) represents the set of forces that are exerted on a single particle.

3. MICROFLUIDIC PLATFORM USING "LIQUID ELECTRODES"

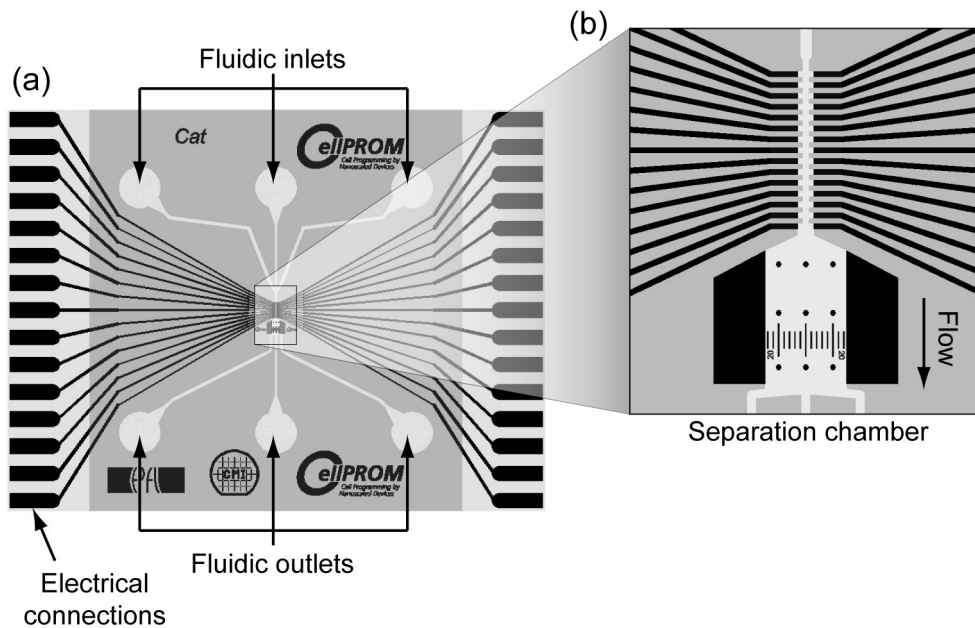


Figure 3.3: (a) Design of the microfluidic platform that consists of two main parts: the electrodes and the fluidic network. The chip contains fifteen electrical connections on left and the right sides and three fluidic connections on the top and the bottom sides. The electrodes converge towards the central channel into which they inject a current. The three fluidic inlets merge to form the central channel which is then split into three fluidic outlets. (b) shows an increased view of separation chamber.

channel. The fifteen electrical connections located on each side of the microfluidic chip have a fingerprint that corresponds to the electrical spring connectors that interface the chip to an electronic circuit (detailed later on in section 3.7). Figure 3.3 shows the metal lines (in black) that start from the sides of the chip and converge towards the center of the chip where is located the central channel (shown in the increased view in figure 3.3b).

Each metal line ends with a typical width of $20 \mu m$ in a separated dead-end chamber defined by the insulator (refer to section 3.1). In these chambers, the metal electrodes are put into contact with the liquid that fills the central channel and the perpendicular chambers. The contact surfaces have typical dimensions of $20 \mu m \times 100 \mu m$ (shown in

figure 3.4b). These contact surfaces create an electric field between successive electrodes by injecting a current into the central channel.

3.2.2 Fluidic network

The fluidic network has three main functions:

- To bring the biological materials suspended in liquids from the fluidic inlets towards the central part of the chip where the separation occurs.
- To define an area downstream from the separation where a good imaging of the separated species can be performed for further characterization of the separation efficiency.
- To allow the collection of the separated fractions of the initial biological materials.

The fluidic design shown in figure 3.3 is basically a network of microchannels. A set of three fluidic inlets with a typical width of $100\ \mu m$ (top side in figure 3.3a) converge towards the middle of the chip. There, they merge to form a unique central channel. The number of three for the inlets increases the flexibility of the microfluidic platform and for example allows the use of sheath flow to align particles. The width of the central channel varies along the length. It has an initial value of $60\ \mu m$ that then narrows to $20\ \mu m$ in the area of the "liquid electrodes" array. Right after this, it widens to a width of $300\ \mu m$. The reason of this widening is to slow down the flow velocity, which facilitates the imaging of the separated populations for characterization. The central channel, the array of "liquid electrodes" on its both sides and the wider channel downstream from the array form together the so called separation chamber (figure 3.3b). Finally, the wider part of the central channel splits into three fluidic outlets (bottom side of figure 3.3a). The split into three outlets offers the possibility to collect distinct fractions of the separated cell types.

3.3 Microfabrication

The objective regarding the microfabrication of the microfluidic platform is to maintain a level of complexity as low as possible. A simple microfabrication process is reliable,

3. MICROFLUIDIC PLATFORM USING "LIQUID ELECTRODES"

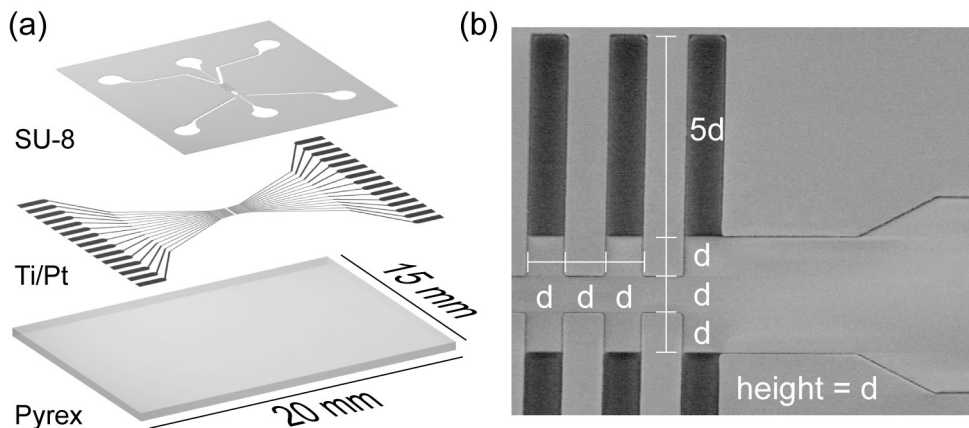


Figure 3.4: (a) Microfabrication process: The Ti/Pt electrodes are deposited by lift-off on a glass substrate prior to the definition of the channels in SU-8 by photolithography. (b) Definition of the characteristic geometrical dimension d of the chip which is $20 \mu\text{m}$ in most applications.

i.e. provides similar chips at each run, and is less time consuming. Thus, fast iterations of chip design and chip production allow to evaluate different configurations and converge towards the optimum microfluidic platform.

The microfabrication of our sorting device is based on a two-masks process. The main fabrication steps are depicted in figure 3.4a. The chip production starts with the deposition of a metal layer on a 4" pyrex wafer. This layer consists of 20 nm of titanium (Ti) and 200 nm of platinum (Pt). The Ti layer is used to enhance the adhesion of the Pt layer on the glass wafer. The electrodes are defined in this layer by a lift-off process (Madou, 2002). The fluidic network is produced on top of the electrodes by photolithography of a layer of SU-8 with a thickness of $20 \mu\text{m}$. This thickness defines the height the channels and can be adjusted to other values according to the biological materials used in applications of separation. The microfabrication of the microfluidic platform finishes with the dicing of the wafer into sixteen single devices. A single device is 20 mm long and 15 mm wide and contains channels that are open on the top. Its electrical and fluidic interfacing is presented in the next section.

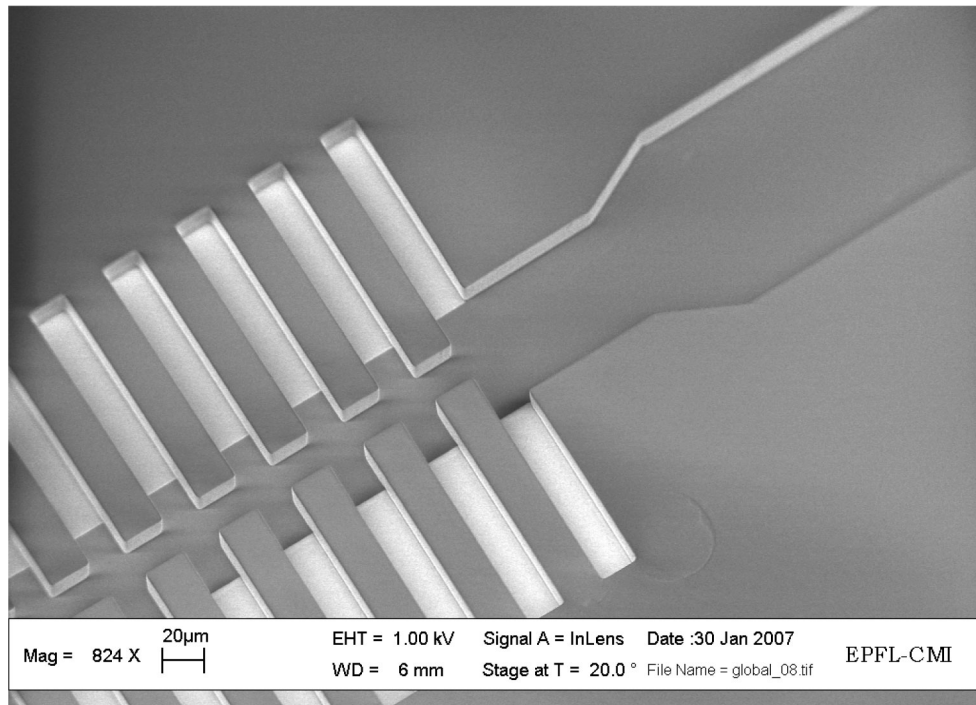


Figure 3.5: SEM image of the central channel sided by the electrode array and the channel widening that facilitates cell observation by slowing down the flow velocity and distributing the cells over a wider area.

The characteristic geometrical dimension d of the microfluidic device is shown in figure 3.4b. Two versions of designs are used throughout all the experiments in this thesis and according to the application targeted and the biological materials to be sorted. The two versions only differ in the value of d ($20 \mu m$ and $40 \mu m$) but both at a constant channel height of $20 \mu m$.

3.4 Chip interfaces

3.4.1 Fluidic setup

The microfabrication process presented previously produces fluidic channels that are open on the top. For the fluidic interfacing, the microfluidic platform is placed on a mechanical support (chip holder). A molded part of silicon (PDMS) is deposited onto

3. MICROFLUIDIC PLATFORM USING "LIQUID ELECTRODES"

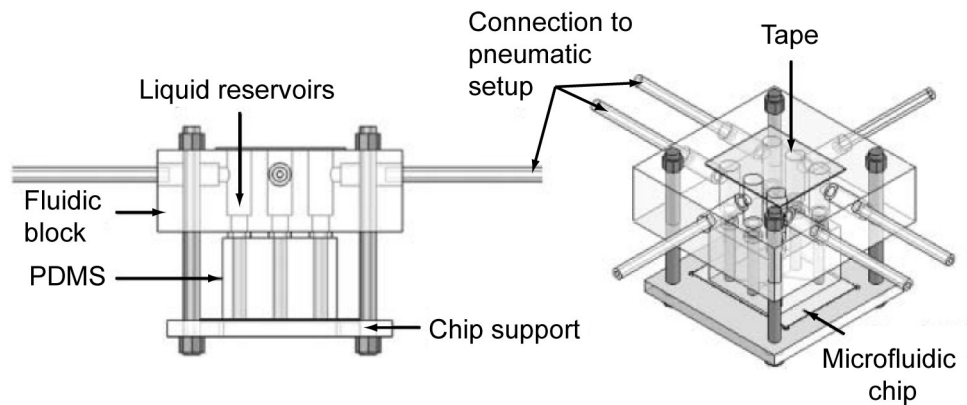


Figure 3.6: Fluidic interface: the microfluidic chip is held by a plastic chip support and assembled with a PDMS cover. A fluidic interface block with embedded reservoirs is mounted on top and connects the reservoirs to the pneumatic setup. *Image published in Braschler et al. (2007)*

the chip, which closes the channels. The sealing of the fluidic network by the PDMS part is obtained by exerting of a mechanical pressure between them with a plastic block. The "sandwich" assembly is shown in figure 3.6.

The handling of liquids is performed by pressure-driven flow (PDF) as described in section 1.4. The liquids are initially loaded into reservoirs that are embedded in the PDMS part. They are then moved through the channels by the pneumatic pressure control, as previously presented by Braschler *et al.* (2007). A oxygen-plasma treatment (40 s at 50 W) of the microfluidic platform and the PDMS part enhances the priming step, *i.e.* the initial filling of channels with liquid. The filling of the perpendicular dead-end chambers is possible only due the gas-permeability property of the PDMS.

3.4.2 Electrical setup

The electrical setup comprises all the electrical equipments required to generate a set of DEP-forces within the central channel of the microfluidic platform. The electric field at the origin of the dielectrophoresis is created by applying a potential difference to consecutive metal electrodes, in total two rows of fifteen electrodes. The function of the

electrical setup is to produce and distribute the right electrical signal to each electrode. The original signal, coming from a function generator, needs to be conditioned before being distributed.

A dedicated home-made printed circuit board (PCB) has been designed for the purpose of amplifying and conditioning two electrical signals coming from function generators and distributing them to each chip electrode. A picture of the PCB is shown in figure 3.7a. The PCB contains two symmetrical electronic circuits, one on each side, to drive independently the two sides of the integrated electrode array. The electronic circuit consists of a combination of an operational amplifier (op-amp) with an inverse op-amp. Both are shown in figure 3.7. Their gain are five and minus five respectively. The conditioning consists of splitting the input electrical signal into two amplified electrical signals with a 180 degrees phase shift. The input can be either a single signal or a superposition of several signals. Each chip electrode can be connected to either the non-inverse amplified signal or the inverse amplified signal, according to the targeted application, by using a set of configurable jumpers . The typical configuration used for the applications reported in this thesis is an alternated distribution of inverse and non-inverse signals.

The electronic circuit provides a constant amplification over a frequency range from 10^2 to 10^7 Hz. The amplified output signals have a maximum peak-to-peak amplitude of ≈ 28 V each. The combination of op-amp with inverse op-amp produces a maximum peak-to-peak potential difference between two consecutive electrodes of ≈ 56 V.

3. MICROFLUIDIC PLATFORM USING "LIQUID ELECTRODES"

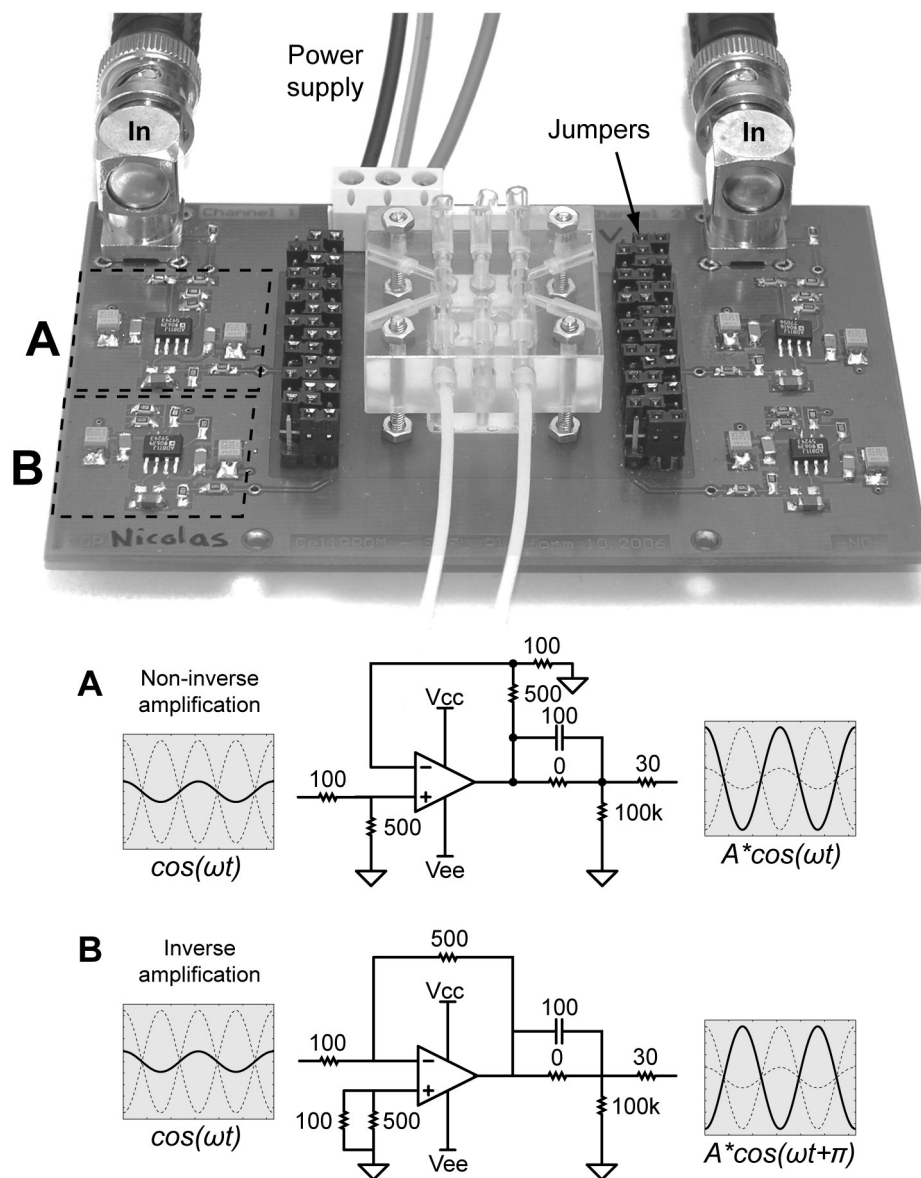


Figure 3.7: Electrical interface. The electronic circuit of printed circuit board is designed for purpose of signal amplification and distribution to the chip electrodes. The input electrical signal is amplified by a pair of (A) non-inverse and (B) inverse amplifiers (see electronic circuits in boxes with resistance value in Ω and capacitance in nF). Each chip electrode can be connected to either the inverse or non-inverse amplified signal by using jumpers. The PCB contains two sites of amplification (on the left and on the right) to drive independently the two rows of the electrode array of the microfluidic platform.

Bibliography

Braschler T, Metref L, Zvitov-Marabi R, Van Lintel H, Demierre N, Theytaz J and Renaud P, 2007: *A simple pneumatic setup for driving microfluidics*. Lab on a Chip - Miniaturisation for Chemistry and Biology, vol. 7(4): 420–422.

Madou MJ, 2002: *Fundamentals of microfabrication* (CRC Press).

Renaud P, Linderholm P, Braschler T, Demierre N and Seger U, 2006: *Apparatus for manipulating, modifying and characterising particles in a micro channel*. International Patent Application PCT/IB2007/050338.

Wang L, Flanagan L, Jeon N, Monuki E and Lee A, 2007: *Dielectrophoresis switching with vertical sidewall electrodes for microfluidic flow cytometry*. Lab on a Chip - Miniaturisation for Chemistry and Biology, vol. 7(9): 1114–1120.

BIBLIOGRAPHY

Chapter 4

Electrical manipulation and characterization of particles

Summary This chapter reports on basic electrical manipulations of cells in the microfluidic platform. The deviation of particles as a function of the flow velocity is evaluated as well as the efficiency of particle focusing from two counteracting DEP-forces. Finally, a method to characterize the dielectric properties of the particles based on the readout of their positions is presented.

4.1 Materials and methods

4.1.1 Suspension medium

For all experiments, we use a solution of phosphate buffered saline (PBS) diluted with deionized water to $60 \text{ mS} \cdot \text{m}^{-1}$. For applications involving the use of biological cells, the PBS solution is supplemented with 0.1% (w/w) of bovine serum albumine (BSA) to reduce cell sticking to the channel walls. BSA contains a tremendous amount of free proteins that saturate and block the adsorption sites of the walls.

4.1.2 Preparation of suspended particles

For the electrical manipulations, polystyrene beads, carboxyl-modified with a diameter of $5.14 \mu\text{m}$ are suspended in the PBS solution. The calculation of the CM factor for

4. ELECTRICAL MANIPULATION AND CHARACTERIZATION OF PARTICLES

these polystyrene beads gives a constant value for our frequency range equal to -0.5 (refer to section 2.2.3). In the applications of focusing, yeast cells are used in addition to the polystyrene beads. Viable yeast cells (> 99% viability according to trypan blue stain) were obtained from a local grocery store (baker's yeast, *Saccharomyces cerevisiae*). Beads and yeast cells are suspended together in the solution of PBS.

4.1.3 Particle tracking

Particle trajectories are obtained by video recordings (high-speed color camera *uEye* up to 80 *fps*) of the trace of green-fluorescent 5.14 μm polystyrene beads. The particle tracking is then performed in two steps of image analysis from the open-source softwares *VirtualDub* and *ImageJ*. The first step converts the videos into sequences - or stacks - of images in greyscale where a color threshold is applied to extract the information of interest. In the second step, the image sequence is loaded into *ImageJ* and processed with the open-source plugin *Mtrack2* which is customized to account for general laminar flow. *Mtrack2* produces a list of particle positions in different frames as its output. Speed vectors and particle positions are finally calculated in the commercial software *Matlab*[©]. The particle tracking is used to evaluate the deviation and focusing (section 4.3).

4.1.4 Image analysis

In order to evaluate the cell separations, all the experiments are recorded using the same camera as in the particle tracking. The camera is focused on the enlarged part of the central channel downstream from the electrode array. The movies are then also converted into stacks of images. The positions of the particles on the images, in particular in the y-axis, are then manually recorded using the plugin *Point Selection* of *ImageJ*. The output data is an array of particle positions that is then manipulated with home-made scripts in *Matlab*[©]. The separation results are generally finally represented in an histogram of cell count as a function of the normalized position across the channel.

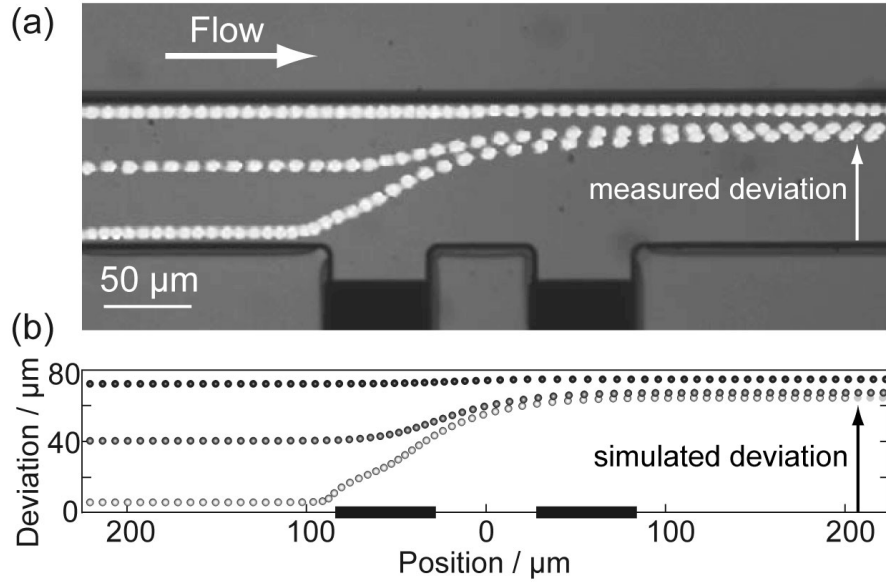


Figure 4.1: Tracking of lateral deviation for $5.14 \mu m$ beads with a constant $\Re \tilde{f}_{CM} = -0.5$. (a) Overlay of video frames taken at a rate of 80 fps , with a fluid flow speed of $140 \mu m \cdot s^{-1}$. (b) Numerical simulation of lateral deviation with identical geometry and parameters as used in (a).

4.2 Deviation of particles

The first electrical manipulation of particles that flow through the central channel is the deflection of their particle trajectories. The results of this section have been published in Demierre *et al.* (2007). The deviation is obtained from a single pair of "liquid electrodes" located on the right side of the central channel. The geometry of the structure for deviation applications is shown in figure 4.1a. The central channel has a width and a height of 80 and $20 \mu m$ respectively. The width of the "liquid electrodes" and the insulator between the two electrodes is equal to $56 \mu m$.

The movement of particles caused by the DEP-force is evaluated by recording and analysis of time-lapse videos. The DEP-force is generated from an electrical signal with a rms (root mean square) amplitude value of 9.75 V at 2 MHz . An overlay of video frames extracted from an experiment of particle deviation is shown in figure 4.1a.

4. ELECTRICAL MANIPULATION AND CHARACTERIZATION OF PARTICLES

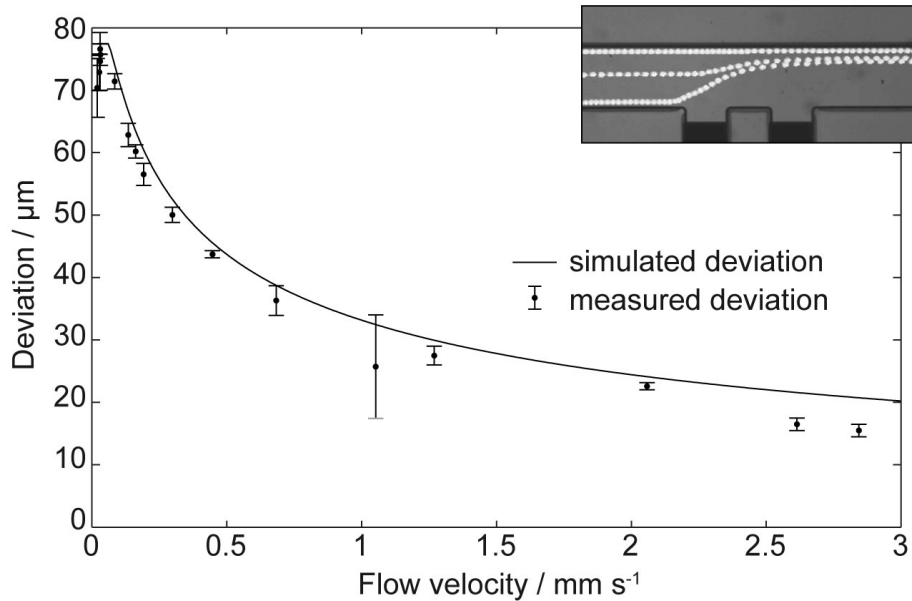


Figure 4.2: Lateral deviation as a function of flow speed in the same structure, both measured (points) and simulated (solid line). For each simulation, a constant flow speed with speed vectors aligned along the x-axis is assumed, as well as a constant $\Re(\tilde{f}_{CM}) = -0.5$ for the $5.14 \mu m$ polystyrene beads.

Figure 4.1b shows simulated particle trajectories for a set of geometrical and electrical parameters similar to the ones used in the video recording in figure 4.1a. The simulated trajectories show a good agreement with the measured trajectories. To obtain a quantitative result, the deviation was evaluated for different flow velocities. The deviation, defined as the width of the particle-free zone in the lower part of the channel downstream from the "liquid electrodes", is represented in figure 4.2 as a function of the flow velocity. Again, one can observe on the graph that the deviation are well predicted by numerical simulations.

The predictions of deviations by numerical simulation could be further improved if we could better evaluate the particle speed. The particle velocities follow a parabolic distribution which is determined by the profile of the pressure driven flow. Moreover, the particle velocities are frequently increased downstream from the deviating structure. These increases are likely due to a vertical centering of particles in the central

channel. The centering phenomenon is a possible consequence of a squeezing of the electric-field lines between the insulating particle and an insulating boundary, which creates local non-uniformities that give raise to a repulsive nDEP-force.

4.3 Focusing of particles

The next electrical manipulation of particles is an application of focusing whose results have been published in Demierre *et al.* (2007). The focusing is an extension of the deviation application and basically consists of two counteracting deviating structures. For this purpose, a combination of two pairs of "liquid electrodes", one on each side of the central channel, is used to achieve the focusing of $5.14 \mu\text{m}$ polystyrene beads (figure 4.3a). Each pair is individually able to deviate the particles towards the opposite sidewall. The combined action of the two pairs focuses the particle stream towards an equilibrium position (refer to section 2.4.3.1). The structure we used in this experiment has a characteristic geometrical dimension d (see section 3.4) and height of $20 \mu\text{m}$ in the active area. The channel width is $100 \mu\text{m}$ apart from the active area.

Two single-frequency DEP-forces $\mathbf{F}_{DEP,1}$ and $\mathbf{F}_{DEP,2}$ are generated in the central channel whose magnitudes are controlled by $V_{ref,1}$ and $V_{ref,2}$. For the same reason as in section 2.4.4, the two electrical signals are at the same frequency but in quarter phase. The tuning of the focusing position in the channel is controlled by the potential ratio $\lambda = V_{ref,1}/V_{ref,2}$. If $\lambda < 0$, the stream is focused towards a position in the upper half of the channel and vice-versa.

We first investigated the influence of the flow velocity on the performances of the particle focusing towards the midline, *i.e.* $\lambda = 1$. Figure 4.3b shows measurements and numerical simulations of the focusing efficiency in terms of relative width of the particle stream (stream width / channel width) as a function of the flow velocity for two voltages (12 V and 25 V). Below a minimum speed ($0.1 \text{ mm} \cdot \text{s}^{-1}$ for 12 V , $1 \text{ mm} \cdot \text{s}^{-1}$ for 25 V), the DEP-forces act as a physical barrier and accumulate particles in front of the structure. Above this threshold, particles are precisely focused to the channel midline. Due to particle diffusion and collisions, the minimum relative width always remains greater than 0, even at very low flow velocity. Above a second velocity

4. ELECTRICAL MANIPULATION AND CHARACTERIZATION OF PARTICLES

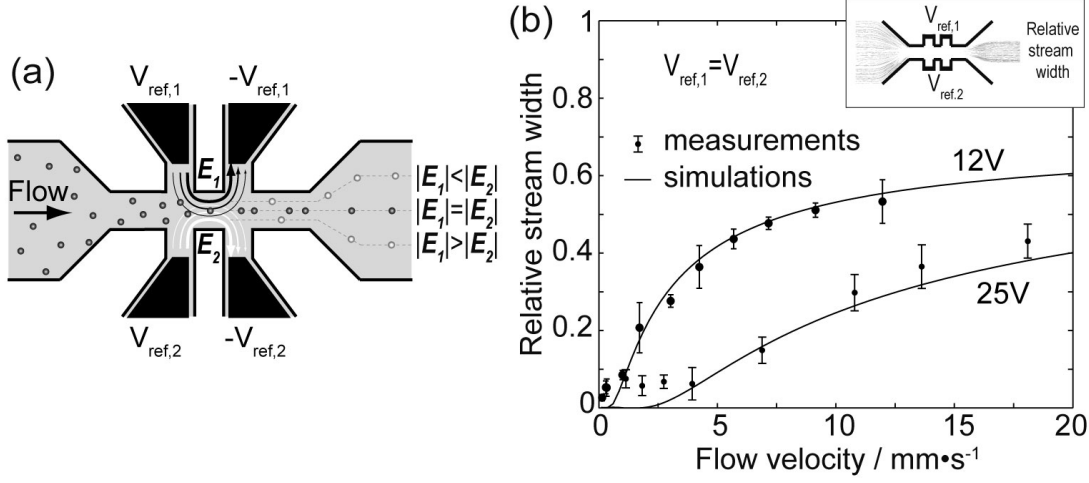


Figure 4.3: Focusing of a particle stream. (a) A four "liquid electrodes" structure where particles flowing from left to right are deflected by two opposite DEP-forces generated by E_1 and E_2 . The position of focusing can be shifted in the y -direction by adjusting the potential ratio λ ($V_{ref,1}/V_{ref,2}$). (b) Focusing of a particle stream towards the channel midline for $V_{ref,1} = V_{ref,2}$ as a function of the flow velocity for two voltages (12 V and 25 V).

threshold (about $0.5 \text{ mm} \cdot \text{s}^{-1}$ for 12 V and about $5 \text{ mm} \cdot \text{s}^{-1}$ for 25 V), the stream gets wider and wider with increasing velocity. The shape of the relative stream width is well predicted by the simulations and is a non-linear function due to the non-linear DEP-force profile across the channel (see figure 2.9). However, up to very high speeds ($> \text{cm} \cdot \text{s}^{-1}$), the particle stream remains reasonably focused.

We then demonstrated the focusing towards a variable position in the central channel as a function of λ at constant flow velocity of $2.7 \text{ mm} \cdot \text{s}^{-1}$. Figure 4.4a is a superposition of particle traces as obtained by particle tracking for 18 different values of λ . The deviation of the particles towards the lower half of the central channel (normalized positions values between 0 and -1) is obtained by keeping $V_{ref,1}$ constant at 25 V while varying $V_{ref,2}$ from 2.5 V to 25 V and similarly towards the upper half (normalized positions values between 0 and 1) by keeping $V_{ref,2}$ constant and while varying $V_{ref,1}$. The DEP-forces define together an equilibrium line where they have equal but opposite y -components. Varying λ shifts this equilibrium line vertically across the chan-

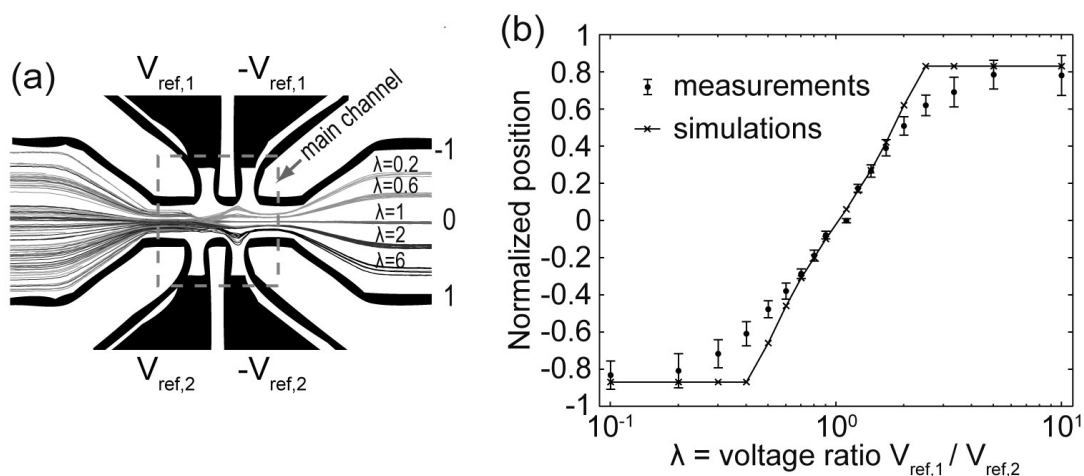


Figure 4.4: (a) Shift of the focused position of the particle stream from one side to the other side of the central channel as a function of the potential ratio λ ($V_{ref,1}/V_{ref,2}$) and at constant average flow velocity of $2.7 \text{ mm}\cdot\text{s}^{-1}$. We show 5 sets of traces obtained for 5 different λ . (b) Focusing positions as a function of λ from simulations (solid line) and from measurements (mean value and standard deviation for more than 20 particles each set).

nel as well as the focused stream. Figure 4.4b compares the simulated and measured positions of stream focusing for different λ . The measured values are reported as the mean value and the standard deviation of more than 20 particle traces for each λ value.

In general, simulations and measurements are in good agreement although the measured particle stream is closer to the midline than calculated for small and large λ values. The simulation predicts that the particles should be completely pushed towards the channel sidewall for λ smaller than 0.4 and bigger than 2.5. The particles are more repulsed from the sidewalls than calculated. This is most likely due to the discrepancy between the exact fluidic path and the one considered in the numerical calculations. The streamlines partially enter the "liquid electrodes" and bring the particles closer to the regions of strong DEP-force. In addition, it is seen that the standard deviation of the position increases as λ deviates from 1. Since we keep the higher voltage constant, values far from 1 signify on one hand a very weak opposite DEP-force and on the other hand, larger movements are needed for some particles to reach their equilibrium posi-

4. ELECTRICAL MANIPULATION AND CHARACTERIZATION OF PARTICLES

tion. The flow velocity could be too high for these λ values. Despite minor deviations, our device demonstrated high performances to focus a particle stream towards a tunable equilibrium line up to high flow velocity. It turns out to be an efficient focusing method for high-throughput microfluidic applications.

4.3.1 Effect of the particle size

We then evaluated the effect of the particle size on the focusing at constant frequency. In order to do so, a mixture of 2, 4 and 5 μm polystyrene beads was focused towards different positions across the channel. As discussed earlier, their dielectric response $\Re(\tilde{f}_{CM})$ is assumed constant and equal to -0.5 for the considered frequency range. The focusing effect was again obtained by generating two opposite negative DEP-forces from two quadrature signals at 50 kHz . The normalized output positions of the beads downstream from the electrode array, where the focusing occurs, is plotted in figure 4.5 for different voltage ratios λ . The position distributions of the three bead sizes are centered for each λ value although the distribution of the 2 μm beads is wider. This is due to a weaker force amplitude since this latter is proportional to the particle volume (equation 2.9).

As a result, particles of different sizes but similar dielectric response are focused towards the same positions. Thus, under certain conditions, the focusing is size independent. This is particularly useful when working with biological sample such as cells where size distribution is inherent to life.

4.3.2 Focusing at two frequencies

In the next set of experiments, a mixture of 5 μm beads and yeast cells were similarly focused in the central channel by the electrode array (see figure 3.2). The electrical signal driving the left side of the electrode array ($V_{ref,1}$ $f_{ref,1}$) had rms amplitude value of 10.4 V at frequencies varying from 60 kHz to 7 MHz whereas the right-side signal ($V_{ref,2}$ $f_{ref,2}$) had a rms amplitude value of 10 V at a constant frequency of 50 kHz .

The frequency sweep of the left signal aimed to evaluate the dielectric responses - or polarizations - of the two populations and highlight differences in their behaviors. Figure

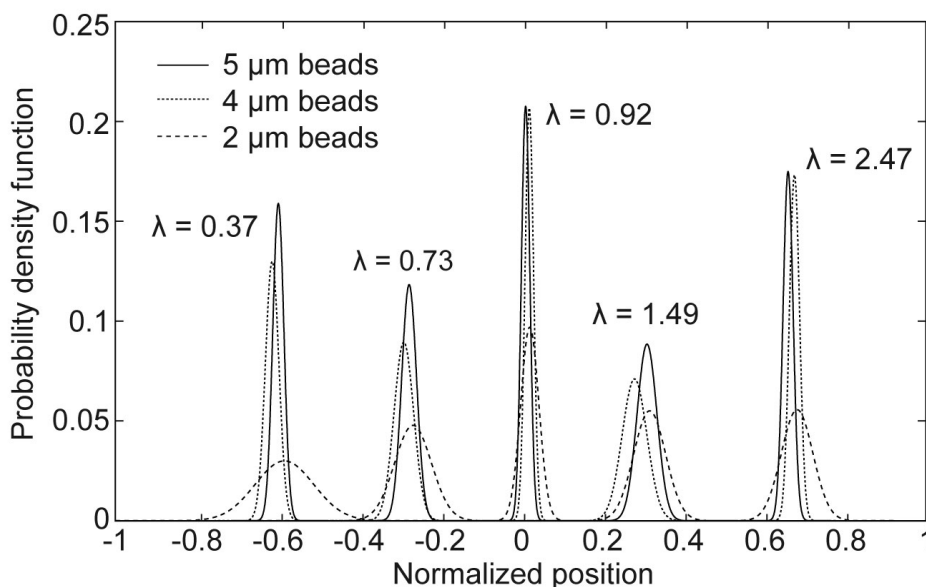


Figure 4.5: Focusing experiments of three populations of polystyrene beads (2, 4 and 5 μm) for five different voltage ratios λ . For each λ value, the two quadrature signals at a constant frequency of 50 kHz define similar equilibrium positions for the three populations. This illustrates the size independency of the focusing under these particular conditions.

4.6 shows the mean values and standard deviations of measured output positions. At frequencies below 400 kHz , both populations were focused towards the same position. But at frequencies above 400 kHz , the DEP-forces focused the two populations towards distinct positions. This critical value of 400 kHz is dependent on dielectric properties of the particles and the medium. This simple experiment shows divergences in the dielectric responses of two different populations over frequency. This results in distinct equilibrium positions and therefore spatial separation of the two species. However, with only one single-frequency signal on each side of the electrode array, it is impossible to extract information about dielectric properties of the species. For example, it is not defined if the yeast cells are focused towards negative positions (at frequencies > 400 kHz) either because they experienced a weaker nDEP-force or in contrary because they turned into a regime of pDEP. This dielectric characterization requires the use of an additional third signal. Applications where dielectric particles are characterized are

4. ELECTRICAL MANIPULATION AND CHARACTERIZATION OF PARTICLES

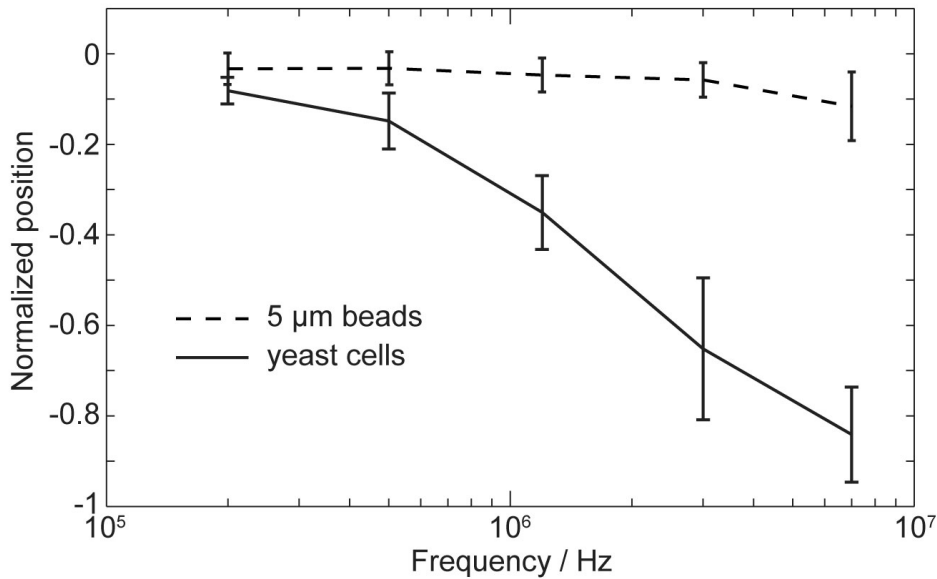


Figure 4.6: Focusing experiments with one signal at constant frequency and the other signal at frequency varying from 200 kHz to 7 MHz . The two populations are 5 μm beads and yeast cells. They remain similarly focused for frequency under the critical value of 400 kHz but separate for frequencies above the critical value. This shows the frequency-dependence of the dielectric response of the yeast cells. Frequencies below the critical value have to be used in focusing application whereas frequencies larger than the critical value are required for particle separation.

presented later on in sections 5.2 and 5.3 but the principle is explained just below.

Conceptually, the frequencies that produce a similar dielectric response of two species should be used for focusing applications. But as soon as the responses differ in a particular frequency range, the two populations are not focused anymore towards similar positions. This frequency range should rather be used in separation applications. The critical frequency value above which separation can be obtained from only two signals is a complicated function of the dielectric properties of the both populations and the medium.

4.4 Dielectric characterization of particles

The concept of multiple-frequency dielectrophoresis and the principle of equilibrium coming from the opposition of the two DEP-forces, as presented in sections 2.4 and 2.4.3.1 respectively, can be used to extract information about dielectric properties of particles involved by observing their output positions downstream from the electrode array. Beyond separating cell types according to their dielectric responses, MFDEP characterizes dielectric properties of particles in a flow manner, meaning that our microfluidic platform also acts as a flow cytometer.

4.4.1 Force balance

The dielectric characterization of particles necessitates the calibration of the device to relate the observed output position of a particle to the set of DEP-forces that it experiences. The concept of force balance is introduced to represent this set of DEP-forces. The force balance is ratio between the total DEP-force generated by the left side of the electrode array ($\mathbf{F}_{DEP,1}$) and the total DEP-force generated by the right side ($\mathbf{F}_{DEP,2}$).

To do so, independent electrical signals are applied to both sides of the electrode array to produce two opposite DEP-force fields, $F_{DEP,1}$ and $F_{DEP,2}$. Although the DEP-forces can have multiple-frequency contributions, the definition of the force balance considers opposite DEP-forces with a single-frequency contribution. Only the y-component of the DEP-force is considered since it is the only contribution to the particle movement perpendicular to the flow. In a first step, the output position of a cell is related to the force balance. The force balance is defined by the ratio between the amplitudes of two opposite DEP-forces corresponding to the midline of the central channels. Two quadrature signals at 50 *kHz* are applied to the electrode array to focus a stream of 5.14 μm polystyrene beads with nDEP. The CM factor of the beads is assumed constant and equal to -0.5 as demonstrated in section 2.2.3. It is therefore canceled in the definition of the force balance. Considering the divergences of the two electric fields responsible for the DEP-force are the same, the force balance is defined as follows:

$$force\ balance = \frac{F_{DEP,1}}{F_{DEP,2}} = \frac{V_1^2}{V_2^2} \quad (4.1)$$

4. ELECTRICAL MANIPULATION AND CHARACTERIZATION OF PARTICLES

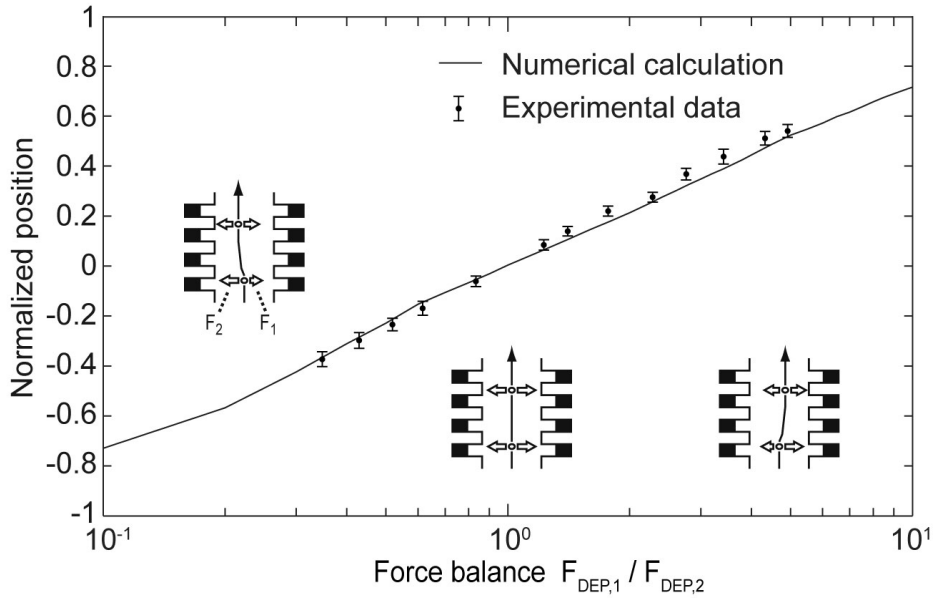


Figure 4.7: Calibration using $5.14 \mu m$ polystyrene beads. The particle stream is focused towards different normalized positions in the channels as a function of the force balance (F_1/F_2). The two opposite forces are generated by two AC signals at $50 kHz$ in quarter phase. The insets show the influence of the force balance on the particle trajectories and the dashed line represent in good agreement the results obtained by numerical simulation.

The next step is to relate the output position of the particle to the force balance. To do that, values of force balance are scanned from 0.1 to 10 by adjusting the two applied voltages V_1 and V_2 . The results of this electrical manipulation with the polystyrene beads are shown in figure 4.7, *i.e.* the normalized output position as a function of the force balance. By convention, the normalized position -1 corresponds to the left wall and $+1$ to the right wall as seen by the flowing particle. Each measurement point of the graph is the mean value and the standard deviation of the positions of a particle stream (> 20 particles). Figure 4.7 is a calibration curve that shows the relationship between the observable output positions of the particle stream and the force balance acting on the particles as follows:

$$force\ balance = f(output\ position) \quad (4.2)$$

For identical forces (*force balance* = 1), the particles are focused towards the channel midline (*normalized position* = 0). An increase of the force on one side shifts the output position towards the other side. Note that the focusing remains good, as seen by the errorbars, even at force balances far from 0. On figure 4.7 are also reported the predictions of the positions based on numerical calculation. These predictions consider the exact 3D flow distribution and correspond well with the experimental values. The small divergence probably comes from the behavior of the last electrode pair where the electric-field distribution is slightly different.

At this point it is of importance to note that all the output positions are actually equilibrium positions where the local force ratio is 1 but corresponds to a force balance reported to the midline that can be different from 1. In addition, all the particles end in the same output - or equilibrium - positions for a given force balance for whatever initial positions.

4.4.2 Definition of "opacity"

This section further exploits the calibration curve of figure 4.7 to relate the output position directly to intrinsic dielectric properties of the particles such as biological cells. The dielectric characterization is obtained from the combination of multiple-frequency dielectrophoresis (see section 2.4) and the force balance (see section 4.4.1). The typical set of electrical signals applied to the electrode array is shown in figure 3.2. It consists of a combination of a low-frequency signal ($V_{ref,1}$ $f_{ref,1}$) and an additional signal at scanning frequency (V_{scan} f_{scan}) on the left side and a single low-frequency signal ($V_{ref,2}$ $f_{ref,2}$) on the right side. Thus, $F_{DEP,1}$ of equation 4.1 corresponds to the vectorial sum of the contributions at multiple frequencies. According to equation 2.25, the force balance at multiple frequencies can be written as follows:

$$force\ balance = \frac{\Re(\tilde{f}_{CM,ref,1})V_{ref,1}^2 + \Re(\tilde{f}_{CM,scan})V_{scan}^2}{\Re(\tilde{f}_{CM,ref,2})V_{ref,2}^2} \quad (4.3)$$

The two low-frequency electrical signals are chosen such that $\Re(\tilde{f}_{CM,ref,1}) = \Re(\tilde{f}_{CM,ref,2}) = \Re(\tilde{f}_{CM,ref})$ by either considering signals with frequencies close enough (but not too

4. ELECTRICAL MANIPULATION AND CHARACTERIZATION OF PARTICLES

much to avoid beat effect) or preferentially by considering quadrature signals. Consequently, equation 4.3 simplifies as follows:

$$force\ balance = \frac{V_{ref,1}^2 + \frac{\Re(\tilde{f}_{CM,scan})}{\Re(\tilde{f}_{CM,ref})} V_{scan}^2}{V_{ref,2}^2} \quad (4.4)$$

where the only factor not determined by the experimental settings is the ratio of the CM factors. This term is called "opacity" by analogy to the terminology used in the field of flow cytometry (Gawad *et al.*, 2001) and is expressed as:

$$Opacity = \frac{\Re(\tilde{f}_{CM,scan})}{\Re(\tilde{f}_{CM,ref})} \quad (4.5)$$

Thus, the "opacity" is indeed an intrinsic dielectric property of the particle. By combining equations 4.2 and 4.4, it becomes:

$$Opacity = \frac{f(output\ position) V_{ref,2}^2 - V_{ref,1}^2}{V_{scan}^2} \quad (4.6)$$

This last equation is important and indicates that the "opacity" of a particle type can be evaluated from the readout of its output position. The "opacity" is a function of the frequency and can be fully determined by reporting the output positions at different frequencies. This dielectric characterization is enabled by the following features:

- The output position of a particle does not depend on its position upstream from the separating chamber.
- The output position of a particle, in a large extent, does not depend on the time spent in the separating chamber.

However, the "opacity" is a relative measurement according to equation 4.5 and needs a reference measurement $\Re(\tilde{f}_{CM,ref})$. Determining the CM factor of the particle requires an additional characterization in order to define this reference value $\Re(\tilde{f}_{CM,ref})$. This latter can be determined for example by evaluating a DEP-force where no equilibrium occurs or by electrorotation (Holzel and Lamprecht, 1992). In addition to separate cell types in a continuous flow, our method further allows to characterize and extract their dielectric properties, which makes our microfluidic device a flow cytometer.

Bibliography

- Demierre N, Braschler T, Linderholm P, Seger U, Van Lintel H and Renaud P, 2007: *Characterization and optimization of liquid electrodes for lateral dielectrophoresis*. Lab on a Chip - Miniaturisation for Chemistry and Biology, *vol. 7*(3): 355–365.
- Gawad S, Schild L and Renaud P, 2001: *Micromachined impedance spectroscopy flow cytometer for cell analysis and particle sizing*. Lab on a Chip - Miniaturisation for Chemistry and Biology, *vol. 1*(1): 76–82.
- Holzel R and Lamprecht I, 1992: *Dielectric properties of yeast cells as determined by electrorotation*. Biochimica et Biophysica Acta - Biomembranes, *vol. 1104*(1): 195–200.

BIBLIOGRAPHY

Chapter 5

Continuous-flow separation of cells using MFDEP

Summary In this chapter reports on the capability of our continuous cell sorting device to solve biological problems. The concepts previously introduced are combined to efficiently and continuously separate viable and nonviable yeast cells and to purify a culture of red blood cells which is subjected to a parasitic attack. The last biological application presented in this chapter is the synchronization of a cell culture based on the extraction of cells at a particular phase within their cell cycle.

5.1 Materials and methods

A brief reminder of the main aspects involved in the continuous-flow cell sorting is first given. The array of "liquid electrodes" consists of two rows that are driven with distinct electrical signals. For the purpose of continuous-flow cell sorting, a particular set of electrical signals (as schematized in figure 3.2) is applied to the electrodes in order to separate two cell types such as viable and nonviable yeast cells (presented in section 5.3) or normal and parasitized red blood cells (presented in section 5.4). The left side of the electrode array is driven by a combination of a low frequency signal that produces a nDEP-force ($V_{ref,1}$ $f_{ref,1}$) and a second signal at a varying frequency that induces a difference in the dielectric responses - or polarizations - of the two cell types (V_{scan}

5. CONTINUOUS-FLOW SEPARATION OF CELLS USING MFDEP

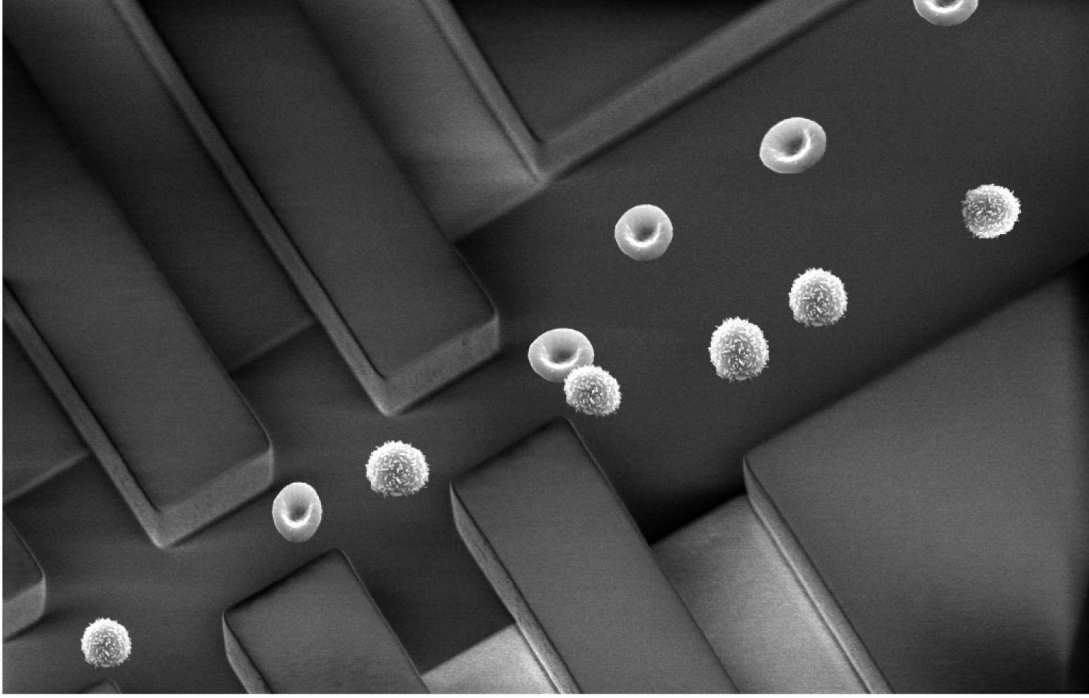


Figure 5.1: Conceptual image of the separation of cells in suspension that flow through the electrode array. Cells of different types are spatially separated because of their different dielectric response to AC electric fields. Pre fractions of each cell type can then be collected at the corresponding fluidic outlets.

f_{scan}). The right side is driven by a single-frequency signal ($V_{ref,2}$ $f_{ref,2}$) that also produces a nDEP-force and which is in quadrature with the opposite low-frequency signal.

Conceptually, the two nDEP signals focus all the cells towards an equilibrium position that depends on the voltage ratio of the two signals. This configuration avoids on the one hand the need of an additional focusing method and on the other hand cell sticking against the channel sidewalls. The third signal disturbs the equilibrium positions which were so far similar for both cell types by producing a difference in the polarization of the two cell types. The result is that the new equilibrium definitions are consequently depending on the dielectric properties of cells. The equilibrium position is therefore particular to each cell type and its position readout serves meanwhile as a

dielectric characterization of the cell properties. Contrary to Doh and Cho (2005), the separation does not necessarily come from the opposition of negative positive responses of the two cell types but more generally comes from a difference in their "opacity" (defined in equation 4.5). Thus, both cell types can exhibit the same affinity to negative or positive DEP but at different strength and still being separated in a continuous flow. Figure 5.1 is a conceptual image that illustrates the separation of two cell types, here red blood cells and white blood cells.

5.1.1 Suspension medium

For all experiments, we use a solution of phosphate buffered saline (PBS) diluted with deionized water to $60 \text{ mS} \cdot \text{m}^{-1}$. For all the application involving the use of biological cells, the PBS solution is supplemented with 0.1% (w/w) of bovine serum albumine (BSA) to reduce cell sticking to the channel walls. Indeed, the BSA contains a tremendous amount of free proteins that saturate and block the adsorption sites of the walls. When working with red blood cells in particular, the medium is furthermore adjusted to physiological osmolarity (between 280 to $310 \text{ mOsm} \cdot \text{l}^{-1}$) by adding saccharose to the suspension medium.

5.1.2 Preparation of yeast cells

Viable yeast cells, *Saccharomyces Cerevisiae*, (>99% viability according to trypan blue stain) are obtained in conditioned cubes from traditional food stores. A small amount of the sample is then diluted into the PBS solution and the cell concentration is roughly adjusted according to the application. The nonviable yeast cells are obtained from the same sample after heat treatment (20 minutes at 90°C). They are stained by methylene blue in concentration of 0.1% (w/v) for optical control.

5.1.3 Culture of infected RBCs

The protocol of infected red blood cells (RBCs) culture was developed by our partners from the biological field in Portugal¹ that investigate the cycle of *Babesia Bovis* para-

¹Instituto de Biologia Experimental e Tecnológica / ITQB, Universidade Nova de Lisboa, 2781-901 Oeiras, Portugal

5. CONTINUOUS-FLOW SEPARATION OF CELLS USING MFDEP

site (Nascimento *et al.*, 2007). *Babesia Bovis* parasite infects only bovine but presents similarities to the parasite of human malaria.

The Mo7 strain of *Babesia bovis* is grown in vitro according to the method of Levy and Ristic (1980). The cultures are maintained at a parasitemia between 1% and 3% by splitting and dilution with fresh normal bovine erythrocytes and medium. Parasitemia is monitored by microscopic examination of Giemsa-stained smears. For the experiments, cells with 1 to 20% parasitemia are suspended at a concentration of $\approx 10^5$ *cells* · *ml*⁻¹ in PBS. To quantitatively detect the degree of separation, the cells are labeled with 25 $\mu\text{g} \cdot \text{ml}^{-1}$ of ethidium bromide, a nucleic acid intercalator (red blood cells do not contain DNA except when they are infected). Label-free sorting experiments is also performed where the fraction of sorted cells is stained afterwards.

5.1.4 Image analysis

Refer to section 4.1.4 for the description of the image analysis performed to evaluate the separation performances and to characterize the dielectric particles.

5.2 Separation of beads and yeast cells

As a first separation example, an initial mixture of 5 μm beads and yeast cells was continuously separated into pure sub-populations. These results have been published by Demierre *et al.* (2007). The particles were suspended in PBS solution with an electric conductivity of 126 $\text{mS} \cdot \text{m}^{-1}$. Two low-frequency quadrature signals (50 kHz) were applied to the electrode array, one on each side (as defined in figure 3.2), for the control experiment. They focused all the particles towards a position of equilibrium centered at the normalized position of -0.26 ± 0.13 as illustrated in figure 5.2a. In order to get a separation, a third signal at varying frequency is superimposed on the left side of the array (the side of negative values of normalized positions). The two combined signals induced a multiple-frequency dielectrophoresis (see section 2.4). This frequency dependency of the particle response is illustrated in figure 5.2 where the varying frequency was swept from 200 kHz to 5 MHz .

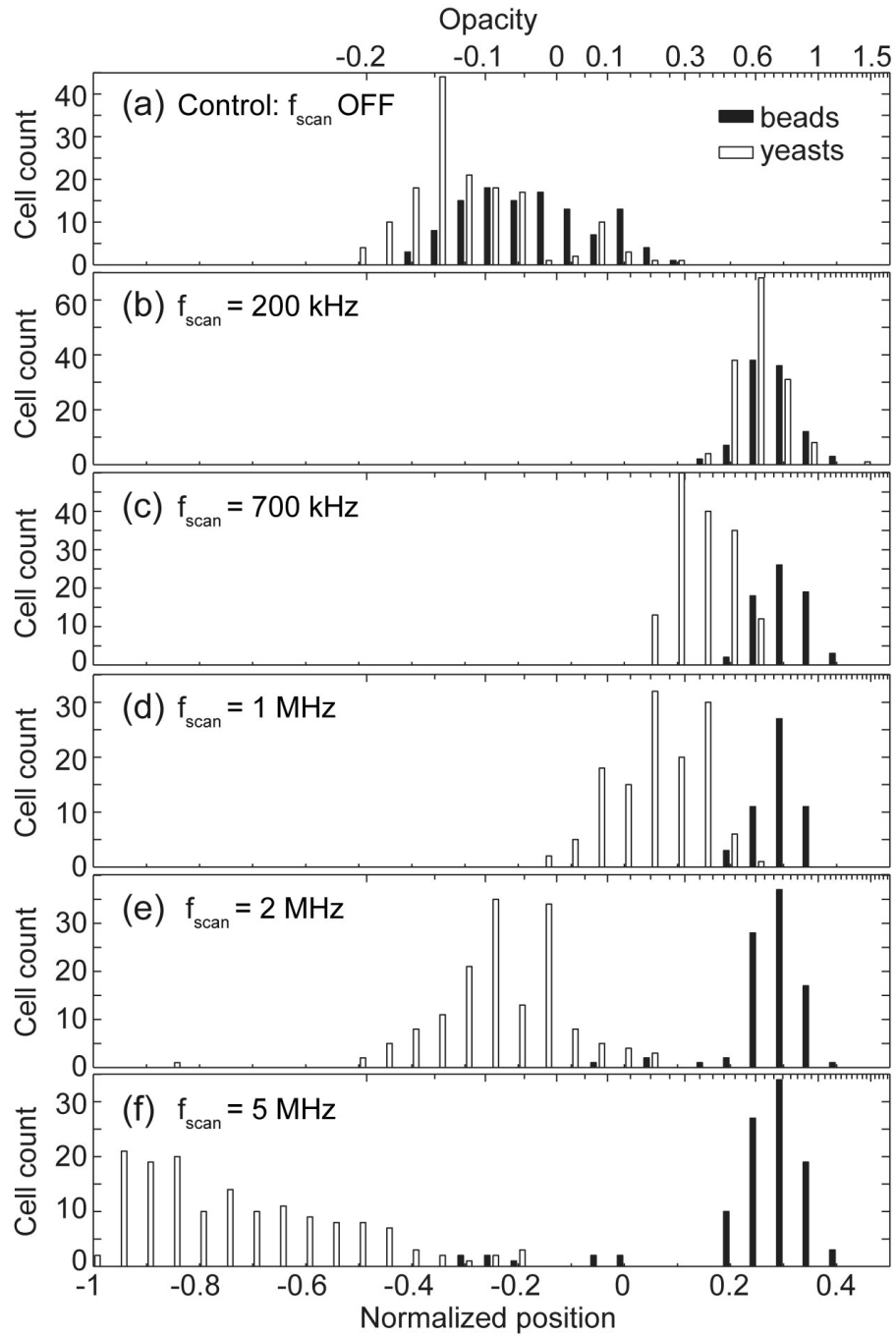


Figure 5.2: Continuous-flow separation of $5 \mu\text{m}$ beads and yeast cells. The control experiment in (a) is obtained from two counteracting nDEP-forces. For the separation, an additional DEP-force is superimposed on the left side of the electrode array. The histograms (b) to (f) show the positions of the two populations for different frequencies of the third signal. Frequencies below 2 MHz produce a nDEP-force on the yeasts whereas a pDEP-force is produced at the frequencies above 2 MHz . All frequencies produce a nDEP-force on the beads.

5. CONTINUOUS-FLOW SEPARATION OF CELLS USING MFDEP

Frequency	200 kHz	700 kHz	1 MHz	2 MHz	5 MHz
Mean meas. "opacity"	0.61	0.35	0.21	-0.07	-
Calculated "opacity"	0.90	0.38	0.19	-0.06	-0.22

Table 5.1: Comparison between the mean values of the measured "opacities" and the calculated "opacities" using a double-shell model with the parameters listed in table 2.1 except $\sigma_m = 126 \text{ mS} \cdot \text{m}^{-1}$.

At 200 kHz both populations, beads and yeast cells, experienced nDEP and were therefore indistinctly pushed towards the positive positions and centered at $+0.26 \pm 0.05$. The separation started occurring at frequencies above 700 kHz where the yeast cells experienced a weaker nDEP-force than the beads. At 2 MHz the yeasts cells are close to the same positions as in the control experiment (0.13 ± 0.24 compared to -0.26 ± 0.13). The DEP-force at 2 MHz is therefore approximately zero. This indicates the crossover frequency f_{co} for this population, *i.e.* the frequency at which the DEP changes from negative to positive. Another effect is observable. The spreading of positions increased with the increasing f_{scan} , due to the natural dispersions of sample properties such as shape, age and viability that influence the dielectric response of the particles. Histogram in figure 5.2f presents the largest spreading of cell positions over the negative normalized values due to pDEP. In contrary, the positions of the beads remained unchanged for all the frequency values. In summary, an increase in the frequency enhances the spatial separation of beads and yeasts and allows collecting pure sub-populations at the chip outlets.

5.2.1 Characterization of dielectric properties

The observation of the particle positions downstream from the electrode array gives valuable insights into the dielectric properties of the particles (as previously presented in section 4.4). We use the parameter of "opacity" to characterize the dielectric response as described in equation 4.6, where the rms values of voltages are $V_{ref,1} = 5.94 \text{ V}$, $V_{ref,2} = 4.95 \text{ V}$ and $V_{scan} = 9.11 \text{ V}$. The calculated "opacity" as a function of the positions is given in a secondary upper logarithmic scale in figure 5.2. Our device works as an "opacity meter" that correlates the output positions of particles with their intrinsic dielectric properties through the "opacity". The "opacity" of the beads is

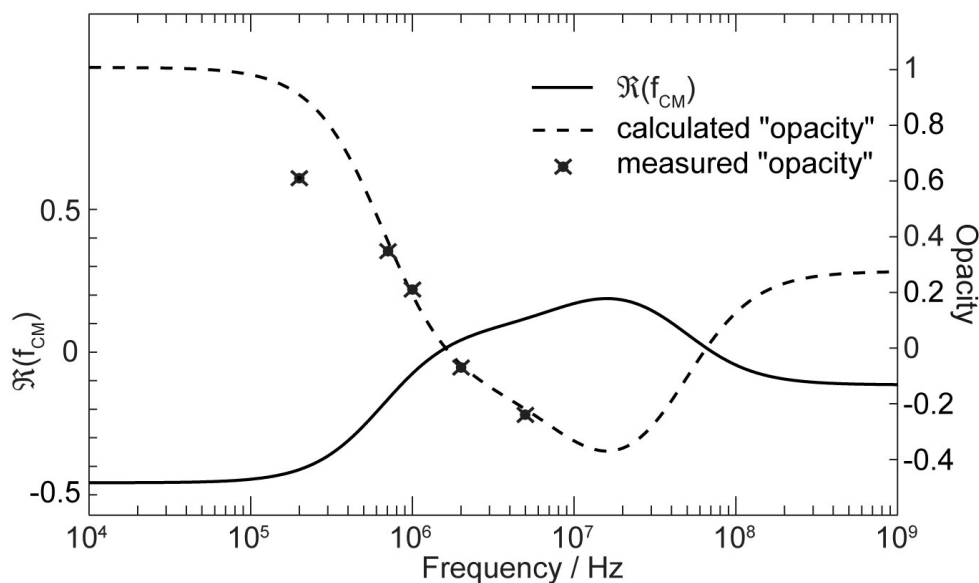


Figure 5.3: Real part of the Clausius-Mossotti factor $\Re(f_{CM})$ for a viable yeast cell (solid line) according to the double-shell model (with the parameters listed in table 2.1 except for $\sigma_m = 126 \text{ mS} \cdot \text{m}^{-1}$ as well as calculated (dashed line) and measured (points) "opacities" for a reference frequency at 50 kHz .

constant for all the frequencies. This means that beads experienced a constant nDEP-force, *i.e.* the polarization presents no relaxation mechanism over these frequencies. Inversely, the yeast cells are more and more attracted towards the negative positions with the increasing f_{scan} . Their "opacity" ranges from 0.6 down to values < -0.2 . It allows tracing the general shape and relative magnitude of the CM factor (similar to the effective CM factor in section 2.4.2). The measured "opacities" at 200 kHz , 700 kHz , 1 MHz , 2 MHz and 5 MHz are reported in figure 5.3 and compared to calculated "opacities" that were computed from the double-shell model (refer to section 2.2.2) with the parameters listed in table 5.1. The measured and calculated "opacities" presented in this figure show good agreement. These measurements validate the use of our device as a flow cytometer to characterize dielectric particles in a continuous flow.

5.3 Separation of viable and nonviable yeast cells

The next application is the continuous-flow separation of viable and nonviable yeast cells. The results of this application have been published by Demierre *et al.* (2008). Histograms of positions as a function of f_{scan} are shown in figure 5.4. In histogram (a), only the low-frequency quadrature signals at 50 kHz are applied on the electrode array, one on each side. The flow velocity was constant for all the experiments at the value of $900 \mu m \cdot s^{-1}$. Under these conditions, all the cells were focused towards a common equilibrium line. Viable and nonviable cells are not discriminated in that case. Superimposing a second electrical signal on the left side of the electrode array ($V_{scan} f_{scan}$) at 100 kHz pushed the particle stream towards the right side (positive values of positions) which indicates that a nDEP-force was generated at that frequency (figure 5.4b). But still no discrimination between viable and nonviable cells is observable.

However, when f_{scan} is increased from 100 kHz up to 5 MHz , the viable cells are more and more attracted towards the left side, from where the third signal is applied. At a frequency around 860 kHz , the viable yeast cells end in the same positions as in the control experiment (figure 5.4a). This means that the DEP-force generated by the third signal has no effect and is in fact the crossover frequency f_{co} . This is a simple method to determine the f_{co} of a cell type under particular experimental settings. Above f_{co} , the third signal generated a pDEP-force for that cell type. The other cell type, the nonviable yeast cells, still experienced nDEP, so that viable and nonviable yeast cells were separated and ended in distinct portions of the central channel. Thus at a frequency of 5 MHz , the two populations appeared clearly separated on the histogram of figure 5.4c. Images of cells flowing in the output channel downstream from the separation are shown in figure 5.5 when f_{scan} is *OFF* on the left side and $f_{scan} = 5 MHz$ on the right side.

Our device allows to collect sub-populations of viable and nonviable yeast cells at particular positions in the channel with approximately 100% of purity as shown in table 5.2. Note that 100% of purity means 100% of viability for the viable cell fraction and 0% of viability for the nonviable cell fraction. For $f_{scan} = 5 MHz$, the portion of the channel with only viable yeast cells is the position range from -1 to -0.1 and the

5.3 Separation of viable and nonviable yeast cells

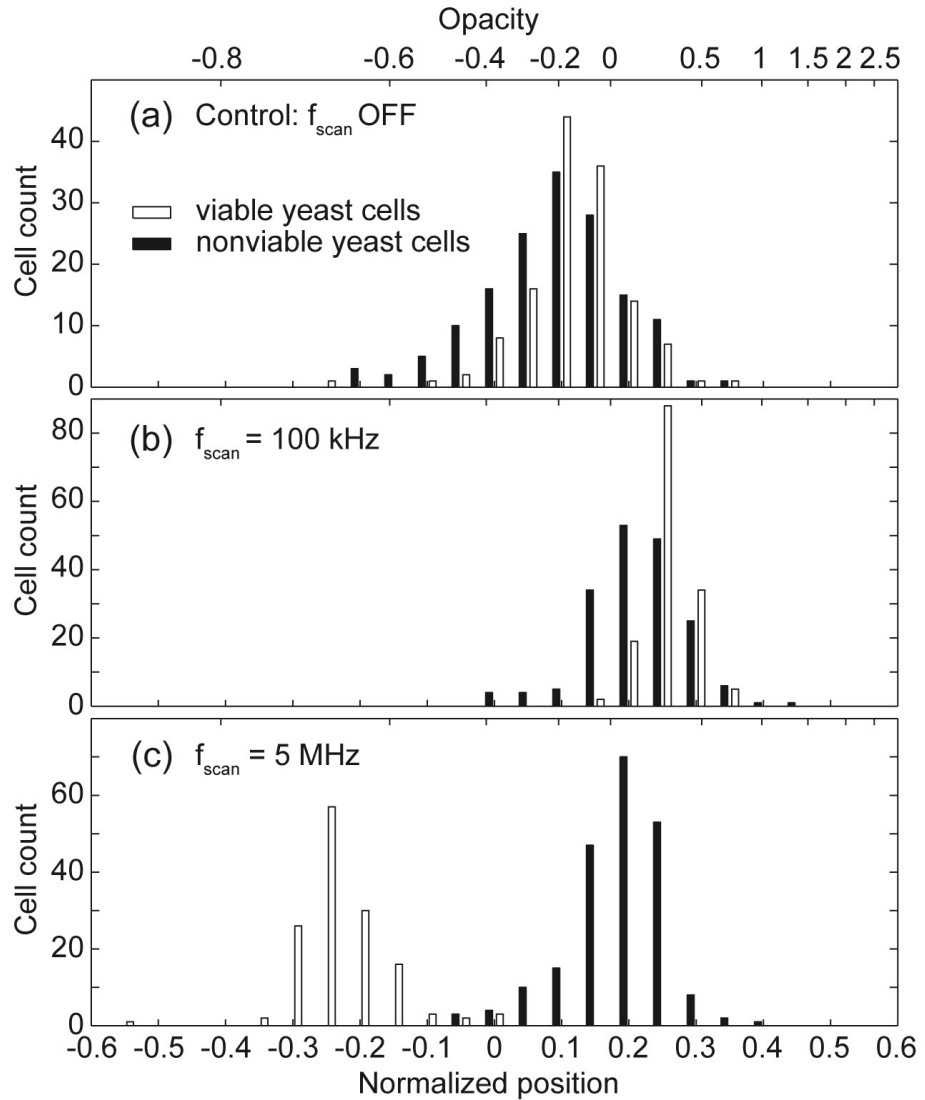


Figure 5.4: Separation of viable and nonviable yeast cells. (a) is the control experiment for which the high frequency is switched off. The two low frequency signals focus all particles towards the same positions. In (b) a 100 kHz signal at $4.45 V_{rms}$ is added to the low frequency signal on the left side of the electrode array and produces an additional nDEP-force. In (c) the frequency of the third signal is increased to 5 MHz . The viable cells now clearly end in the left side, which means that they are subjected to a pDEP-force. In accordance, their "opacity" is negative. The nonviable cells however still experience a nDEP-force at this frequency, as indicated by positive "opacity" values.

5. CONTINUOUS-FLOW SEPARATION OF CELLS USING MFDEP

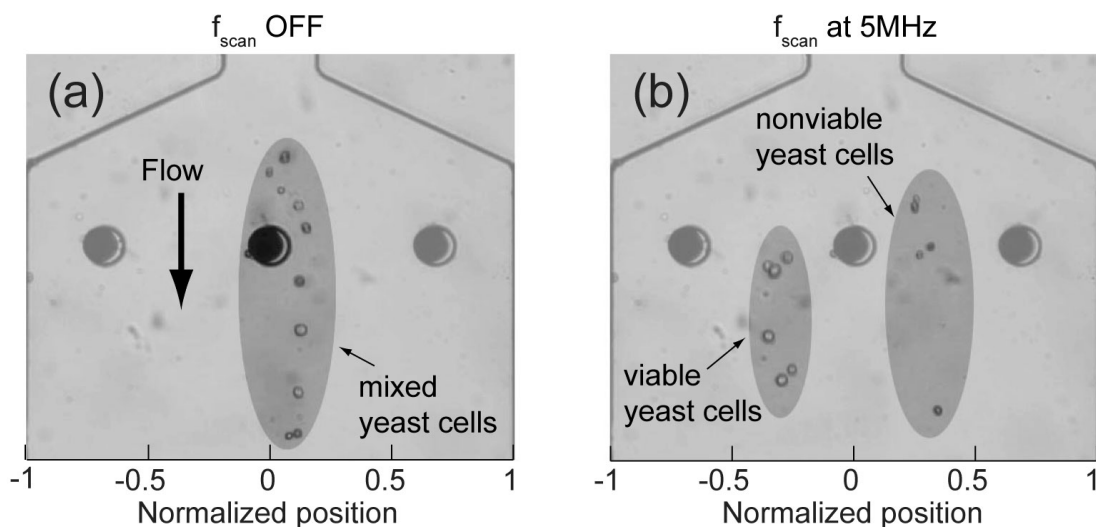


Figure 5.5: Image of two populations of viable and nonviable yeast cells flowing in the channel. The nonviable yeast cells appear darker due to blue staining. The populations are focused but mixed in (a) due to two opposite nDEP-forces whereas they are separated in (b). The separation is induced by the addition of a third DEP-force only on one side, that produces differences in the dielectric responses of the two species at a frequency f_{scan} of 5 MHz in that particular case.

position range of the pure sub-population of nonviable yeast cells is from 0.1 to 1. At this frequency, 132 viable cells and 0 nonviable cells in the position range of viable cells were counted and 0 viable cells and 181 nonviable cells were counted in the position range of nonviable cells. The initial viability percentage of the mixture of viable and nonviable yeast cells before separation was 40%. A small portion of the channel (position range from -0.1 to 0.1) contains a small amount of the two species. Cells ending in this position range have to be rejected prior to the fraction sampling in order to preserve the purities of the other channel portions. This is done by dedicating the middle fluidic outlet to waste. The results of continuous-flow cell separation performed by Doh and Cho (2005) reported purities of 97% for the viable cell fraction and 70% for the nonviable cell fraction. In comparison, our separation method presents significant improvements, in particular for the nonviable cell fraction. This improvement is likely due to the use of an equilibrium between two opposite DEP-forces at multiple frequencies rather than a binary separation based on the opposition of nDEP and pDEP at

5.3 Separation of viable and nonviable yeast cells

	f_{scan} kHz	Cell count -	Cell viability %
Initial mixture	Off	283	46.3
	100	330	44.9
	5000	353	39.7
Position = [-1;-0.1]	Off	6	16.7
	100	0	0
	5000	132	100
Position = [-0.1;0.1]	Off	162	43.8
	100	13	0
	5000	40	20
Position = [0.1;1]	Off	115	51.3
	100	317	46.7
	5000	181	0

Table 5.2: Population statistics for viable and nonviable yeast cells according to their output positions in the central channel downstream from the electrode array. The two low frequency signals in quarter phase at 50 kHz remain constant while the frequency of the third signal is successively off, 100 kHz and 5 MHz . The data correspond to figure 5.4.

a single frequency. The quality of separation also shows that the difference in dielectric properties between viable and nonviable populations is larger than the variations within each population.

5.3.1 Estimation of the dielectric response

As in the previous section, the readout of the output positions of the cells downstream from the electrode array defines the "opacity" of viable and nonviable yeast cells. The output positions are related to "opacities" using the equation 4.6 with the rms voltages of 3.39 V , 4.38 V and 4.45 V for $V_{ref,1}$, $V_{ref,2}$ and V_{scan} respectively.

In order to compare the "opacities" obtained experimentally to published work, we calculated the dielectric response of the viable and nonviable yeast cells based on a double-shell model with the parameters listed in table 2.1. The real part of the CM

5. CONTINUOUS-FLOW SEPARATION OF CELLS USING MFDEP

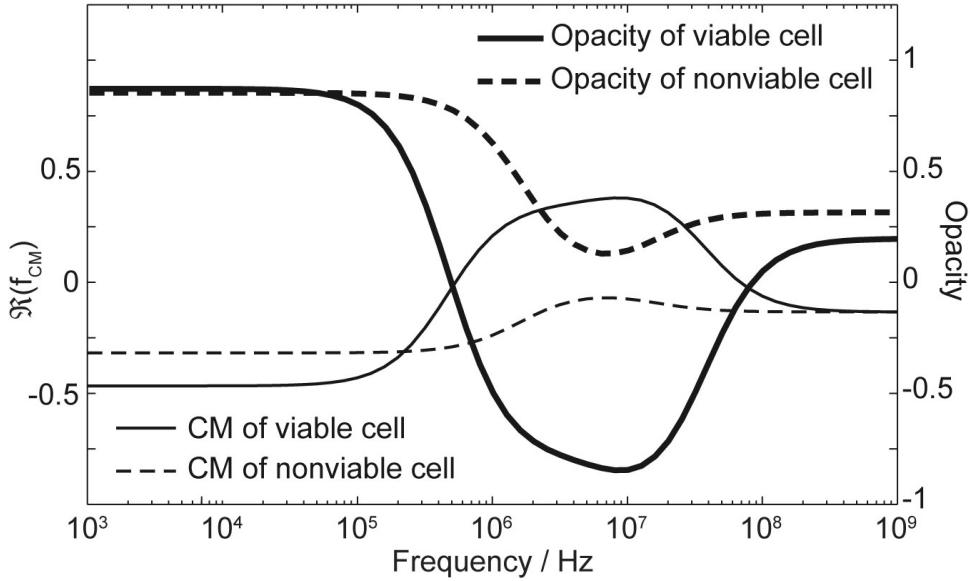


Figure 5.6: Graph of $\Re(\tilde{f}_{CM})$ for both viable and nonviable yeast cells computed from a double-shell model with the parameters listed in table 2.1. The "opacities" for both populations plotted on the same graph (thick solid / dashed lines) are calculated from the double-shell model with respect to $\Re(\tilde{f}_{CM,ref})$ at 50 *kHz*.

factors and the "opacities" computed from these parameters are plotted in figure 5.6 for both viable and nonviable yeast cells. For f_{scan} at 5 *MHz* and both $f_{ref,1}$ and $f_{ref,2}$ at 50 *kHz*, the calculated "opacities" are -0.8 for the viable cells and +0.23 for the nonviable cells whereas the measured "opacities" are -0.67 for the viable cells and 0.065 for the nonviable cells. The values for the viable cells correspond but one observe a significant difference between the experimental and calculated values of "opacities" for the nonviable cells. The major source of error probably comes from the configuration of applied signals. In some early experiments, the two low-frequency signals were at 50 *kHz* and 60 *kHz* (or even 60 *kHz* and 90 *kHz*) instead of being two quadrature signals. These two configurations have basically the same effect on the total DEP-force, which is the vectorial sum of the contributions at each single frequency as demonstrated in section 2.4. However, the first configuration, the one used for these experiments, has a negative influence on the separation and on the measurement of the "opacity" because of a difference in the dielectric responses of the cells at 50 *kHz* and 60 *kHz*. This

also explains that the populations are not exactly centered at the "opacity" value of 0 in the control experiment in figure 5.4a. This discrepancy indicates that the choice of two distinct frequencies, *e.g.* 50 *kHz* and 90 *kHz*, is unfortunate and degrades the separation performances. A better precision is reached if using two quadrature signals at a lower frequency.

5.4 Isolation of parasitized RBCs

5.4.1 Separation of infected and non-infected RBCs

The objective in this application is to increase the percentage of red blood cells that are infected with *Babesia bovis* within a cell culture. This percentage is commonly called the parasitemia percentage (PPE). *Babesia bovis* is an eukaryotic tick-borne unicellular parasite similar to the parasite that causes malaria. The protozoan parasite *Babesia bovis* infects bovines. Current concentration methods of *Babesia bovis* infected erythrocytes are time consuming and require expensive reagents or equipments (Rodriguez *et al.*, 1986, Alkhalil *et al.*, 2007). We propose to apply our continuous-flow separation method to concentrate parasitized cells at one fluidic outlet of microfluidic device. This biological problem has been addressed in collaboration with the Biomolecular diagnostic laboratory of IBET, Oeiras, Portugal in the framework of the European project *CellPROM*¹. The results have been published by Demierre *et al.* (2008).

The starting hypothesis is that *Babesia bovis* causes changes in the cellular dielectric response of the host which is similar to what was observed in malaria by Gascoyne *et al.* (2004). The two pathogens have similarities in their biosystematics and their physiology. Both pathogens are apicomplexans, *i.e.* characterized by the presence of a unique organelle called an "apical complex" and both cause changes in membrane conductance but from different molecular mechanisms as reported by Alkhalil *et al.* (2007). We previously demonstrated that indeed changes occur in the dielectric properties between infected and non-infected RBCs by impedance spectroscopy (Kuttel *et al.*, 2007). Here we intend to separate infected and non-infected RBCs in a continuous flow in a label-free manner. The separation method has to be sensitive enough to detect small

¹(2008) <http://www.cellprom.org/>

5. CONTINUOUS-FLOW SEPARATION OF CELLS USING MFDEP

differences in the dielectric responses of infected and non-infected RBCs. So, it would be possible to increase the percentage of infected cells, which is generally not exceeding 7%. Our method should increase the PPE up to 50% in order to compete against the best performances of traditional label-free methods (Rodriguez *et al.*, 1986).

The results of the enrichment experiments for *Babesia bovis* are shown in figure 5.7. The two populations were optically discriminating based on the fluorescent staining of the DNA content of the parasites. The evaluation of the separation efficiency and the statistics on cell populations required the acquisition of two types of images; one bright-field image to distinguish the RBCs and one fluorescent images to localize the parasites and therefore identify the infected RBCs. An example of two superimposed images is shown in figure 5.8. The settings of rms voltage values and frequencies were 9.0 V at 90 kHz and 4.7 V at 4 MHz on the left side and 6.8 V at 60 kHz on the right side. The sub-population distributions downstream from the electrode array are shown in (b), while (a) is the control experiment where only the low frequency signals ($V_{ref,1}$ $V_{ref,2}$) were applied ($f_{ref,1} = 90$ kHz on the left side and $f_{ref,2} = 60$ kHz on the right side). When the third electrical signal at varying frequencies (V_{scan} f_{scan}) is superimposed as in figure 5.7b, the infected cells get more concentrated at the right side whereas the non-infected at the left one. By comparing figure 5.7a and 5.7b it clearly appears that both infected and non-infected RBCs experience pDEP at $f_{scan} = 4$ MHz. However, the pDEP is stronger for the non-infected cells, which produces to a partial separation of the population. We confirm therefore that the *Babesia bovis* parasite causes changes in the dielectric response of the hosting cells. The presence of the parasite within the cell population also contributes to increase the dispersion of the population by causing cell damage such as membrane degradation. Thus, the positions of the non-infected cells are widespread over a large channel portion (see figure 5.7). The spread of positions would be much smaller in a control experiment with a homogeneous population of healthy cells. This observable dispersion is also explained by the use of the strong pDEP which is required to separate infected and non-infected RBCs. The strong high-frequency signal induces differences in the frequency responses of the sub-populations due to natural cell variations such as the age and the shape.

The weaker pDEP experienced by the infected cells at high frequencies indicates that

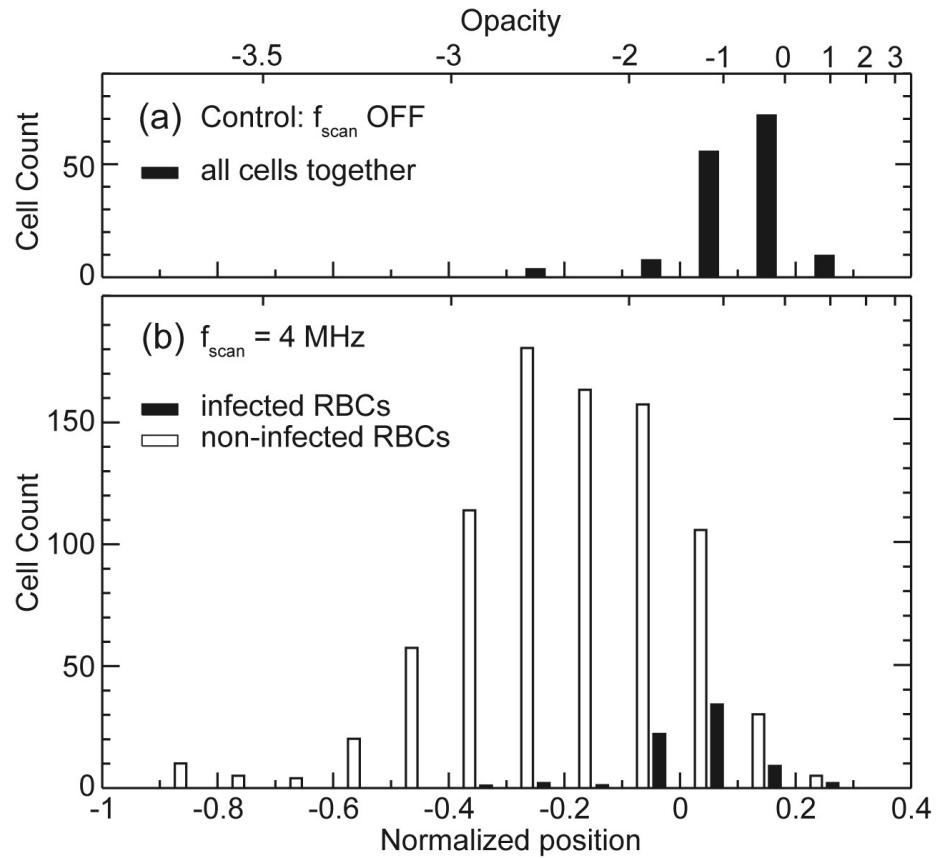


Figure 5.7: Enrichment of red blood cells parasitized by *Babesia bovis*. For the control experiment in (a), only two opposite flow frequency signals are applied to focus all the cells. In (b) the additional high frequency signal (4 MHz) on the left side produces a pDEP-force for all cells. It results in a shift of all cells towards the left side as compared to the control (a) where the high frequency is off. However, the pDEP is stronger for non-infected than for infected cells which increases locally the parasitemia percentage of the right channel portion.

5. CONTINUOUS-FLOW SEPARATION OF CELLS USING MFDEP

these cells have a lower intracellular conductivity. As in malaria (Gascoyne *et al.*, 2004), there are probably two main contributions to the decrease in the effective intracellular conductivity:

- The presence of the parasite itself inside the cell that forms an obstacle to the current flow and therefore increases the cytoplasmic resistance.
- The loss of internal ions to the medium which is probably due to an increase in the permeability of the cell membrane caused by the parasite.

It is also clear from figure 5.7b that with these particular experimental settings, no clean separation of the two populations can be achieved. We suspect that the dielectric changes caused by the *Babesia bovis* parasite are rather small compared to the large intrinsic variations within both infected and non-infected populations.

5.4.2 Estimation of the enrichment factor

An enrichment of infected cells on one portion of the channel (position range from -0.1 to 0.4) was observed rather than a clean spatial separation of the two populations. The other channel portion (position range from -1 to -0.1) got a population almost free of infected cells. Two different techniques were used in order to quantify the percentage of infected cells and evaluate the enrichment factor. The first method consists of collecting and counting the enriched fraction in one chip outlet and the non-infected in another outlet. In this way, the PPE was estimated up to $\approx 50\%$ whereas the initial PPE, before separation, was estimated to $\approx 7\%$. For this first method, similar enrichment values were obtained when the infected cells were stained with ethidium bromide either in the sample preparation step before the separation or after collection of the sorted cells at the corresponding chip outlet.

The second method is based on images that are taken right after the separation, *i.e.* where the central channel gets wider and where the flow velocity is reduced. To do so, the flow is temporarily stopped during the acquisition of the two corresponding images (as described above). The infection rate is then estimated by comparing and counting the sub-populations from the two images. This method yielded to a PPE value of

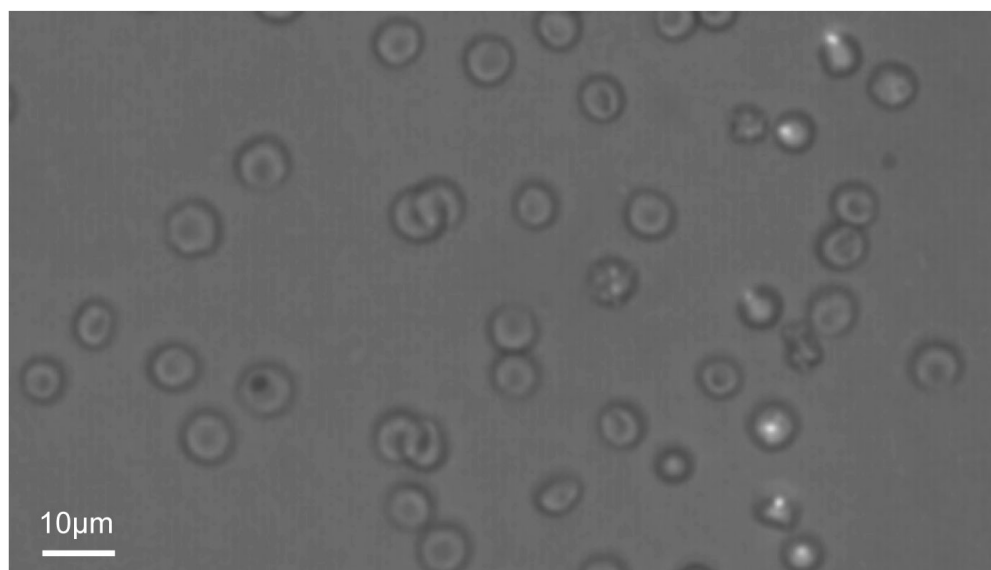


Figure 5.8: Superposition of a bright field image and a fluorescent image of red blood cells that flow (from the top to the bottom) through the output channel downstream from the separation chamber. The RBCs with the fluorescent signals are hosting the *Babesia bovis* parasite. The fluorescent marker, ethidium bromide, marks the DNA content of the parasites.

$\approx 32\%$. This value is smaller than the value of 50% that was obtained with the collecting method. The main reason for this lower infection rate is related to the need of stopping the flow for each acquisition of images. It induced the sticking of the infected cells to the channel floor and therefore decreased the apparent infection rate. However, this second method provided the values of the cell positions right after the separation for the statistics represented in 5.7b. The collecting method would be implemented in applications where the PPE increase is the main issue. These measurements show that our continuous-flow separation method is capable of enriching *Babesia bovis* infected cells up to a PPE of $\approx 50\%$ in a label-free manner.

5.5 Synchronization of a cell culture

In the previous sections, the great potential of our continuous-flow sorting method was demonstrated for sample preparation and isolation of biological sample before bioas-

5. CONTINUOUS-FLOW SEPARATION OF CELLS USING MFDEP

says. This section reports on the use of the method to address another fundamental issue in biology that reveals, meanwhile, the versatility of our microfluidic device. This biological issue is the synchronization of a cell culture. The synchronization of a cell culture increases its homogeneity by providing cells that are at the same phase within their cell cycle. The homogeneity of the cell cultures has a significant importance in biotechnology to develop and improve particular processes such as protein synthesis. The cell synchrony is also an issue in biomolecular biology and in fundamental research at the single cell level. In research fields such as drug discovery, the homogeneity of a cell culture also prevents the need of statistical methods to evaluate a biological process and assess its dynamics. For example, many anticancer drugs target cells at a particular cell-cycle phase (Schiff *et al.*, 1979). The main approach today is the use of metabolic agents that block the cell cycle at a particular phase and accumulate cells at this phase. The arrest of the cell cycle as well as the release are obtained by chemical stimuli. This approach presents the main drawback of disturbing the cell physiology. As an alternative, Davis *et al.* (2001) presented a centrifugal elutriation technique to separate and collect cells according to their size and weight. Although this method preserves the cell physiology, it induces mechanical stress on the cells. More recently, Kim *et al.* (2007) proposed a novel approach to get cell synchrony by the mean of dielectrophoresis, taking advantage of the relationship between the cell volume and the cell cycle. However, the volume of budding cells - or dividing cells - is not intimately related to the internal cell organization such as spindles and microtubules and therefore only allows a rough synchronization level.

We propose to address the synchronization issue by applying our continuous-flow cell separation method. The synchronization is obtained by isolating a group of cells that are all at the same phase within their cell cycle. The shape and the internal arrangement of the cells that are at this particular phase enhance the polarization mechanism and provide to them a stronger pDEP affinity than to the others. By being sensitive to internal structures of the cells that are deeply involved in the cell division, our method is potentially able to achieve high level of cell synchrony.

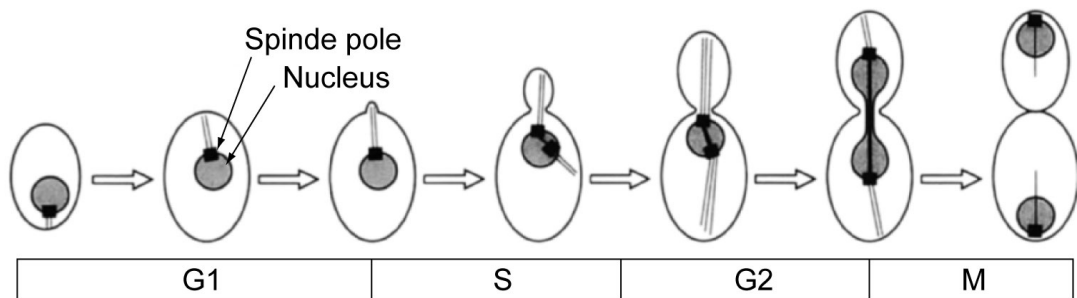


Figure 5.9: Phases of the division cycle of the yeast cell by budding mechanism and arrangements of the spindle poles and nucleus; unbudded cell in the starting G1 phase; bud emergence in S phase till the creation of a ring between mother and daughter cells; nucleus migration towards the bud neck in G2 phase; nucleus extension during mitosis (M) phase. The cell cycle finishes at the cytokinesis where the two daughter cells separate from each other. *Adapted from Lew and Reed (1995)*

5.5.1 Cell model

The division of a cell, the mother cell, into two cells, the daughter cells, can be performed by different mechanisms. Fission and budding two main division mechanisms responsible for cell proliferation. Basically, in the former mechanism, the cell grows longitudinally. When a critical length is reached, the cell simply splits into two parts of half length each (McCully and Robinow, 1971), whereas in the latter mechanism, the proliferation occurs from the emergence of a bud at the cell surface that increases until the two parts separate into two daughter cells (Lew and Reed, 1995).

The cell cycle of budding cells is split into the interphase (G_1 , S and G_2) and the mitotic phase (M) as depicted in figure 5.9. The shape, the volume and the internal arrangement temporally change within the cell-cycle progression. The cell cycle starts in G_1 with the emergence of a bud at the cell surface and with production of enzymes for the next phase. During the S phase, the DNA is synthesized until all the chromosomes are replicated. The two spindle poles separate and start migrating and microtubules appear in the continuously increasing bud. The increase is pursued in G_2 where the microtubules develop and align along the cell-bud axis. At the end of G_2 , the nucleus elongates and enters in the bud whose current size is comparable to the cell

5. CONTINUOUS-FLOW SEPARATION OF CELLS USING MFDEP

one. In the M phase, the nucleus divides (mitosis) as well as the cytoplasm (cytokinesis) through a reduction of the bud neck to finally form two independent daughter cells. For the synchronization of cell culture with MFDEP, we concentrate only on the budding mechanism for which the different phases within the cycle are easier to identify by optical inspection than for the fission mechanism.

The cell model considered for these experiments is again the yeast cell, or more specifically the *Saccharomyces cerevisiae*. The yeast cell has the characteristic to proliferate either by fission mechanism or budding mechanism according to the particular strain. Moreover, the cell cycle of the yeast has been widely investigated in the past by numerous research groups (Hartwell, 1974, Byers and Goetsch, 1975). Likewise all eucaryote cells, the yeast possesses tubulin and actin, two major structural proteins that compose the microtubules. The yeast presents an arrangement of microtubules and in general a spindle apparatus that resemble strongly to those of higher eukaryotes - or higher organisms (Kilmartin and Adams, 1984). The yeast cell has however a shorter cell cycle than general eukaryotes, in particular the resting time between two cycles. This increases the fraction of dividing cells in the sample and avoid resorting to any pre-concentration procedure. The yeast cell exhibits a close temporal correlation between the cell cycle progression and the shape changes (Lew and Reed, 1995). All these characteristics make the yeast cell a good and representative model for the synchronization experiments with MFDEP. The cell strain is kindly provided by the group of Prof. Yves Barral¹ from ETHZ (Swiss Federal Institute of Technology, Zurich). A genetic modification allows to express green-fluorescent microtubules caused by GFP-tubulin (green fluorescent protein). The GFP staining allows to assess the phase of the cell within its cycle by fluorescent imaging.

5.5.2 Numerical modeling of budding yeast cell

The common models presented in section 2.2 are inappropriate to a budding cell whose geometry is more complicated than concentric spheres. Note that models based on ellipsoidal shape exist with two different polarization axes. They are better than sphere-based models but still far from the budded geometry. Moreover, an ellipsoidal-based

¹<http://www.bc.biol.ethz.ch/people/groups/yvbarral>

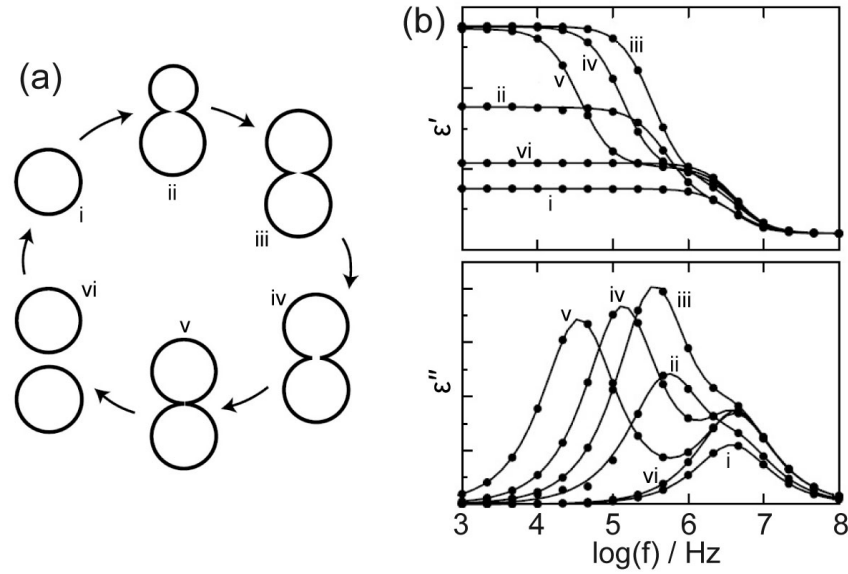


Figure 5.10: Numerical modeling of a budding yeast cell at 6 different stages within the cell cycle. In (a) are shown the geometries corresponding to the 6 stages (from i to vi). Numerical calculation of the complex permittivity (ε' for the relative effective permittivity and ε'' for the loss factor) are plotted in (b) for the 6 stages. A clear additional dispersion is observable for the stage iii to v which also indicates a stronger polarization for the cells in these stages. After the separation (stage vi), the additional dispersion is canceled and the permittivity curve converges to the initial stage i . Adapted from Asami and Sekine (2007)

model would never take into account the bud neck, *i.e.* the opening between the cell and the bud, whose section varies during the cell cycle. This highlights the difficulty to define a good analytical model of budded geometry.

Asami and Sekine (2007) proposed a numerical approach to investigate the bud influence on the cell polarization at the different phases within the cell cycle (shown in figure 5.9). They used a boundary element method (BEM) to evaluate the polarization of a budding yeast in an electric field. The orientation of the budding yeast and the field is of importance and they proposed a numerical model for both parallel and perpendicular alignments. Videos taken during our experiments indicate that the budding yeast is aligned with the electric-field gradient, *i.e.* parallel to the electric field.

5. CONTINUOUS-FLOW SEPARATION OF CELLS USING MFDEP

In this particular case and according to Asami and Sekine, the low-frequency polarization of budding cell is stronger than normal cell. Understand by low frequency the frequencies under f_{MW} (c.f. section 2.2) and by normal cell the cells that are not currently dividing. The stronger polarization is accompanied by an additional dispersion - or relaxation mechanism. This relaxation frequency shows dependency on the bud-neck geometry. Asami and Sekine proposed 6 different cell geometries related to the cell-cycle progression as shown in figure 5.10a. Numerical calculation are then performed for the 6 geometries to compute the complex permittivity $\tilde{\epsilon}$ over frequency. Note that the calculated values at a particular frequency for the 6 geometries give changes over time, *i.e.* permittivity changes associated with the cell-cycle progression. The real part ϵ' and the imaginary part ϵ'' are shown in figure 5.10b and represent respectively the relative permittivity and the dissipated energy. The strongest polarization corresponds to the geometries *iii* to *v* in figure 5.10a within the cell cycle. These 3 geometries have however different relaxation frequencies, the highest being related to the geometry *iii*. The relaxation frequency decreases with the narrowing of the bud neck and disappears when the neck is closed according to the numerical models. Nevertheless, the relative permittivity of the geometry *vi* remains higher than the one of geometry *i* because of the proximity of the two daughter cells that interact with the electric field.

All of this essentially means that indeed cells in division could be separated from non-dividing cells due to differences in polarization magnitudes at certain frequencies. The separation frequency should be centered around the relaxation frequency corresponding to the geometry *iii*. Thus, only cells in geometry *iii* would be attracted by pDEP stronger than any other cells.

5.5.3 Materials and methods

5.5.3.1 Microfluidic device

The only difference with the device described in section 3.3 lies on the substrate thickness. The standard 550 μm thick glass wafer is replaced by a 170 μm thick one. The reason is imparted to the imaging of the GFP-tubulin. Since the stained structure are submicrometric, a good imaging with enough resolution requires static conditions, high magnification factor (typically 100 \times) and high numerical-aperture objectives. All of these

requirements can only be achieved with short-working distance objectives, meaning a maximum wafer thickness of 170 μm .

5.5.3.2 Sample preparation

The yeast cells are cultured at 20°C on YPD agar plates (1000 *ml* of deionized water, 10 *g* of BactoYeast Extract, 20 *g* of BactoPeptone, 20 *g* of Dextrose and 20 *g* of Agar). For the experiments, cells in logarithmic growth phase are transferred to YPD liquid media which is adjusted with deionized water to a conductivity of $\approx 60 \text{ mS} \cdot \text{m}^{-1}$.

5.5.4 Estimation of the synchrony level

Since the objective of this section is the synchronization of a cell culture, it is essential to have a method that evaluates the synchrony level of a cell population. In our application, this method is applied to the isolated cells, which are expected to be synchronous. It is an optical method that consists of observing the internal arrangement of the GFP-marked spindle apparatus of the isolated cells with high numerical-aperture microscopy. The length of the microtubules and the localization of the two spindle poles correspond to a particular phase of the cell cycle. The relationship between the arrangement of the spindle apparatus and the cell cycle is represented in figure 5.9. The imaging of the spindle apparatus under fluorescent illumination is shown in figure 5.11a and figure 5.11b shows the corresponding image obtained by differential interference contrast (DIC) microscopy. Both images show asynchronous yeast cells where different bud sizes can be observed. The comparison of the two images allow to determine the cell-cycle phase of each cell.

5.5.5 Isolation of cells in division

We intend to address synchronization issues by applying our continuous separation method based on multiple-frequency dielectrophoresis. Based on the observations during sorting experiments of viable and nonviable yeast cells (see section 5.3) and on the numerical modeling, the dividing cells are more strongly affected by the pDEP-force than the non-dividing cells. A continuous-flow separation of dividing and non-dividing yeast cells has been performed to confirm that the dividing cells indeed enter into pDEP

5. CONTINUOUS-FLOW SEPARATION OF CELLS USING MFDEP

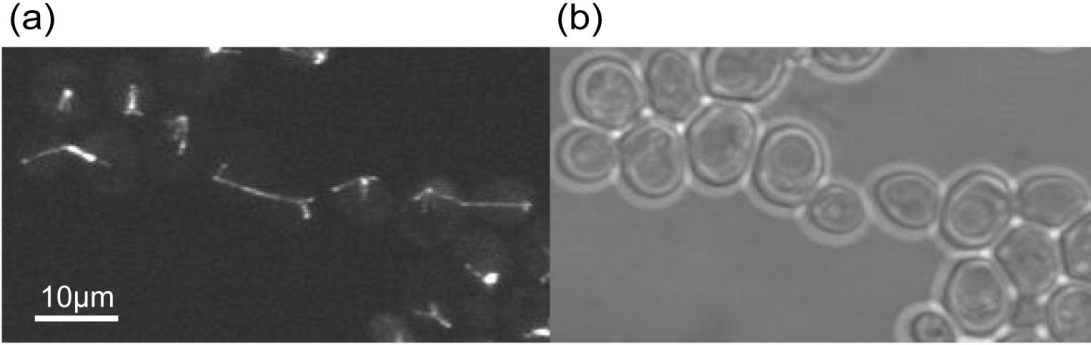


Figure 5.11: Fluorescent microscopy of asynchronous yeast cells with GFP-marked spindle apparatus in (a) and corresponding differential interference contrast microscopy of yeast cells in (b). The microtubules are clearly identified on the fluorescent image. Thus, an optical analysis of the fluorescent image, in comparison to the bright image, allows to determine the cell-cycle phase of each individual cell.

regime earlier ($f_{co,dividing} < f_{co,non-dividing}$) and stronger ($\epsilon'_{dividing} > \epsilon'_{non-dividing}$) than the non-dividing cells. For these experiments, a typical set of electrical signals was used, *i.e.* one low frequency signal ($f_{ref,1} = f_{ref,2} = 50 \text{ kHz}$) on each side of the electrode array to focus the cells and one additional signal at scanning frequency (f_{scan}) superimposed on the left side to distinctly modify the equilibrium positions of each cell type.

Figure 5.12 shows the histograms of output positions of both dividing and non-dividing cells for 6 different frequency values of f_{scan} (OFF , 200 kHz , 500 kHz , 700 kHz , 1 MHz and 1.5 MHz). One observes that the sub-population of dividing cells is earlier attracted by the pDEP (for $f_{scan} > 500 \text{ kHz}$). In figure 5.12d for $f_{scan} = 700 \text{ kHz}$, the dividing cells are clearly more strongly attracted towards the left side than the other cells, as expected from the numerical model of section 5.5.2. The second observation we can do from figure 5.12 is that the dividing-cell population is spread out over a large channel portion (normalized position values between -1 and 0.19). This spreading reveals large variations within the sub-population. This is the result of dispersions of shape, volume and cell-cycle phase within the sub-population since all of these three parameters influence the dielectric response of the cells.

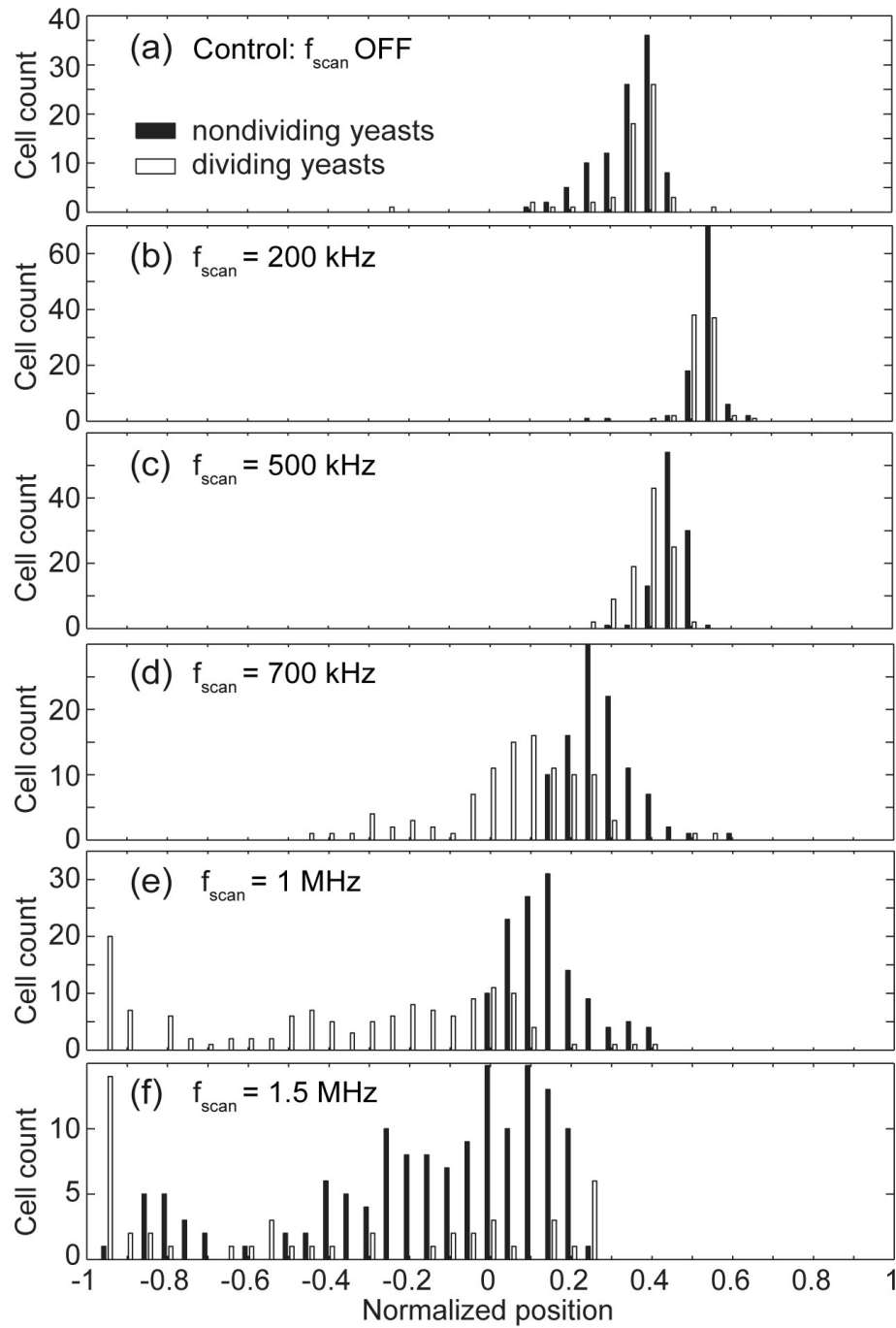


Figure 5.12: Separation of yeast cells in division. The superimposed signal on the left side of the electrode array at $f_{scan} = 1$ MHz exerts stronger pDEP on cells on division compare to normal yeast cells due to the lower crossover frequency f_{co} . The cells in division are spread over a large portion of the channel due to large dispersions in size and dielectric properties. A sub-population of cells in division seems more attracted to the left side than the average, probably related to the stage in the cell division cycle.

5. CONTINUOUS-FLOW SEPARATION OF CELLS USING MFDEP

The histogram (e) at $f_{scan} = 1 \text{ MHz}$ also shows the presence of groups within the sub-population of dividing cells. One group completely on the left side (position range between -1 and -0.8) is particularly visible. Due to its extreme position, one can conclude that this group exhibit the strongest affinity to pDEP. We draw the hypothesis that all these cells are at the particular phase *iii* of figure 5.10b for which the polarizability at that frequency of 1 MHz is maximum. Other observations during the experiments reveal that the small-budded yeasts are not differently affected by the pDEP than the normal yeast cells. When the buds increase, they get more attracted by the pDEP. Although the tendency of the budding cells is a strong pDEP affinity, few of them end in the similar channel portion than the non-dividing yeast cells. This abrupt change in the dielectric response is suspected to be intimately related to the inner cell morphogenesis and in particular to the bud neck. A possible explanation involves the polarization mechanism occurring at low frequencies ($< 1 \text{ MHz}$) for which the ion movement is partially responsible. In these conditions, one can easily imagine that budding yeast cells whose bud neck is still open would exhibit a different dielectric response than the one of budding yeast cells whose bud neck is already closed. These two species would therefore exhibit a different pDEP affinity although they look similar from the outside. However, they would be different in a fluorescent imaging of their internal arrangement of microtubules (as in figure 5.11a). Unfortunately, this validation has not been performed during these experiments but should be addressed shortly. Figure 5.12f shows that the separation of the two species disappears at frequencies above 1 MHz since all the cells are strongly attracted towards the left side and spread over a large channel portion.

So far, the only reported synchronization method based on DEP separates dividing cells according to their volumes (Kim *et al.*, 2007). This manipulation requires nDEP and synchronizes cells due to the relationship between the cell volume and the cell cycle. However, the volume is a cell property that is subjected to a natural dispersion within a cell population. Moreover, the cell volume is roughly limited to the cell cycle. For example, significant internal changes of the cells occur during the M-phase whereas their volume remains more or less constant, as shown in figure 5.9. The continuous-flow separation method that we propose uses multiple-frequency dielectrophoresis to synchronize a cell culture based on the different polarization mechanisms of cells that

5.5 Synchronization of a cell culture

are associated to their cell-cycle phases. Cell properties such as the polarization and relaxation mechanisms are likely more related to the cell cycle than the volume, which neglects the arrangement of microtubules and the neck opening. Thus, our method, which is capable of isolating particular cells according to their internal arrangement, constitutes a highly specific synchronization technique that preserves the cell physiology. To our best knowledge, our method is the most sensitive synchronization technique based on multiple-frequency dielectrophoresis for lab-on-a-chip applications.

5. CONTINUOUS-FLOW SEPARATION OF CELLS USING MFDEP

Bibliography

- Alkhalil A, Hill DA and Desai SA, 2007: *Babesia and plasmodia increase host erythrocyte permeability through distinct mechanisms*. Cellular Microbiology, vol. 9(4): 851–860.
- Asami K and Sekine K, 2007: *Dielectric modelling of cell division for budding and fission yeast*. Journal Of Physics D-Applied Physics, vol. 40(4): 1128–1133.
- Byers B and Goetsch L, 1975: *Behavior of spindles and spindle plaques in the cell cycle and conjugation of Saccharomyces cerevisiae*. Journal of Bacteriology, vol. 124(1): 511–523.
- Davis P, Ho A and Dowdy S, 2001: *Biological methods for cell-cycle synchronization of mammalian cells*. BioTechniques, vol. 30(6): 1322–1331.
- Demierre N, Braschler T, Muller R and Renaud P, 2007: *Focusing and continuous separation of cells in a microfluidic device using lateral dielectrophoresis*. Sensors and Actuators, B: Chemical, vol. DOI:10.1016/j.snb.2007.09.078.
- Demierre N, Braschler T, Nascimento E, Silva T, Oliva AG and Renaud P, 2008: *Continuous separation of cells by balanced dielectrophoretic forces at multiple frequencies*. Lab on a Chip - Miniaturisation for Chemistry and Biology, vol. 8(2): 280–286.
- Doh I and Cho YH, 2005: *A continuous cell separation chip using hydrodynamic dielectrophoresis (DEP) process*. Sensors And Actuators A-Physical, vol. 121(1): 59–65.
- Gascoyne P, Satayavivad J and Ruchirawat M, 2004: *Microfluidic approaches to malaria detection*. Acta Tropica, vol. 89(3): 357–369.

BIBLIOGRAPHY

- Hartwell L, 1974: *Saccharomyces cerevisiae cell cycle*. Bacteriological Reviews, vol. 38(2): 164–198.
- Kilmartin J and Adams A, 1984: *Structural rearrangements of tubulin and actin during the cell cycle of the yeast Saccharomyces*. Journal of Cell Biology, vol. 98(3): 922–933.
- Kim U, Shu CW, Dane K, Daugherty P, Wang J and Soh H, 2007: *Selection of mammalian cells based on their cell-cycle phase using dielectrophoresis*. Proceedings of the National Academy of Sciences of the United States of America, vol. 104(52): 20708–20712.
- Kuttel C, Nascimento E, Demierre N, Silva T, Braschler T, Renaud P and Oliva AG, 2007: *Label-free detection of Babesia bovis infected red blood cells using impedance spectroscopy on a microfabricated flow cytometer*. Acta Tropica, vol. 102(1): 63–68.
- Levy MG and Ristic M, 1980: *Babesia-Bovis - Continuous Cultivation In A Micro-Aerophilous Stationary Phase Culture*. Science, vol. 207(4436): 1218–1220.
- Lew D and Reed S, 1995: *Cell cycle control of morphogenesis in budding yeast*. Current Opinion in Genetics and Development, vol. 5(1): 17–23.
- McCully E and Robinow C, 1971: *Mitosis in the fission yeast Schizosaccharomyces pombe: a comparative study with light and electron microscopy*. Journal of Cell Science, vol. 9(2): 475–507.
- Nascimento EM, Nogueira N, Silva T, Braschler T, Demierre N, Renaud P and Oliva AG, 2007: *Dielectrophoretic sorting on a microfabricated flow cytometer: Label free separation of Babesia bovis infected erythrocytes*. Bioelectrochemistry, vol. In Press, Accepted Manuscript: –.
- Rodriguez SD, Buening GM, Vega CA and Carson CA, 1986: *Babesia-Bovis - Purification And Concentration Of Merozoites And Infected Bovine Erythrocytes*. Experimental Parasitology, vol. 61(2): 236–243.
- Schiff P, Fant J and Horwitz S, 1979: *Promotion of microtubule assembly in vitro by taxol*. Nature, vol. 277(5698): 665–667.

Chapter 6

Conclusion and outlook

Summary This last chapter comes back to the main achievements in terms of applications but also in terms of technical developments that allowed such performances. It summarizes the fields where our method of continuous cell sorting brought contributions regarding to the state of the art. Finally, the chapter gives perspectives where "liquid electrodes" and multiple-frequency dielectrophoresis offer new opportunities for lab-on-a-chip applications.

6.1 Summary of achievements

The main objective of this thesis was to develop a continuous-flow cell separation method that can be applied to a wide panel of biological materials. Efforts were focused on optimizing the resolution of the method to allow separating cell types with only small changes in their intrinsic dielectric properties. The integration of the method on a microfluidic platform is regrouped under four main fields of achievements. The novelty of this research mainly lies on the integration of the method using "liquid electrodes" and multiple-frequency dielectrophoresis. A few technological developments provide an easy-to-use microchip that achieves a separation efficiency exceeding the performances of the other DEP-based methods reported so far.

6. CONCLUSION AND OUTLOOK

6.1.1 The "liquid electrode"

The technological development aimed to replace top and bottom microelectrodes by planar electrodes. This avoids critical micromachining steps such as alignment and bonding of wafers. Investigations in these directions provided us with the new concept that we named "liquid electrode". The "liquid electrode" has to be seen as the major technological achievement of this work, the basis of all further developments. The concept is really attractive by its simplicity and by the opportunities that it offers:

- The microfabrication is a simple two-masks process to structure one layer of Ti/Pt for the electrodes and another layer of SU-8 for the fluidic network. The channel closing by a non-permanent sealing (PDMS part) allows to recycle the chips many times.
- The metal electrodes are robust due to their large size ($\geq 20 \mu m$) and thus would not suffer from local defect, *e.g.* caused by electrochemical reaction on the metal layer.
- The large interfacial capacitance of the metal electrodes provides sufficient current injection at low frequencies for a large band of operation
- The generation of the electric field and the shaping of its distribution are decoupled by the use of a patterned insulator. Thus, the DEP-force and its direction can be generated at particular and desired locations in the central channel.
- The most important characteristic is that simple design rules of "liquid electrodes" provide vertical equipotential surfaces in the central channel, or in other words that the "liquid electrode" behaves like a solid 3D vertical electrode.
- The potential homogeneity in the height ($\nabla E_z = 0$) allows generating an horizontal DEP-force, *i.e.* parallel to the channel bottom. The observation by microscopy of cell manipulations in the central channel is therefore facilitated.

A simple structure with one pair of "liquid electrodes" only was used to efficiently deviate particles in a channel with nDEP. However, the deviation of the particles was unidirectional and depended on the flow velocity as we demonstrated in Demierre *et al.* (2007).

6.1.2 The electrode array

The simplest manner to get a bidirectional positioning of particles across the central channel from nDEP was to symmetrically arrange another pair of "liquid electrodes" on the opposite side of the central channel. This new arrangement of facing pairs was duplicated many times along the central channel to give new possibilities:

- The arrangement produces two DEP-forces that are opposed and whose respective magnitudes are determined by independent external electrical signals (potentials and frequencies).
- In the nDEP regime, the two DEP-forces focus flowing particles towards a position in the central channel.
- The position of focusing is determined by the ratio of the applied potentials (an easy external control) and can be swept from one side of the channel to the other.
- The duplication of the arrangement into a whole array of fifteen electrodes on both sides increases the total efficiency by summing the effect of each pair.
- The focusing position is actually a position of equilibrium - or a line of equilibrium - defined by the two opposite nDEP-forces.
- Particles with different volumes but similar dielectric responses end in the same equilibrium position which is an advantage when working with samples subjected to size dispersion.

The notion of equilibrium is essential for the continuous-flow cell separation method proposed in this thesis. The equilibrium implies that the output positions of the particles are independent of their initial positions, upstream from the electrode array, and thus prevents resorting to a focusing step prior to separation, such as a sheath flow. Moreover, the tunable position of equilibrium is quickly reached by the particles and is then kept during the rest of the fluidic path thanks to the laminar flow. Thus the deviation imparted on the particles by the nDEP-forces is no longer depending on the flow velocity.

6. CONCLUSION AND OUTLOOK

6.1.3 Multiple-frequency dielectrophoresis

The second main achievement of this research, after the "liquid electrode", is to combine on one side of the electrode array two signals at different potentials and frequencies. This superposition introduces the multiple-frequency dielectrophoresis and the principle of superposition has been demonstrated for adding the contributions of each frequency in the total DEP-force (section 2.4). The multiple-frequency dielectrophoresis offers the following advantages:

- An additional DEP-force is combined with the two previous opposite nDEP-forces that still act to focus the particles.
- The additional DEP-force that can either be negative or positive modifies - or unbalances - the former positions of equilibrium.
- The new position of equilibrium is determined by the dielectric response of the particles to the set of frequencies and is therefore function of the additional frequency as well as of the dielectric properties of the particles.
- The additional frequency can be set such that the dielectric response of two types of particles differ at that particular frequency.
- The resulting equilibrium are distinct for the two species that get spatially separated in the electrode array and that end in the output channel focused at different positions.
- The separation is continuous and make use of a large range of frequencies.
- The multiple-frequency dielectrophoresis separates types of particles based on differences between their dielectric response within a large spectrum. It is therefore much more flexible than separation only based on the duality nDEP vs. pDEP.
- The particle types can be directed towards dedicated fluidic outlets by physically splitting the output channel into several branches where the pure sub-populations can be collected.

- The readout of the output position of a particle type characterizes its dielectric properties in term of "opacity". In other words, besides a continuous-flow separator, our device is also a flow cytometer (but this relies on the quality of the equivalent models).

The challenge is to define the best set of parameters such as the potentials and the frequencies of the three applied signals to get the performances in the continuous separation of particles. The only requirement is the use of two opposite nDEP-forces in order to really create equilibriums and to avoid the cells to enter the "liquid electrodes" due to unbalanced pDEP attraction. In practice, the two nDEP-forces are generated by two independent signals in quadrature ($\omega_1 = \omega_2 + \frac{\pi}{2}$). In case of particles that are more polarizable than the medium, this separation method will be limited since nDEP would be impossible to get. And therefore, the positions of equilibrium could not be defined. A separation could still be obtained but would require on one hand a hydrodynamic focusing prior to the separation and on the other hand would strongly depend on the flow velocity. In summary, the efficient method of continuous particle sorting is provided by the combination of two concepts, the multiple-frequency dielectrophoresis and the "liquid electrode".

6.1.4 Biological applications

The continuous-flow separation method that we developed was applied to biological samples in which the particles were living cells such as yeast cells or red blood cells. The first biological demonstration was the use of the method as sample preparation for a biological analysis. Viable and non-viable yeast cells were separated into fractions approaching 100% in purities. The yeast cell was chosen as model in order to compare our method to worldwide competitors. Our performances are among the best, if not the best, for an application of continuous cell sorting. Obviously, the yeast separation has no relevance in the biological field except as proof of principle.

We focused then on an application with biological significance. The sorting method provided support in the investigation of the cycle of a parasite, *Babesia bovis*, that infects bovine red blood cells. The goal of the sorting device was to maintain a high

6. CONCLUSION AND OUTLOOK

level of PPE in cell culture by isolating infected cells from non-infected cells. This application revealed to be critical because of the small changes in the dielectric properties of the infected RBCs in comparison to the intrinsic variations within the populations. The experiments indeed confirmed our hypothesis that the parasite induces changes in dielectric properties of the host, in particular a decrease of the cytoplasmic conductivity, but did not allow to get pure sub-populations. Instead of clear separation, an enrichment of infected cells was obtained in a portion of the channel. The initial 7% of parasitemia percentage was increased up to 50% in this particular portion. This result competes with current best methods of isolation daily used in laboratories.

The last biological function we intended to address with our flow separator and cytometer device is the synchronization of a cell culture. Our method is a good candidate to get fast and natural cell synchrony without disrupting the cell physiology. We firstly observed that a particular group of cells in division were strongly attracted by pDEP. Since only a few cells among all the cells in division exhibited the "super polarization effect", we assumed that this was somehow correlated to a particular phase within the cell cycle and more specifically to a particular internal arrangement of the spindle apparatus or to geometry of the bud neck. If the hypothesis is confirmed, our continuous cell sorting can benefit from polarization effects related to the cell cycle in order to isolate only synchronous cells. Recent works on numerical modeling (Asami and Sekine, 2007) tend to confirm our hypothesis by pointing out an additional polarization mechanism of budding cell whose relaxation frequency is intimately related to the cell cycle. Preliminary experiments carried out in our lab with genetically modified yeast cells to express GFP-microtubules should allow in a near future to quantify the level of synchrony within a separated sub-population of dividing cells. This could be the most sensitive DEP-based method for lab-on-a-chip application of cell synchronization.

6.2 Contribution to knowledge

Our contribution to knowledge occurs at several levels from concepts to applications. The main conceptual contribution is the "liquid electrode" which behaves like a vertical electrode, or 3D electrode, in the channel sidewall. Integration of such electrodes has been recently reported by Wang *et al.* (2007) and was used to focus a particle

stream. Their focusing application is identical to our focusing application which was already published (Demierre *et al.*, 2007). Wang *et al.* did not yet apply their vertical electrodes to the cell separation. For potentially similar performances, the "liquid electrodes" remain simpler in terms of microfabrication and prove that simple microfabrication process can still produce devices to address complicated biological issues.

Moreover, the "liquid electrodes" provide an homogeneous electric field in the channel height which offers advantages such as the generation of horizontal DEP-forces. They further allow to oppose two DEP-force fields to create an equilibrium position. The principle of equilibrium is important in applications of cell separation by reducing effects of experimental parameters such as the flow velocity. In addition, equilibrium-based manipulations of cells allow to relate the equilibrium position to cell properties. Vahey and Voldman (2008) recently reported on an equilibrium-based cell separation method using DEP-forces in a medium with a conductivity gradient.

The superposition of signals at multiple frequencies for generating dielectrophoresis is itself not new even though only few works have been reported so far. A phenomenological description of MFDEP was issued end of last year by Urdaneta and Smela. Our contribution to knowledge in the field of MFDEP is the opposition of horizontal DEP-forces at multiple frequencies. The use of multiple frequencies in cell separation applications increases the efficiency by considering intrinsic dielectric properties of the particles to be separated over a large frequency spectrum. It is in this way that our separation method brings novelty and improved performances compared to the state-of-the-art of continuous-flow DEP-based cell separation for lab-on-a-chip application.

Most of the biological applications addressed by the combination of multiple-frequency dielectrophoresis with "liquid electrodes" achieved improved performances such as extremely high purities of both viable and nonviable yeast cell fractions. Our separation method was applied to new biological issues such as the isolation on chip of *Babesia bovis* infected RBCs. Moreover, the equilibrium-based separation method can also be applied to flow cytometry applications to characterize the dielectric properties of biological samples. The characterization is simply done by the readout of the cell positions after separation. A major contribution is brought by the last biological application

6. CONCLUSION AND OUTLOOK

considered in this thesis which is the synchronization of a cell culture. We presented a novel method of on-chip cell synchronization by isolating cells that are in the particular phase within their cell-cycle. This method preserves the cell physiology in contrary to classical synchronization methods based on metabolic agents that arrest the cells at a particular cell-cycle phase. Recent work published by Kim *et al.* (2007) pointed out the potential of a DEP-based method in cell synchronization. However, their method has a limited resolution in terms of synchrony level due to the discriminating factor they considered and which is the cell volume. By being sensitive to the internal arrangement of cells and in particular to the bud-neck opening, our method contributes to increase the level of cell synchrony achieved on chip.

6.3 Future perspectives

The technology we described is simple and reliable. Slight adaptations of chips and interfaces to particular applications could contribute to increase sensitivity and versatility. One example is the use of thin wafers (170 μm) in the microfabrication process to provide chip compatibility with high numerical aperture microscopy. The technological platform is mature enough to be applied to further biological issues which can be addressed thanks to the miniaturization. I would recommend to focus the future research on three main axes which are the improvement of current applications, the focalization on novel applications and last the technological developments that are required to address these issues.

The improvement of current applications is particularly directed towards the synchronization of a cell culture where many questions remain open. Here is a list of a few points that should be addressed shortly:

- The preliminary results on cell-culture synchronization are promising even though the question whether cells strongly attracted by the pDEP are synchronous is still not addressed. This requires the use of a cell model that reveals in a way its cell-cycle phase, *e.g.* GFP-tubulin strain of yeast cell. The collaboration with a biological group in Zurich¹ has provided the cell model and the fabrication of thin

¹<http://www.bc.biol.ethz.ch/people/groups/yvbarral>

chips for high resolution imaging has been done. It is time to separate dividing cells and quantify their level of synchrony.

- This validation could also be done using temperature-sensitive mutant strains of yeasts that can be arrested at different particular phases within the cell cycle. This should define which phase is the most polarizable one and validate the numerical model.
- The sorting method and the dielectric characterization should be the starting point of the elaboration and validation of accurate numerical model of budding yeast which correlates the polarizability to the cell-cycle phase. This investigation also contributes to a better understanding of the cell morphogenesis and its consequences on the dielectric properties during the cell cycle

The next group of perspectives extends the application fields considered so far by proposing a few research directions in which the continuous-flow separation method could be used:

- The continuous separation method can be applied to other biological problems such as blood filtration or blood separation, isolation of cancerous cells and early diagnostics, etc... These new opportunities should come through collaborations with biological groups in which our technological platform could be introduced. This would contribute to get the biologists familiar with chip technology.
- The device could also be used to monitor the changes in dielectric properties of a cell over time. To do that, a cell could be tracked during a complete cell cycle and its output position or the "opacity" would be monitored over time. Thus the flow cytometer is not only used to take an instantaneous value of "opacity" but evaluates the dynamics of a biological process such as cell cycle or apoptosis.
- Since viable and non-viable cells generally exhibit a different dielectric response, the device could also serve to assess the cell viability. Using this information, the toxicity of a product can be estimated as well as its lethal concentration or its dynamics on the cell metabolism.

6. CONCLUSION AND OUTLOOK

- The method could also be used in the field of diagnostics by revealing an early and low-concentrated presence of cancerous cells or infected cells. It could also be used in the stem-cell research by detecting changes in the cell development or one can even imagine using an electric-field based method to trigger the cell differentiation. This would be an application of cell "electro-activation".

The last group of perspectives are oriented towards technological developments that would help to address the few biological issues cited just above:

- For application where the cells need to be recollected after experiments, the chip interface needs to be improved in order to allow the sample collection after separation. One could imagine to work in a suction mode rather than pushing the liquids through the channels as it is now. The suction would allow to directly load treated sample into tubes or syringes for further manipulations.
- The long-term monitoring of dielectric properties of cells on chip requires the development of a re-circulating chamber where each individual cell is tracked during hours or days. That would provide valuable insights about dielectric changes during the cell cycle or during the differentiation of a cell.

My deep conviction is that this continuous-flow cell separation method is promised to exciting opportunities in lab-on-a-chip applications due to its simplicity and efficiency. Its ease-of-use is an essential factor that could convince clinicians to adopt it.

Bibliography

- Asami K and Sekine K, 2007: *Dielectric modelling of cell division for budding and fission yeast*. Journal Of Physics D-Applied Physics, vol. 40(4): 1128–1133.
- Demierre N, Braschler T, Linderholm P, Seger U, Van Lintel H and Renaud P, 2007: *Characterization and optimization of liquid electrodes for lateral dielectrophoresis*. Lab on a Chip - Miniaturisation for Chemistry and Biology, vol. 7(3): 355–365.
- Kim U, Shu CW, Dane K, Daugherty P, Wang J and Soh H, 2007: *Selection of mammalian cells based on their cell-cycle phase using dielectrophoresis*. Proceedings of the National Academy of Sciences of the United States of America, vol. 104(52): 20708–20712.
- Urdaneta M and Smela E, 2007: *Multiple frequency dielectrophoresis*. Electrophoresis, vol. 28(18): 3145–3155.
- Vahey M and Voldman J, 2008: *An Equilibrium Method for Continuous-Flow Cell Sorting Using Dielectrophoresis*. Anal Chem, pp. –.
- Wang L, Flanagan L, Jeon N, Monuki E and Lee A, 2007: *Dielectrophoresis switching with vertical sidewall electrodes for microfluidic flow cytometry*. Lab on a Chip - Miniaturisation for Chemistry and Biology, vol. 7(9): 1114–1120.

BIBLIOGRAPHY

Appendix A

Curriculum vitae

Curriculum Vitae



Nicolas Demierre

Date of birth	May 10, 1980
Nationality	Swiss
Origin	St-Martin FR

Education

2004 – 2008	École Polytechnique Fédérale de Lausanne (EPFL) Institute of Microsystems Ph.D. (Dr. ès sciences) Thesis: <i>Continuous-flow cell separation of cells in a lab-on-a-chip using "liquid electrodes" and multiple-frequency dielectrophoresis</i>
2003 – 2004	University of Twente, NL, BIOS The lab-on-a-chip group Master thesis: <i>On-chip trapping of living cells.</i>
1999 – 2003	École Polytechnique Fédérale de Lausanne (EPFL) MSc in microengineering with specialization in integrated products
1995 – 1999	Gymnase Cantonal de Ste-Croix, Fribourg Matura type scientific (Highschool)

Professional Experience

from 2008	Project manager in Biocartis SA, Lausanne, Switzerland Point-of-care testing and diagnostics
2003 – 2008	Swiss Federal Institute of Technology Lausanne (EPFL) MSc/Ph.D. studies and research assistant in the field of microsystems
2006	Software development Development of a setup for force measurement on muscles Univ. of Geneva and Santhera Pharmaceuticals AG, Switzerland

Appendix B

Publications

Publications

Peer-reviewed papers

Demierre N, Braschler T, Linderholm P, Seger U, Van Lintel H and Renaud P, 2007: *Characterization and optimization of liquid electrodes for lateral dielectrophoresis*. Lab on a Chip - Miniaturisation for Chemistry and Biology, vol. 7: 355-365.

Demierre N, Braschler T, Muller R and Renaud P, 2007: *Focusing and continuous separation of cells in a microfluidic device using lateral dielectrophoresis*. Sensors and Actuators, B: Chemical, DOI:10.1016/j.snb.2007.09.078.

Demierre N, Braschler T, Nascimento E, Silva T, Oliva A G and Renaud P, 2008: *Continuous separation of cells by balanced dielectrophoretic forces at multiple frequencies*. Lab on a Chip - Miniaturisation for Chemistry and Biology, vol. 8: 280-286

Küttel C, Nascimento E, **Demierre N**, Silva T, Braschler T, Renaud P and Oliva A G, 2007: *Label-free detection of Babesia bovis infected red blood cells using impedance spectroscopy on a microfabricated flow cytometer*. Acta Tropica, vol. 102: 63-68

Braschler T, Metref L, Zvitov-Marabi R, Van Lintel H, **Demierre N**, Theytaz J and Renaud P, 2007: *A simple pneumatic setup for driving microfluidics*. Lab on a Chip - Miniaturisation for Chemistry and Biology, vol. 7: 420-422

Braschler T, Theytaz J, Zvitov-Marabi R, Van Lintel H, Loche G, Kunze A, **Demierre N**, Tornay R, Schlund M and Renaud P, 2007: *A virtual valve for smooth contamination-free flow switching*. Lab on a Chip - Miniaturisation for Chemistry and Biology, vol. 7: 1111-1113

Tornay R, Braschler T, **Demierre N**, Steitz B, Finka A, Hofmann H, Hubbell J and Renaud P, 2008: *Dielectrophoresis-based particle exchanger for the manipulation and surface functionalization of particles*. Lab on a Chip - Miniaturisation for Chemistry and Biology, vol. 8: 267-273

Nascimento E, Nogueira N M, Silva T, Braschler T, **Demierre N**, Renaud P and Oliva A G, 2007: *Dielectrophoretic sorting on a microfabricated flow cytometer: label free separation of Babesia bovis infected erythrocytes*. submitted to Bioelectrochemistry

Publications

Patents

Renaud P, Linderholm P, Braschler T, **Demierre N** and Seger U, 2006: *APPARATUS FOR MANIPULATING, MODIFYING AND CHARACTERIZING PARTICLES IN A MICRO CHANNEL*. International Patent Application PCT/IB2007/050338

Proceedings

Demierre N, Braschler T, Tornay R, Valero A and Renaud P, 2008: *Microfluidic device for continuous dielectrophoretic separation of cells in division*. Accepted to Proceedings of the 12th International Conference on Miniaturized Systems for Chemistry and Life Sciences, MicroTAS, October 12-16, San Diego, CA, USA

Demierre N, Braschler T, Muller R and Renaud P, 2007: *Focusing and Continuous Separation of Cells in a Microfluidic Device using Lateral Dielectrophoresis*. International Solid-State Sensors, Actuators and Microsystems Conference, TRANSDUCERS: 1777-1780

Demierre N, Braschler T, Meyer P and Renaud P, 2007: *Continuous separation of cells in a microfluidic device using lateral dielectrophoresis*. Proceedings of the 11th International Conference on Miniaturized Systems for Chemistry and Life Sciences, MicroTAS: 125-127

Küttel C, Nascimento E, **Demierre N**, Silva T, Braschler T, Oliva A G and Renaud P, 2007: *Impedance spectroscopy on a microfabricated flow cytometer: label-free detection of Babesia Bovis parasites in bovine red blood cells*. Proceedings of the 11th International Conference on Miniaturized Systems for Chemistry and Life Sciences, MicroTAS: 494-496